Numerical Analysis for Tension Membrane Structures and Multiscale Modeling for the Applied Coated Fabrics

Numerieke analyse van voorgespannen membraanstructuren en multischaalmodellering van de bijbehorende textielmaterialen

Tien Dung Dinh

Promotoren: prof. dr. ir. W. Van Paepegem, dr. A. Rezaei
Proefschrift ingediend tot het behalen van de graad van
Doctor in de ingenieurswetenschappen: werktuigkunde-elektrotechniek

UNIVERSITEIT
GENT

Vakgroep Toegepaste Materiaalwetenschappen
Voorzitter: prof. dr. ir. L. Kestens
Faculteit Ingenieurswetenschappen en Architectuur
Academiejaar 2016 - 2017

ISBN 978-90-8578-957-4
NUR 929, 978
Wettelijk depot: D/2016/10.500/89

Promotors

prof. dr. ir. W. Van Paepegem and dr. ir. A. Rezaei

Ghent University
Faculty of Engineering and Architecture
Department of Materials Science and Engineering

Examination Committee

prof. H. Van Landeghem	Ghent University, Belgium
prof. W. Van Paepegem	Ghent University, Belgium
dr. A. Rezaei	Ghent University, Belgium & Katholieke Universiteit Leuven
prof. M. Mollaert	Vrije Universiteit Brussel, Belgium
prof. D. Van Hemelrijck	Vrije Universiteit Brussel, Belgium
prof. S. Reese	RWTH Aachen, Germany
prof. M. Abdel Wahab	Ghent University, Belgium
prof. F.A. Gilabert	Ghent University, Belgium

Research Institute

Ghent University
Department of Materials Science and Engineering
Mechanics of Materials and Structures
Technologiepark 903
B-9052 Zwijnaarde
Belgium

Tel. +32 9 331 04 14
Tiendung.Dinh@UGent.be
Tiendungdinh@gmail.com

This research is funded by Fonds Wetenschappelijk Onderzoek- Vlaanderen (F.W.O).

The computational resources (Stevin Supercomputer Infrastructure) and services used in this work were provided by the VSC (Flemish Supercomputer Center), funded by Ghent University, the Hercules Foundation and the Flemish Government - department EWI.

Acknowledgements

I still remember on Sunday November 11^{th} 2012, I took the earliest train from Bochum to go to Ghent. That date opened a new chapter in my life, I moved to Ghent, Belgium. I have been truly fortunate to live in the beautiful city of Gent and to study and work in the Mechanics of Materials and Structures research group under the supervision of Prof. Wim Van Paepegem and Dr. Ali Rezaei.

First and foremost, I would like to sincerely acknowledge Prof. Wim Van Paepegem for accepting me as a Ph.D. student in his research group and for his great guidance and support in my research over the last four years. He has offered me the freedom to pursue my own ideas in the research project, contributed invaluable advice and got me started in the right direction. I would also like to express my gratitude to my daily supervisor, Dr. Ali Rezaei, for numerous advice, not only in science but also in life.

I am very grateful to Prof. Marijke Mollaert, Prof. Danny Van Hemelrijck, Prof. Lars De Laet, Silke Puystiens and Maarten Van Craenenbroeck from Vrije Universiteit Brussel for their fruitful cooperation, their warm host in many enjoyable project meetings and especially for the valuable experimental data that they generously shared.

I would like to express my sincere gratitude to all members of my Ph.D. examination committee, especially to Prof. Stefanie Reese for her constructive comments in the reading report of my dissertation and also for her time to travel from Aachen to Gent to attend my private Ph.D. defense.

I would also like to take this chance to thank Lode Daelemans from the department of Textile Engineering, Ghent University for his help in doing experiments for the studied coated fabric and sharing his knowledge in the digital element simulation method. I have highly appreciated many technical discussions with David Garoz Gomez, Francisco Gilabert, Reza Vafadari and Stefan Jacques.

My thanks goes to the former master thesis students, who have been involved in my research: Kristine Vandenboer, Kim Carbonez, Sara Minoodt and Thomas Linthout.

This dissertation cannot be complete without the Dutch summary. Many thanks are addressed to Mathias Kersemans and Ilse Vercruysse for their kind help in translating the English summary into Dutch.

This research was funded by the Fonds Wetenschappelijk Onderzoek - Vlaanderen (F.W.O). This funding is gratefully acknowledged.

I would also like to thank Jana Faes and Joren Pelfrene for joining me at the courses in Barcelona and in Hannover. My trips would have been much less pleasant without their company.

My special thanks go to the colleagues who have been working in the research group of Mechanics of Materials and Structures for many technical and social discussions in the coffee break and in the lunch time during my time at Gent. Many thanks to my Vietnamese friends in Gent, who treated me like their younger brother, Truong Quoc Thai, Huynh Thanh Toi, Nguyen Viet Dung, Nguyen Van Hung, Nguyen Thi Hanh Tien, Pham Huu Ha Giang and Phan Ngoc Thanh Phuong.

My deepest thank goes to my family, especially, my parents and my eldest brother, for their love and unconditional support they have given me. Last but not least, I would like to thank my beloved wife for her care, balancing distraction, relaxation and joy over the years.

Tien-Dung Dinh
Gent, November 25, 2016

Summary

Nowadays, tensioned fabric membrane structures (TFMS) are widely used in large-scale buildings, such as sports stadia, shopping malls, etc. Indeed, TFMS are classified as unconventional structures as the coated fabric material has both cladding and supporting functionality. At present, there is limited guidance, let alone a unified approach in designing and analyzing of these structures. Therefore, the design and analysis of TFMS strongly depend on numerical simulations.

Understanding the behavior of TFMS is a challenging task because of involvement of different sources of nonlinearity. The mechanical behavior of the fabric membrane is severely nonlinear and this membrane experiences a finite deformation during loading. Thus, material and geometrical nonlinearities have to be considered in the analysis of TFMS. In addition, the nonlinear kinematical interaction between different constituents of TFMS, *i.e.*, the fabric membrane and the boundary cables, has also a profound effect on the structural behavior of this kind of structures. Therefore, it is crucial to account also for boundary nonlinearity in the analysis step. In the literature, there are numerous works on numerical analyses of TFMS. However, most of them ignore the material and boundary nonlinearities and only consider the geometrical nonlinearity in their analyses. In addition, validation of these numerical studies is missing, making it difficult to assess their performance and accuracy.

This study aims to gain a better understanding of the mechanical behavior of the fabric membrane materials on one hand and the structural behavior of TFMS on the other hand. In the first part of the study, a material constitutive law for the fabric membrane materials is developed. This material model is aimed for numerical simulations of large scale membrane structures, therefore, it should be computationally inexpensive, but sophisticated enough to capture the peculiar mechanical be-

havior of the fabric membrane material in detail. Based on experimental data from uniaxial tension tests in both the warp and fill directions, two 1D elasto-plastic models were proposed respectively for each direction. Subsequently, the mechanical behavior in case of multiaxial stress states can be taken into account by adjusting the Poisson's ratios, which were identified based on the data from the biaxial tension tests. Even though the proposed material model is purely phenomenological, the idea behind was motivated by the discrete nature of the fabric membrane materials. In the remainder of this dissertation, the proposed material model is referred to as fabric plasticity model. The fabric plasticity model was implemented in ABAQUS/Standard as user material (UMAT). Afterward, the model was verified with the experimental data from the uniaxial and biaxial tension tests. It is clear from the obtained results that the fabric plasticity model can capture well the peculiar mechanical behavior of the fabric membrane material, such as strong orthotropy, irreversible deformation and load-ratio dependence. Furthermore, the fabric plasticity model was validated for a large-scale polyvinyl chloride (PVC) coated fabric membrane under in-plane multiaxial loading. The numerical results were discussed and critically compared to the corresponding experimental data. The numerically computed strain fields in the membrane were qualitatively compared to the corresponding experimental data obtained from the digital image correlation (DIC) technique. Also quantitative comparison was made by considering three paths in the membrane in horizontal, diagonal and vertical direction. The strains in the membrane were then extracted along these paths and quantitatively compared to the counterparts in the experiments. In addition, the linear orthotropic elasticity model, which is widely used now in practice, has also been used for the fabric membrane and the obtained results were then also compared to the experimental data. In these comparisons, the results obtained from the fabric plasticity model have a good correlation with the corresponding experimental data and are significantly better than the counterparts obtained from the linear orthotropic elasticity model.

In the second part of the study, it was explained why the nonlinear material model for coated fabrics in general and the fabric plasticity model in particular cannot be used for 3D fabric membrane structures in the conventional design method. As a consequence, a novel design and analysis method was proposed within the framework of shape optimization. In this method, the shape of an intermediate membrane, which is formed by assembling different fabric panels, was adjusted in such a way that

the stress fields in the deployed membrane are uniform and close to the targeted values. The shape adjustment was done automatically by using an optimization algorithm. At first, a genetic algorithm was used for this process, but this algorithm demanded a large number of the objective function evaluations making it computationally inefficient. Therefore, the Pattern Search and Bayesian optimization methods were also used in this study. Moreover, in practice, designers have to apply compensation for the fabric cutting panels. This amount of compensation, which is originated from the usage of the simplified material models for the fabrics, is highly dependent on the curvature level of the structures as well as the types of the applied fabric material. By employing the proposed design and analysis method and comparing the obtained fabric cutting patterns when using respectively the fabric plasticity and linear orthotropic elasticity model for the membrane, the amount of compensation can be attained.

Moreover, the origin of the peculiar macroscopic mechanical behavior of the fabric membrane material resides in the properties and interaction of its constituents in meso- and micro- scales. Therefore, to gain a better understanding of the deformation mechanisms of this kind of material, a hybrid micro-meso-scale unit cell model for coated fabrics was proposed in the third part of this study using the multiscale modeling strategy. This model not only provides local information of the fabric membrane materials under loading but can also be used to generate virtual experimental data. These data are indeed crucial to further develop the macroscopic material law for the fabric membrane materials but are still missing in the literature. To build up this hybrid unit cell model, a CT-scan measurement of the considered fabric, *i.e.*, the PVC coated polyester fiber fabric, was done to characterize the geometrical data. Afterward, the mechanical characterization of PVC coating and polyester fiber was done. Subsequently, an in-house software was used to create the finite element model of the hybrid unit cell in ABAQUS/Explicit. In this model, while the PVC coating was modeled with 3D solid elements, the polyester yarns were modeled as assemblies of truss elements. Thus, the material constitutive law used in this model is far simpler than the one in which the yarn is modeled with solid elements and the interaction among the fibers can be taken into account. The developed hybrid model has been verified with the uniaxial test data in both the warp and fill directions. It was then validated with the experimental data from the biaxial test. It is clear that the numerical results are in good agreement with the corresponding experimental data. Finally, it was employed to create the virtual experi-

mental data when the unit cell was subjected to different stress ratios.

Samenvatting

Tegenwoordig worden steeds meer membraanstructuren met gespannen textieldoek (Engels: Tensioned Fabric Membrane Structures - TFMS) gebruikt in grootschalige architectuur, zoals stadions, winkelcentra, etc. Deze membraanstructuren worden beschouwd als onconventioneel aangezien het textielmateriaal zowel een overkappende als ondersteunende functie heeft. Momenteel zijn er dan ook heel weinig richtlijnen, laat staan een uniforme aanpak, bij het ontwerpen en analyseren van deze structuren, wat dan weer leidt tot een grote afhankelijkheid van numerieke simulaties.

Inzicht in het gedrag van TFMS is een uitdagende taak, omdat hier verschillende bronnen van non-lineariteit spelen.Een gespannen doek membraanstructuur vertoont een sterk niet-lineair mechanisch gedrag en vertoont een eindige vervorming bij belasting. Dit betekent dat men bij het analyseren van TFMS rekening moet houden met geometrische niet-lineariteit, alsook met de niet-lineariteit van het materiaal. Bovendien wordt het structurele gedrag van dergelijke membraanstructuren ook beïnvloed door de kinematische niet lineaire interactie tussen de verschillende bestanddelen van TFMS, nl. het doek en de kabels. Het is daarom van groot belang om tijdens de analytische stappen rekening te houden met niet-lineariteit van de interactie tussen kabels en textieldoek.In de literatuur zijn er talrijke studies terug te vinden over numerieke analyse van TFMS. De meeste van deze studies negeren echter het bestaan van niet-lineariteiten van materiaal en/of kabel-doek interactie en houden in hun analyses enkel rekening met de geometrische niet-lineariteit. Bovendien ontbreekt elke validatie in deze numerieke studies waardoor het moeilijk is om de resultaten en de nauwkeurigheid te evalueren.

Dit doctoraatsonderzoek heeft tot doel om een beter inzicht te krijgen in het mechanisch gedrag van de membraanmaterialen enerzijds, en het

structurele gedrag van TFMS anderzijds. In het eerste deel van het onderzoek wordt een constitutieve wet voor de membraanmaterialen ontwikkeld. Dit materiaalmodel moet performant zijn voor numerieke simulaties van grootschalige membraanstructuren. Het moet derhalve rekenkundig efficiënt zijn, maar tegelijk geavanceerd genoeg om het bijzondere mechanische gedrag van het membraanmateriaal in detail te bestuderen. Op basis van de experimentele gegevens van eenassige trekproeven in zowel de ketting als inslag richtingen werden twee 1D elasto-plastische modellen voorgesteld respectievelijk voor elke richting. Vervolgens kan het het mechanisch gedrag bij meerassige spanningstoestanden in rekening gebracht worden door de Poisson-coëfficiënten aan te passen, die geïdentificeerd zijn op basis van de gegevens van de biaxiale trekproeven. Hoewel het voorgestelde materiaalmodel louter fenomenologisch is, werd het idee erachter ingegeven door de discrete aard van de membraanmaterialen. In de rest van deze studie wordt naar het voorgestelde materiaalmodel verwezen als een plasticiteitsmodel voor membranen. Het plasticiteitsmodel werd in ABAQUS/Standard geïmplementeerd als een nieuw materiaalmodel (Umat) . Daarna werd het model geverifieerd met de experimentele gegevens van de één-assige en twee-assige trekproeven. Uit de verkregen resultaten is gebleken dat het plasticiteitsmodel zeer goed de bijzondere mechanische eigenschappen van het membraanmateriaal kan weergeven, waaronder de sterke orthotropie, de onomkeerbare vervorming en de afhankelijkheid van de belastingsverhouding. Verder werd het plasticiteitsmodel gevalideerd voor een grootschalige constructie van polyvinylchloride (PVC) gecoat membraan onder een meer-assige belasting in het vlak. De numerieke resultaten werden besproken en kritisch vergeleken met de overeenkomstige experimentele gegevens. De numeriek berekende spanningsvelden in het membraan werden kwantitatief vergeleken met de overeenkomstige experimentele gegevens van de digitale beeldcorrelatie (DIC) techniek. Tevens werd een kwantitatieve vergelijking gemaakt waarbij drie paden in het membraan werden bestudeerd, in een horizontale, diagonale en verticale richting. Vervolgens werden langs deze paden de spanningen in het membraan afgeleid en kwantitatief vergeleken met de tegenhangers in de experimenten. Bovendien werd voor het membraan ook een vergelijking gemaakt met het op grote schaal in de praktijk gebruikte lineaire orthotropische elasticiteitsmodel. Uit deze vergelijkingen blijkt dat de resultaten verkregen uit het plasticiteitsmodel, een goede correlatie vertonen met de overeenkomstige experimentele gegevens en deze ook significant beter zijn dan de tegenhangers verkregen

uit het lineaire orthotrope elasticiteitsmodel.

In het tweede deel van de studie wordt verklaard waarom het niet-lineaire materiaalmodel voor gecoat textiel in het algemeen, en het plasticiteitsmodel in het bijzonder, niet kan worden gebruikt voor 3D membraanstructuren in de conventionele ontwerpmethode. Bijgevolg werd een nieuwe ontwerp- en een nieuwe analysemethode in het kader van vormoptimalisatie voorgesteld. Bij deze werkwijze werd de vorm van een tussenliggend membraan, dat werd gevormd door het samenvoegen van verschillende panelen, zodanig aangepast dat de spanningsvelden in het samengevoegde membraan uniform zijn en dicht bij de vooropgestelde waarden liggen. De vormaanpassing werd automatisch uitgevoerd via een optimalisatie algoritme. Aanvankelijk werd een genetisch algoritme gebruikt voor dit proces, maar dit vereiste een groot aantal functie-evaluaties waardoor het rekenkundig inefficiënt was. Derhalve werden ook de Pattern Search en Bayesiaanse optimalisatie methoden gebruikt in dit onderzoek. Bovendien passen ontwerpers in de praktijk compensatie toe bij het knippen van de individuele panelen. Deze compensatie, die ontstaat uit het gebruik van vereenvoudigde materiaalmodellen voor de weefsels, is sterk afhankelijk van de krommingscurve van de structuren en van het soort weefselmateriaal dat gebruikt wordt. Indien het voorgestelde ontwerp en de analyse methode worden toegepast, wordt de compensatie meteen mee berekend. De verkregen knippatronen van de weefsels werden opnieuw vergeleken, dit met behulp van respectievelijk het plasticiteitsmodel en het lineaire orthotrope elasticiteitsmodel .

De oorsprong van het bijzondere macroscopische mechanische gedrag van het membraanmateriaal ligt bovendien in de eigenschappen en in de interactie van zijn bestanddelen in meso- en micro- schalen. Om tot een beter begrip te komen van de vervormingsmechanismen van dit soort materialen, werd in het derde deel van deze studie een hybride micromeso schaalmodel voorgesteld voor gecoat weefsel, waarbij gebruik gemaakt werd van een multischaal model-strategie. Dit model geeft niet alleen lokale info over het membraanmateriaal onder belasting, maar kan ook worden gebruikt om virtueel experimentele gegevens te genereren. Deze gegevens zijn van cruciaal belang voor de verdere ontwikkeling van de macroscopische materiaal wet voor de membraanmaterialen, en zijn momenteel nog niet terug te vinden in de literatuur. Voor de opbouw van dit hybride eenheidscel-model, werd een CT-scan meting gedaan van de betrokken stof, i.e. PVC-gecoate polyestervezel, om zodoende de geometrische gegevens te genereren. Nadien werd de mechanische karakte-

risering van de PVC coating en de polyestervezel uitgevoerd. Vervolgens werd het eindige elementenmodel van de hybride eenheidscel in ABAQUS / Explicit berekend. In dit model werden de polyester garens gemodelleerd als een geheel van staafelementen, terwijl de PVC coating werd gemodelleerd met 3D continuum elementen. Bijgevolg is de materiaal constitutieve wet die gebruikt werd in dit model veel eenvoudiger dan die waar het garen wordt gemodelleerd met continuum elementen en kan er rekening gehouden worden met de interactie tussen de vezels. Het ontwikkelde hybride model is geverifieerd met de één-assige testgegevens in zowel de ketting als inslag richtingen. Vervolgens werd het model gevalideerd met de experimentele gegevens van de twee-assige testopstelling. Het is duidelijk dat de numerieke resultaten goed overeen stemmen met de corresponderende experimentele gegevens. Tot slot werd het hybride model gebruikt om virtuele testdata te genereren voor biaxiale spanningstoestanden met verschillende spanningsverhoudingen.

Curriculum

Tien-Dung Dinh was born on July 14, 1987 in Binh Thuan, Vietnam. He received his B.Sc. in Engineering Mechanics from Ho Chi Minh City University of Technology, Vietnam in April 2010 and his M.Sc. degree in Computational Engineering from Ruhr University Bochum, Germany in September 2012. With the interest in the fields of mechanics of composite materials and structures and computational mechanics, he started his research work in the Department of Materials Science and Engineering at Ghent University in November 2012. The work presented in this dissertation has been accomplished under the guidance of prof. dr. ir. Wim Van Paepegem and dr. ir. Ali Rezaei, in collaboration with prof. dr. ir. Marijke Mollaert and prof. dr. ir. Danny Van Hemelrijck from Vrije Universiteit Brussel. His research work entitled "Numerical analysis for tension membrane structures and multiscale modeling for the applied coated fabrics" has been financially supported by a Ph.D. grant of Research Fund-Flanders (FWO) for the project "Integrated analysis and experimental verification of kinematic form active structures (KFAS) for architectural applications". Tien-Dung Dinh is author of four publications in international journals of the Science Citation Index, of which 3 publications as the first author, and one publication in an international conference proceeding.

Publications

List of scientific publications by Tien-Dung Dinh.

A1 - Peer reviewed journal publications included in Science Citation Index

1. **T.D. Dinh**, A. Rezaei, L. De Laet, M. Mollaert, D. Van Hemelrijck and W. Van Paepegem. A new elasto-plastic material model for coated fabric. *Engineering Structures*, 71:222-233, 2014 (SCIE-IF: 1.893).

2. **T.D. Dinh**, A. Rezaei, S. Puystiens, M. Van Craenenbroeck, K. Carbonez, L. De Laet, M. Mollaert, D. Van Hemelrijck and W. Van Paepegem. A study of tension fabric membrane structures under in-plane loading: Nonlinear finite element analysis and validation. *Composite Structures*, 128:10-20, 2015 (SCIE-IF: 3.853).

3. P. Phung-Van, Lieu B. Nguyen, Loc V. Tran, **T.D. Dinh**, Chien H. Thai, S.P.A. Bordas, M. Abdel Wahab and H. Nguyen-Xuan. An efficient computational approach for control of nonlinear transient responses of smart piezoelectric composite plates. *International Journal of Non-Linear Mechanics*, 76:190-202, 2015 (SCIE-IF:1.920)

4. **T.D. Dinh**, A. Rezaei, W. Punurai, L. De Laet, M. Mollaert, D. Van Hemelrijck and W. Van Paepegem. A shape optimization approach to integrated design and nonlinear analysis of tensioned fabric membrane structures with boundary cables. *International Journal of Solids and Structures*, 83:114-125, 2016 (SCIE-IF: 2.081).

Publications under review

1. **T.D. Dinh**, A. Rezaei, T. Linthout, M. Mollaert, D. Van Hemelrijck and W. Van Paepegem. A computational compensation method for fabric panels of tensioned membrane structures using a shape optimization method based on gradientless algorithms *(submitted for publication in International Journal of Solids and Structures)* (SCIE-IF: 2.081).

2. **T.D. Dinh**, A. Rezaei, L. Daelemans, M. Mollaert, D. Van Hemelrijck and W. Van Paepegem. A hybrid micro-meso-scale unit cell model for homogenization of the orthotropic material behavior of coated fabrics used in tensioned membrane structures *(submitted for publication in Composite Structures)* (SCIE-IF: 3.853).

C1 - Publication in conference proceedings

1. **T.D. Dinh**, A. Rezaei, M. Van Craenenbroeck, S. Puystiens, L. De Laet, M. Mollaert, D. Van Hemelrijck and W. Van Paepegem. A new elasto-plastic material model for coated fabric in membrane structures. 16^{th} *European conference on Composite Materials (ECCM-16)*, 01/2014.

C3 - Conference abstract

1. **T.D. Dinh**, A. Rezaei and W. Van Paepegem. Shape optimization for cable reinforced tension fabric membrane structures. *VII International Conference on Textile Composites and Inflatable Structures, STRUCTURAL MEMBRANES*, 2015.

Contents

List of Figures

List of Tables

Chapter 1

Introduction

In this chapter, an overview of the tensioned fabric membrane structures and coated fabrics modeling is presented. It commences with a brief introduction about the membrane structures, then the motivation and objectives of this work are given. At the end of this chapter, the details of subsequent chapters in this dissertation are also summarized.

1.1 General overview

Tensioned fabric membrane structures have been widely used for the last five decades since the pioneering work of Frei Otto [1]. In these structures, coated fabrics are used due to their high ratio of strength to weight. This salient feature enables fabric membrane structures to be used in large scale structures, such as sports stadia, shopping malls and tent-like structures [2] (*cf.* figs. 1.1 to 1.3). Moreover, fabric membranes provide the surfaces with high levels of curvature that makes them look aesthetic and can serve as an architecturally striking solution [3].

Compared with conventional structures made from concrete, steel or timber, fabric structures are more structurally efficient and cost-effective. Moreover, in this kind of structure the material can be used optimally because there is no need to design the membrane section for bending or buckling [4]. However, due to the lack of bending and compression stiffness, compressive stresses will lead to buckling and wrinkling in architectural fabrics. It can eventually lead to the collapse of the fabric structures [5]. To circumvent this issue, the fabric membrane structures

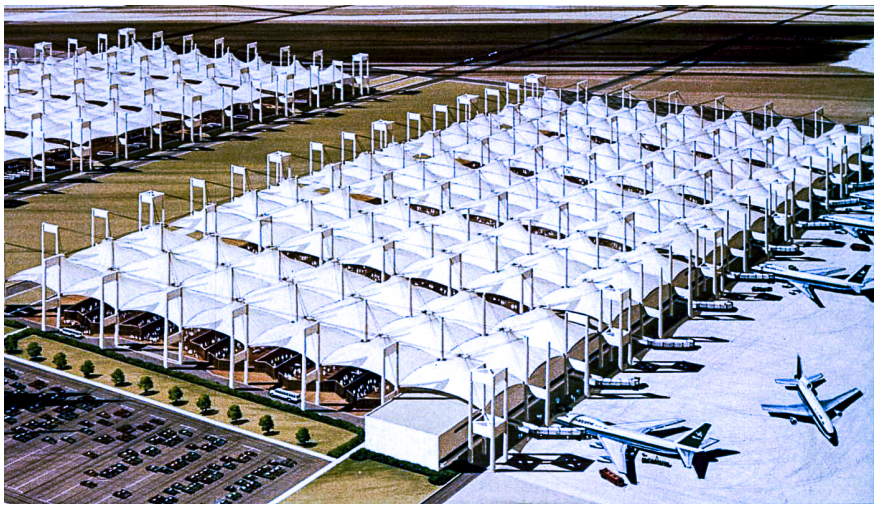

Figure 1.1: The most significant membrane structure, the Hajj Terminal in Saudi Arabia.

Figure 1.2: Tensioned membrane structures were used as temporary structures in Gent Floraliën 2016 (courtesy of Han Nguyen).

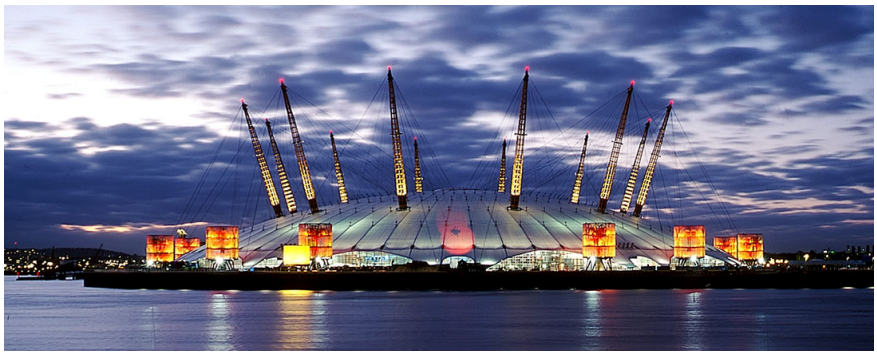

Figure 1.3: The Millennium dome in Greenwich, United Kingdom.

have to be designed in such a way that they will be always in tension under any kind of loads for their whole life cycle. Indeed, prestresses are usually introduced in the membrane by stretching the boundary cables at the edges of the membrane.

Design and analysis of tensioned membrane structures is challenging and *'no other class of architectural structural systems is as dependent upon the use of digital computers as are tensile membrane structures.'* [6]. The fabric membrane materials are much softer compared to conventional materials used in civil engineering, *i.e.*, concrete, timber and steel. Because of that, the fabric membrane experiences a finite deformation during the course of loading. Furthermore, the mechanical behavior of the coated fabrics is also severely nonlinear, including orthotropy, stress ratio dependence, hysteresis effect and irreversible deformation [7]. In addition, the boundary cables may fit within the fabric sleeves and may slide when the membrane structure is loaded. Therefore, to simulate a tensioned fabric membrane structure true-to-nature, one has to consider three different kinds of nonlinearities, *i.e.*, material, geometrical and boundary nonlinearities. Thus far several software packages have been developed, such as EASY, Sofistik, etc. However, most of them are working with largely simplified material models and thus cannot capture properly the mechanical behavior of the coated fabrics. Even though there are numerous numerical analyses for these structures available in the literature, most of them only take the geometrical nonlinearity into account and validation of these analyses is missing. It leaves these numerical simulations in dubiety [8].

Thus far, there has been limited guidance and no unified approach in design and analyses for these structures. Therefore, round robin exercises

have been conducted to evaluate the current state of analysis as well as to assess the level of consistency in practice [8]. However, there are visible discrepancies in the results obtained from the participants, it thus raises doubt about the degree of confidence in the analysis of these structures using current design procedures.

The current design procedures for tensioned membrane structures can be divided into two methods, *i.e.*, the conventional design method and the integrated one. In the former one, which has been employed ubiquitously in the field, the design and analysis are split into four steps, *viz.*, form finding, materialization, load analysis and cutting pattern generations [9]. In the integrated design and analysis method, these stages are combined in a single step [10]. There are several unrevealed problems associated with the aforementioned design and analysis methods. For the conventional design method, many methods have been proposed for the form finding, however, comparisons remain rare and it is not clear to what extent these methods differ [11]. In materialization and load analysis stages, the importance of incorporating the nonlinear mechanical behavior of the fabric membranes has been emphasized in several works [12–16], however, the linear orthotropic elasticity model is still widely used [17]. Designers try to compensate these weaknesses in the design and analysis stages by applying compensation to the fabric panels. However, up to now the method to apply this compensation has been rarely mentioned in the literature. For the integrated design and analysis method, all stages are combined in a single loop. Thus the information is well-transferred among them. It has been shown in the literature that this approach facilitates the incorporation of material and boundary nonlinearities, which are difficult to include when using the conventional design method. Two factors that are important in this method are the sources of nonlinearities, which are considered in the structural analysis stage, and the way the shape of the membrane and the length of the boundary cables are adjusted. Thus far, most of the works using this design and analysis method either simplified the sources of nonlinearity in their analysis or adjusted the membrane's shape crudely.

Moreover, in order to develop the material constitutive law for the coated fabrics, it is necessary to perform numerous experiments. These experiments are time-consuming and costly. Therefore, computational models that can predict the mechanical behavior of the coated fabrics are demanded. Indeed, the coated fabrics used in tensioned membrane structures can be considered as a special kind of textile composites. However,

the coating material is much less stiff compared to the conventional textile composites. Moreover, the coating material is not fully-impregnated inside the fabric yarns. Hence, the fabric fiber can slip relatively on each others during the course of loading. This phenomenon does not happen in the conventional textile composites and is one of the major challenges in modeling the coated fabrics.

1.2 Motivation and objectives

In the present dissertation, nonlinear finite element analyses for tensioned fabric membrane structures and the applied coated fabric are presented. These simulations are carefully validated with corresponding experimental data. It hence ensures the degree of confidence of these simulations. As mentioned, in the conventional design and analysis method, there are some non-validated assumptions. Among them, the oversimplification in the material model for the fabric membrane and the way designers apply compensation for fabric panels are critical issues. The present author believes that by solving these issues, we can make a big step in providing more reliable simulation results, which can be used for verification and benchmarking for membrane analysis software packages as well as to contribute to the development of an international design code for tensioned membrane structures in future.

From tensioned fabric membrane structures point of view, the works presented in this dissertation can be considered as a continuing study of the integrated design and analysis method in tensioned fabric membrane structures. The novelties in this dissertation include:

- The development of a new material law for the considered coated fabric
- A novel design and analysis method for tensioned membrane structures using shape optimization method was proposed, in which all sources of nonlinearities can be incorporated in the structural analysis step and the adjustment of the membrane's shape and boundary cables' length can be done automatically.
- From material modeling point of view, the work presented in this dissertation is one of the first studies that proposes a direct link be-

tween the micro-meso structure of the coated fabrics and its macroscopic mechanical behavior.

1.3 Collaborators of the project

This dissertation is a part of the project *"Integrated analysis and experimental verification of kinematic form active structures (KFAS) for architectural applications"*, funded by Research Fund-Flanders (FWO), Belgium. This project was executed in strong collaboration of the three following partners:

- The research group Mechanics of Materials and Structures (MMS) of the Department of Materials Science and Engineering at Ghent University.
- The architectural engineering research laboratory (ae-lab) of the department of Architectural Engineering at Vrije Universiteit Brussel.
- The research group Mechanics of Materials and Constructions (MeMC) at Vrije Universiteit Brussel.

In this project, the numerical simulations were performed under supervision of the MMS research group and the experiments were performed under supervision of the ae-lab and the MeMC groups, with a continuous feedback between the two research activities. The list of experiments done at VUB is presented in appendix A.

1.4 Outline of this dissertation

This dissertation can be divided into three mutually connected parts (*cf.* fig. 1.4), *viz.*, (i) development of a material constitutive law for coated fabrics and its validation, (ii) integrated design and analysis of tensioned fabric membrane structures and (iii) multiscale modeling of the applied coated fabric. The first part is organized as follows:

Chapter 2 presents a structural material model for coated fabrics (*viz.*, fabric elasto-plasticity), which can be considered as the core of the first part of the thesis. This material model is proposed based on the experimental data obtained from uniaxial tests, a uniaxial bias extension test,

and biaxial tests. In this chapter, the present author will present how these data are transferred to the fabric elasto-plastic model and how the parameter calibration is done. At the end of the chapter, an analysis for a hypar structure is considered when the fabric elasto-plasticity and orthotropic elasticity are respectively used for the membrane.

Chapter 3 presents a case study where a structural analysis was conducted for a 2-D membrane that was subjected to in-plane loading. The aim of this case study is two-fold: firstly, to validate the fabric elasto-plasticity model developed in the previous chapter; secondly, to propose a benchmark for numerical analysis in the research field of tensioned fabric membrane structures.

The part dedicated to the integrated design and analysis of tensioned fabric membrane structures consists of two following chapters:

Chapter 4 presents a method in which all stages in design and analysis of tensioned fabric membrane can be incorporated seamlessly within the framework of shape optimization. Moreover, in this chapter the deficiencies of the current design procedures are also discussed in detail.

Chapter 5 presents a further development of the proposed method in chapter 4, so that it can be used for highly curved membrane structures. In this chapter, a computational approach for fabric panels used in tensioned membrane structures is also discussed in detail. Moreover, different gradientless optimization algorithms are employed to find the optimum shape of the membrane and their performances are compared.

It is worth mentioning that the material model used for the membrane in chapters 4 and 5 is the fabric plasticity model developed in chapter 2.

The content of the last part of this dissertation is presented in the following chapters:

Chapter 6 presents the elements of homogenization-based multiscale modeling of woven fabrics, *viz.*, the periodic boundary conditions, the numerical homogenization and the digital element method. Simulation of a dry fabric under shear loading is also presented in this chapter.

Chapter 7 presents a hybrid micro-meso-scale unit cell model for the applied coated fabrics within the framework of homogenization-based multiscale modeling of woven fabrics (*cf.* chapter 6). In this chapter, the experimental data for each phase of the material, *i.e.*, PVC coating and polyester fiber are presented. Afterward, the homogenized stress strain curves from the uniaxial tests are compared with the counterparts from

the experiments (*cf.* chapter 2). Finally, the virtual experimental data for different strain ratios in the biaxial tests are presented.

?? concludes the present dissertation with some remarks on numerical analysis for tensioned membrane structures and woven fabric materials modeling. Possibilities to extend the present research are also discussed.

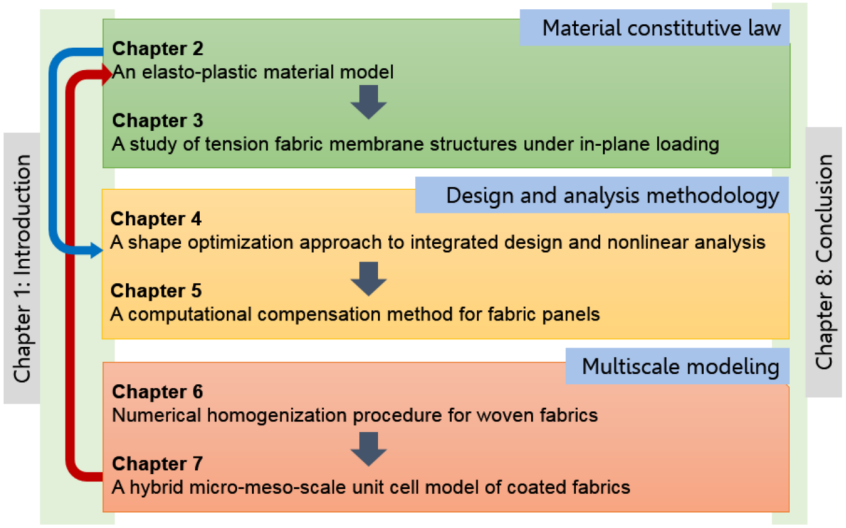

Figure 1.4: An illustration for the connection among different parts of the research presented in this dissertation

Bibliography

[1] F. Otto, Tensile Structures; Design, Structure, and Calculation of Buildings of Cables, Nets, and Membranes, M.I.T. Press, 1967.

[2] B. Bridgens, M. Birchall, Form and function: The significance of material properties in the design of tensile fabric structures, Engineering Structures 44 (2012) 1–12. doi:10.1016/j.engstruct.2012.05.044.

[3] B. N. Bridgens, P. D. Gosling, Direct stress–strain representation for coated woven fabrics, Computers & Structures 82 (23–26) (2004) 1913–1927. doi:10.1016/j.compstruc.2003.07.005.

[4] K.-U. Bletzinger, J. Linhard, R. Wüchner, EXTENDED AND INTEGRATED NUMERICAL FORM FINDING AND PATTERNING OF MEMBRANE STRUCTURES, Journal of the International Association for Shell and Spatial Structures 50 (1) (2009) 35–49.

[5] K.-U. Bletzinger, Shape optimization by homotopy methods with special application to membrane structures, in: 6th Symposium on Multidisciplinary Analysis and Optimization, American Institute of Aeronautics and Astronautics, 1996.

[6] D. M. Campbell, The unique role of computing in the design and construction of tensile membrane structures, in: American Society of Civil Engineers Second Civil Engineering Automation Conference, 1991.

[7] J. B. Pargana, D. Lloyd-Smith, B. A. Izzuddin, Advanced material model for coated fabrics used in tensioned fabric structures, Engineering Structures 29 (7) (2007) 1323–1336. doi:10.1016/j.engstruct.2006.09.001.

[8] P. Gosling, B. Bridgens, A. Albrecht, H. Alpermann, A. Angeleri, M. Barnes, N. Bartle, R. Canobbio, F. Dieringer, S. Gellin, W. Lewis, N. Mageau, R. Mahadevan, J.-M. Marion, P. Marsden, E. Milligan, Y. Phang, K. Sahlin, B. Stimpfle, O. Suire, J. Uhlemann, Analysis and design of membrane structures: Results of a round robin exercise, Engineering Structures 48 (2013) 313–328. doi:10.1016/j.engstruct.2012.10.008.

[9] F. Masahisa, K. Osamu, F. Seiichiro, Analysis of fabric tension structures, Computers & Structures 32 (3) (1989) 537–547.

[10] R. B. Haber, J. F. Abel, D. P. Greenberg, An integrated design system for cable reinforced membranes using interactive computer graphics, Computers & Structures 14 (3–4) (1981) 261–280. doi:10.1016/0045-7949(81)90012-2.

[11] D. Veenendaal, P. Block, An overview and comparison of structural form finding methods for general networks, International Journal of Solids and Structures 49 (26) (2012) 3741–3753. doi:10.1016/j.ijsolstr.2012.08.008.

[12] J. B. Pargana, D. Lloyd-Smith, B. A. Izzuddin, Fully integrated design and analysis of Tensioned Fabric Structures: Finite elements and case studies, Engineering Structures 32 (4) (2010) 1054–1068. doi:10.1016/j.engstruct.2009.12.032.

[13] T. D. Dinh, A. Rezaei, L. De Laet, M. Mollaert, D. Van Hemelrijck, W. Van Paepegem, A new elasto-plastic material model for coated fabric, Engineering Structures 71 (2014) 222–233. doi:10.1016/j.engstruct.2014.04.027.

[14] Z. Yingying, Z. Qilin, L. Ke, K. Bei-lei, Experimental analysis of tensile behaviors of polytetrafluoroethylene-coated fabrics subjected to monotonous and cyclic loading, Textile Research Journal 84 (3) (2014) 231–245. doi:10.1177/0040517513494259.

[15] T. D. Dinh, A. Rezaei, S. Puystiens, M. Van Craenenbroeck, K. Carbonez, L. De Laet, M. Mollaert, D. Van Hemelrijck, W. Van Paepegem, A study of tension fabric membrane structures under in-plane loading: Nonlinear finite element analysis and validation, Composite Structures 128 (2015) 10–20. doi:10.1016/j.compstruct.2015.03.055.

[16] T. Dinh, A. Rezaei, W. Punurai, L. De Laet, M. Mollaert, D. Van Hemelrijck, W. Van Paepegem, A shape optimization approach to integrated design and nonlinear analysis of tensioned fabric membrane structures with boundary cables, International Journal of Solids and Structures 83 (2016) 114–125. doi:10.1016/j.ijsolstr.2016.01.004.

[17] T. Nouri-Baranger, Computational methods for tension-loaded structures, Archives of Computational Methods in Engineering 11 (2) (2004) 143–186. doi:10.1007/BF02905937.

Chapter 2

An Elasto-plastic Material Model for Coated Fabrics

One of the contemporary issues in the research field of tension fabric membrane structures is to find an adequate material model for coated fabrics that not only can capture the complicated mechanical behavior of coated fabrics, but also has a good performance in computation. This chapter presents an elasto-plastic model that can capture quite well the nonlinear behavior of coated fabrics and shows a good performance in computation. This material constitutive model is referred to as fabric elasto-plastic model in subsequent chapters of this dissertation. The results of this chapter were published in [1].

2.1 Introduction

Coated fabrics are generally composed of a base fabric and a coating. There are several types of coated fabric used in the tension membrane structures. Among them, the PVC coated fabric is very popular because it is flexible to fold and unfold, which is a very important consideration for temporary structures. In addition, designers find the PVC coated fabric an economic solution because of its reasonable price compared with other types of coated fabric, such as Teflon coated fabric, Silicone coated fabric and PTFE coated fabric [2].

Design of tension membrane structures is a challenging task due to the complicated mechanical response of coated fabrics under biaxial tension

loads in which coated fabrics exhibit a severely nonlinear relation between strain and stress, orthotropic nature, irreversible strains, load ratio and load history dependence [3]. Some material models have been proposed for coated fabrics, however, many parameters are involved and demand high computational resources, which prevent them from being widely used in realistic applications [4]. At the moment, only linear elastic models are mostly used for the numerical simulation of coated fabrics. Due to this oversimplified assumption, the safety factor in the design stage for fabric membrane is very high, ranging from 5 to 10 [5]. From the aforementioned problems, it is feasible to demand a material model that is not only sophisticated enough to capture the salient features of coated fabrics, but is also computationally inexpensive.

This chapter is commenced by briefly introducing the material behavior as well as the deformation mechanisms of the PVC coated fabric under tension load. A literature review is conducted to give an overview of what has been done on material constitutive models for coated fabrics. From that we can gain a better understanding about the pros and cons of the existing models. The experiments that were carried out in uniaxial and biaxial loading are then presented. Subsequently, the proposed model is developed. This is followed by verification and validation with the experimental data in uniaxial tests and biaxial tests, respectively.

2.2 Material behavior

The material in this study is a coated fabric that consists of woven polyester fibers and PVC coating (*cf.* figs. 2.1 and 2.2). The woven fabric is composed by two orthogonal yarn families, *viz.*, warp and fill. Due to the weaving method, the yarns are not straight and this waviness is referred to as crimp in the literature [6]. Moreover, the crimp levels in the warp and fill directions are not identical. As a result, the behavior of the coated fabric in the warp and fill directions is remarkably different. Applying an external load in the warp direction reduces the crimp in this direction but simultaneously increases the crimp in the fill direction and vice versa. In other words, the crimp in the warp and fill yarns remain complementary and this effect is called crimp interchange [6]. According to Pargana et al. [3], crimp interchange together with the interaction between yarn filaments as well as between yarns and coating cause severe nonlinearities in the behavior of coated fabrics. Moreover, the above interaction

leads to permanent strains in the macroscopic behavior after the fabric is subjected to the first loading cycle [3].

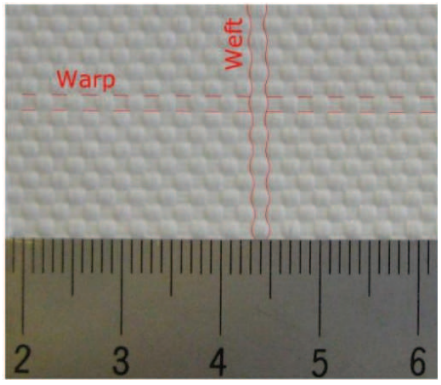

Figure 2.1: The PVC coated fabric that is used in this work.

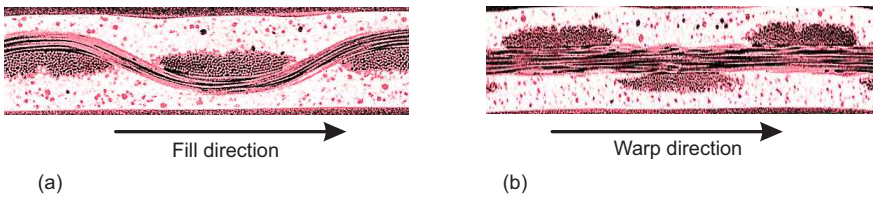

Figure 2.2: Microscopic images of the coated fabric. (a) Cross section in the warp direction and (b) cross section in the fill direction.

2.3 Material constitutive models for coated fabrics

Several methods have been used for coated fabrics modeling in which there are two main approaches. In the first one, the yarns and coating are substituted by an equivalent mechanical system [3, 7–11] (*cf.* fig. 2.3). In general, models in this approach can be distinguished by their geometric complexity and element constitutive properties [9]. Although the models in this group can capture the behavior of coated fabric well, there are too many parameters involved in the models and they demand too much time in computation, which prevents them from practical use in tension membrane structures design. In the second approach, the behavior of coated

fabric is directly modeled from experimental data by using multi-linear methods and response surfaces [2, 6, 12–15]. To apply this approach, it is necessary to conduct many experiments and the models cannot reflect the permanent strains as well as load history dependence in the behavior of coated fabrics.

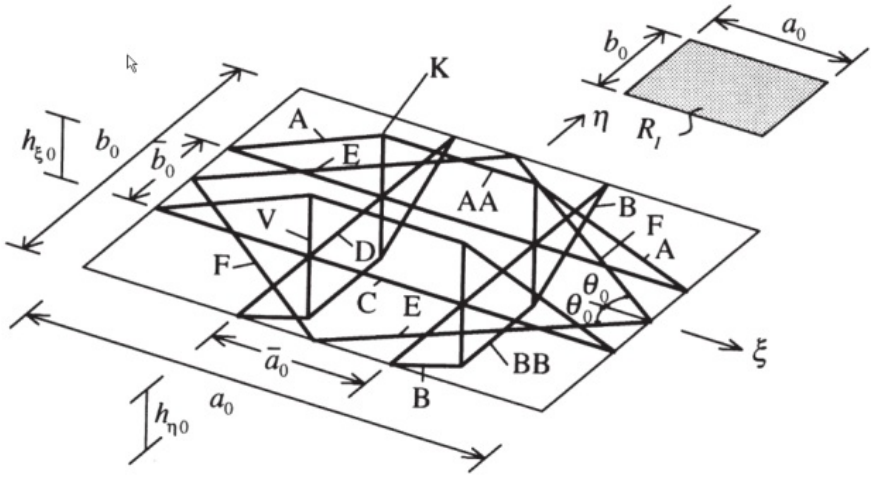

Figure 2.3: Equivalent mechanical system is used to substitute for the fabric yarns and the coating (reprinted from [11]).

In the pioneering work in fabric research, Peirce proposed a geometrical for dry fabrics in which the cross section of the fabric yarn is assumed to be a circle [7]. That model was then further developed in the work of Kawabata et al. [8] when these authors substituted the yarns by a truss system. The first model for coated fabric was proposed by Testa et al. [6], in which the authors also used the geometry proposed by Peirce, but included a linear elastic isotropic coating membrane. In that study, the considered geometry was a square coated fabric and the constitutive law was built from the in-plane strains of coating membrane, yarn strains and crimp. However, the validation for their mathematical model was not presented. In all studies cited hitherto, anisotropic and nonlinear properties of coated fabrics have been studied, but some peculiarities have not been considered yet, such as sudden changes in gradient of fabric loading response. It was only in 1984 that Thomas and Stubbs [16] extended the works of Testa et al. [6] and Stubbs and Thomas [10] by including material inelasticity caused by plastic deformation in the yarn-coating system. Moreover, a systematic method of evaluating model

parameters was also outlined. In the work of Kato et al. [11], the authors proposed a new formulation for continuum constitutive equations based on a fabric lattice model in which the material nonlinearities of yarns and coatings as well as crimp interchange were taken into account. While the trusses representing the yarns were only active in tension, the counterparts for coating were active in both tension and compression. That work was considered as a milestone in the field of coated fabric modeling because of its precision when verified by experimental data, however, that model is too complex for practical application [3]. The most advanced model in this approach is the one proposed by Pargana et al. [3]. In this model the yarn was composed by a system of nonlinear elastic elements, frictional elements and rigid links. In addition, an isotropic plate was used to model the coating. The model was then calibrated and verified by the experimental data obtained from the work of Kato et al. [11]. A good agreement between numerical simulations and experiments was observed. Especially, there were very good agreements in case the load ratios are equal to (2:1) and (1:2). These load ratios are frequently met in design and construction of tension membrane structures, that model is thus promising for practical use. Moreover, in that paper the authors also conducted the parameter sensitivity analysis; from the results they concluded that it would be possible to reduce some degrees of freedom in the model to improve the computational performance. Nevertheless, in that model thirty five elements are involved, they can lead to a high demand in computation. Recently, in [17] the authors have reduced the number of elements in that model, but there are still 60 parameters involved in their new model. Moreover, that new model and the one presented earlier in [3] can only predict the behavior of the coated fabric well in the elastic regime, but they are unable to capture the irreversible deformation.

Additionally, there have been many attempts to model behavior of coated fabrics directly from experimental data. One of the first works in this approach is the method suggested by Testa and Yu [13]. In that work, the authors considered the mechanical response of Teflon and Silicone coated fabric that exhibit nonlinear and orthotropic nature. In addition, Teflon fabric shows inelastic behavior due to crimp interchange. More specifically, in that work the authors assumed that the crimp strains depend on the load ratio α, load level r and load history. They also used empirical formulas to calculate the crimp strain when either the load ratio or load level varies. From these formulas, a parametric study was conducted. By keeping the load level constant and increasing the load ratio, the natural

crimp states were formed. From these states, if the load ratio changes, the unnatural states will appear; this causes the path dependence of the fabric response. Due to this nature, it is necessary to choose a standard reference state from which the crimp strain is measured. In that paper, the authors chose the loading state in a uniaxial test $(\alpha = \infty, r = 1)$ as reference state. From that state, a complementary set of natural crimp states can be derived by changing the load ratio. From these sets and an increment in load $(\Delta\alpha, \Delta r)$, the crimp strain can be calculated. Nevertheless, when validating this model with experimental data, the discrepancies are quite visible.

In the work of Bridgens and Gosling [12], two methods for representing the fabric response surface were proposed. While in the first method, spline functions were used, stress-strain mean and difference functions were used in the second one. With those methods, the direct correlation between stress-strain was provided without the plane stress assumption. More specifically, in that paper the authors showed some disadvantages of the methods in which the polynomial functions were used to represent the response surface. Due to salient deformation mechanisms of coated fabrics, their response surface must be characterized by sudden changes in gradient, gradient reversal and negative strain [12]. These characteristics cannot be captured by polynomial functions, but can be represented by using non-uniform rational B-splines (NURBS). Especially, the authors mentioned that discontinuities can appear in behavior of coated fabrics and NURBS is an ideal tool to deal with this issue. The obtained results were in good agreement with experimental data in which the crimp interchange was taken into account. However, inelastic behavior was excluded in that work.

Minami [15] suggested another method in which coated fabric was considered to be linear elastic and orthotropic, but its elasticity constants can be changed when load ratios change. Biaxial elongation property surfaces were drawn by using the stress-strain curves obtained from biaxial tests with stress ratios (1:0), (2:1), (1:1), (1:2) and (0:1). The surface was then divided into quadrilaterals and triangles. Elastic constants within each quadrilateral or triangles were subsequently determined by using a least square method. That model can be implemented in a nonlinear FEA code by storing the elastic constants that correspond to a certain load ratio. The method was validated by using an in-plane biaxial tension test under stress ratio (1:1) and another model in which the coated fabric was subjected to air pressure and had out-of-plane deformation. The obtained

results showed excellent agreement with experimental data. However, the shortcomings of that method are that it cannot take into account the time-dependent and load history dependent effects.

Similar to the above approach of response surfaces, Galliot and Luchsinger [2] assumed that the behavior of PVC-coated fabric in plane stress is orthotropic elastic for a particular load ratio, but the elastic properties can vary with load ratio in order to represent the complex interaction between warp and fill yarns. Apart from the response surface method, the authors found that the Young's moduli of warp and fill yarns can be formulated as a linear function of load ratio and the model needs five parameters in calibration. Therefore, that model has a very good numerical performance. However, it assumed linear orthotropic elasticity in a certain load ratio. As a result, that model cannot capture the nonlinear behavior of coated fabrics in the first load cycle as well as the permanent strains.

2.4 Experiments

Since the material properties of a coated fabric are highly dependent on the weaving method and the type of coating, it is essential to conduct experiments to investigate the response of the PVC coated fabrics under loading conditions [18] and later to use them to assess the validity of the proposed material model. Uniaxial and biaxial tensile tests (*cf.* fig. 2.4) are two types of test that have been widely used in fabric research. Moreover, shear tests are also conducted in this work. In this study, *the experimental*

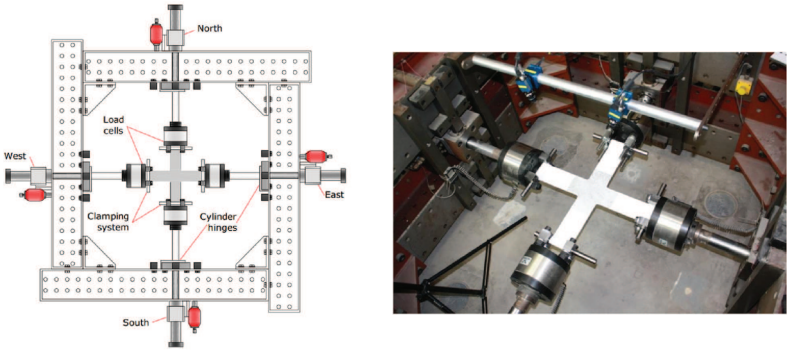

Figure 2.4: Experimental set-up for the biaxial tests [19, 20].

tests were carried out at the department Mechanics of Materials and Constructions at the Vrije Universiteit Brussel [19, 20]. The PVC coated fabric used in this study has a thickness of 0.83 mm and a surface mass density of 1050 $\mathrm{g/m^2}$. In the warp direction, the density of reinforcement is 12 $\mathrm{yarns/cm}$ and 13 $\mathrm{yarns/cm}$ in the fill direction. During the course of the experiments, strains are measured by means of a digital image correlation device (DIC). This is an experimental technique that offers the possibility to determine displacement and deformation fields at the surface of objects, based on a comparison between images taken at different load steps. Two cameras were used in order to measure both in-plane and out-of-plane displacements. In this section, descriptions for these tests as well as the post-processed experimental results are presented and discussed.

2.4.1 Uniaxial tensile tests

In this test, the specimen has a rectangular shape with the width of 50 mm, the length of 200 mm and is cut out along the warp and fill directions. Two types of experiments were performed.

- The load is continuously increased until 24.1 MPa. This value is equal to 25% of the ultimate tensile strength (UTS) of the considered coated fabric. Subsequently, the loading and unloading cycle is applied in which the load is varied between a pre-load of 2.41 MPa and a maximum load of 24.1 MPa.
- Similar to the first experiment, cyclic load is also applied, but this time the load is commenced with a loading cycle in which the maximum load is equal to 200 N. By dividing this value by the cross sectional area of the membrane $(50\mathrm{mm} \times 0.83\mathrm{mm})$, the effective stress is equal to 4.82 MPa. In subsequent cycles, the maximum load is increasing by 200 N, until a maximum load of 1400 N (its corresponding stress is equal to 33.73 MPa) is reached. By doing that, both the initial and stabilized behavior are determined [2].

The relations between strains and stresses in the warp and fill directions in the first and second types of experiment are shown in figs. 2.5 and 2.6, respectively. As can be seen from these graphs, on the contrary to the warp direction, large initial strains are observed in the fill direction during the uniaxial tests, which are related to the straightening of the fibers. During the weaving process, the yarns in the warp direction are kept in

tension, while the yarns in the fill direction have relatively large waviness. Moreover, permanent strains are observed when exceeding the yield stresses of 15 MPa and 5 MPa in the warp and fill directions, respectively [21].

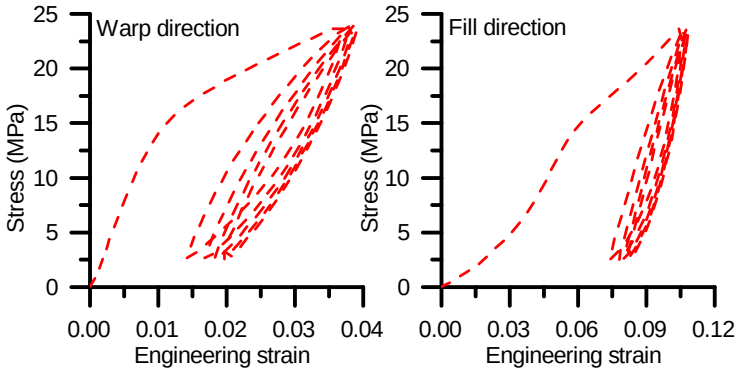

Figure 2.5: The stress-strain curves obtained from the uniaxial tests in the warp and fill directions in case of continuously increasing load until 25% UTS of the coated fabric [19, 20].

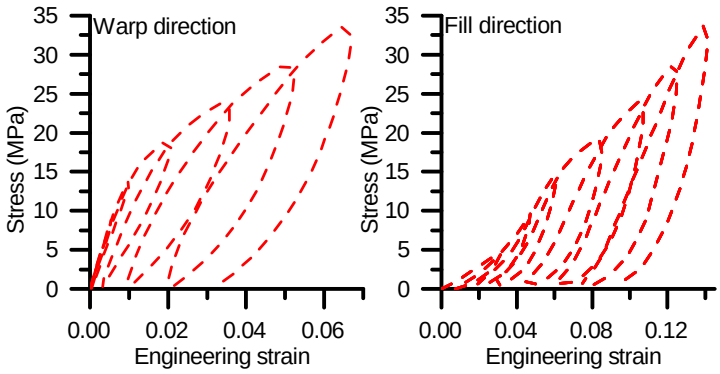

Figure 2.6: The stress-strain curves obtained from the uniaxial tests in the warp and fill directions in case of cyclic load [19, 20].

2.4.2 Biaxial tensile tests

As mentioned in section 2.2, the interaction between yarns affects significantly the mechanical behavior of coated fabric. Consequently, biaxial tests are essential to capture this effect. In this study, the behavior of the coated fabric under biaxial stress state is investigated with a cruciform sample (*cf.* fig. 2.7). This method is widely used to study the behavior of coated fabrics [20, 22, 23]. The biaxial experiments were performed with repetition of load cycles, to explore both the initial and the stabilized behavior of the coated fabric, at limited load levels. During the course of experiments, the applied load and the elongation are recorded at the arms of the biaxial testing device, while the strains in the center of the cruciform are determined by means of DIC. The stresses are subsequently calculated by dividing the applied load by the cross section in the arms. Therefore, the stress-strain curves showed in fig. 2.8 do not represent the true stress at the center of the sample, but the applied stress at the arms. In fig. 2.8, the results of the biaxial tests are shown in which each time 3 cycles of the sequencing load ratios (1:1), (2:1), (1:2), (1:0) and (0:1) with a maximum stress of $\sigma_{\max} = 24.1$ MPa are performed. From these results, it can be seen that coated fabric exhibits different slopes in the stress-strain curves for each load ratio. In addition, when passing on to a next load ratio, a small increase of permanent strains is observed.

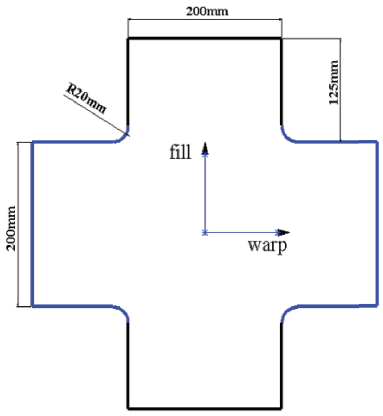

Figure 2.7: Geometry of the cruciform used in the biaxial tests [19, 20].

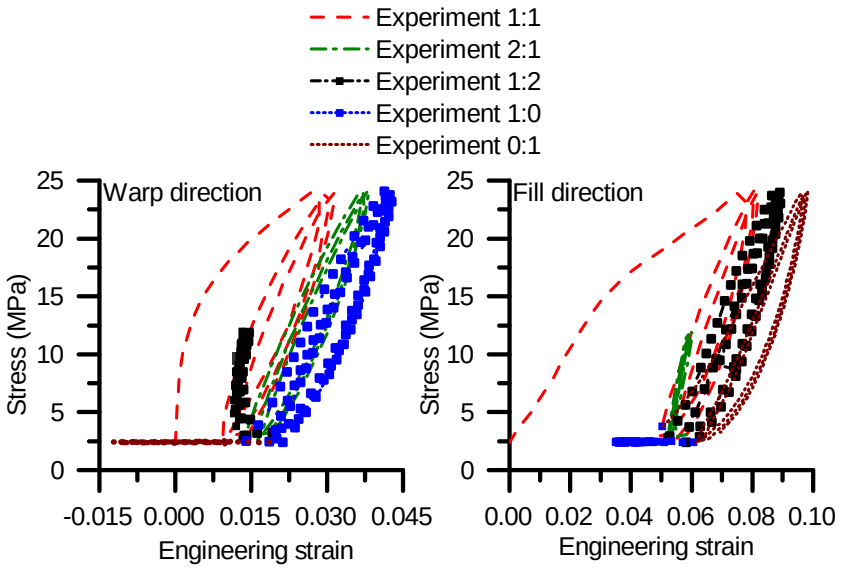

Figure 2.8: The stress-strain curves obtained from the biaxial tests with successive load ratios 1:1, 2:1, 1:2, 1:0 and 0:1. For each load ratio, the load cycle was repeated three times [19, 20].

2.4.3 Uniaxial bias extension test

In tension membrane structures, the shear behavior is important because it can affect the stress distribution in the membrane as well as the final shape of the structure [24]. In this study, uniaxial bias extension tests were performed to characterize the shear behavior. The specimen used in this test had the same size as the one used in the uniaxial tests, but this time the fabric was cut at 45° with respect to the warp fiber directions. Six loading and unloading cycles were applied with a maximum load of 550 N corresponding to a stress of 13.25 MPa in the loading direction. During the course of the experiment, the strain and stress in the loading direction were measured and plotted in fig. 2.9. As can be seen from the figure, the stress-strain curve is similar to the corresponding curves for the uniaxial tests in the warp and fill directions, however, in this case the permanent strain is higher and the low stiffness zone is larger. To convert the stress-strain curve presented in fig. 2.9 into a shear stress-shear angle curve, *i.e.*, the constitutive shear properties of the coated fabric, the method proposed in [25] is used. For the sake of completeness, that method is

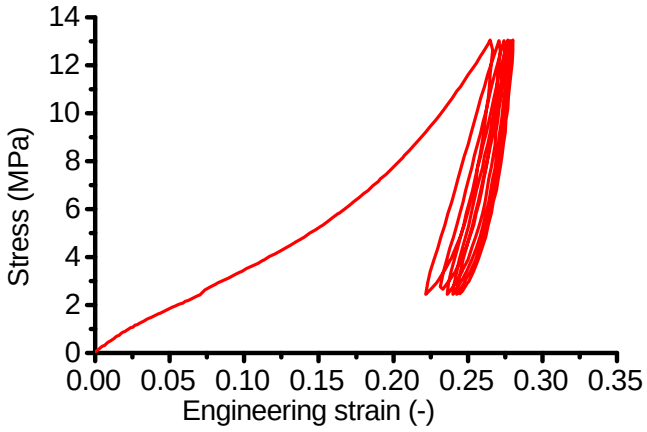

Figure 2.9: The stress strain curve obtained from the uniaxial bias extension test [19, 20].

also presented here. Considering the deformed coated fabric specimen in fig. 2.10, it is supposed that there are three different distinct regions, *viz.*, region A exhibits pure shear, region B has very little or almost no shear and region C exhibits partial shear. The shear angles are measured from the region A as follows:

- In the initial configuration fig. 2.10(b)

$$x = 2a\cos(\pi/4), \tag{2.1}$$

- In the deformed configuration fig. 2.10(c)

$$x + \delta x = 2a\cos(\alpha). \tag{2.2}$$

Therefore,

$$\frac{x + \delta x}{x} = (1 + \epsilon) = \frac{\cos\alpha}{\cos(\pi/4)}, \tag{2.3}$$

where ϵ is the strain in the loading direction. In addition, by reasoning that the region B has no contribution to shear, a corrected shear strain ϵ^c is calculated as follows:

$$\epsilon^c = \epsilon\frac{l_0}{l_0 - w_0}, \tag{2.4}$$

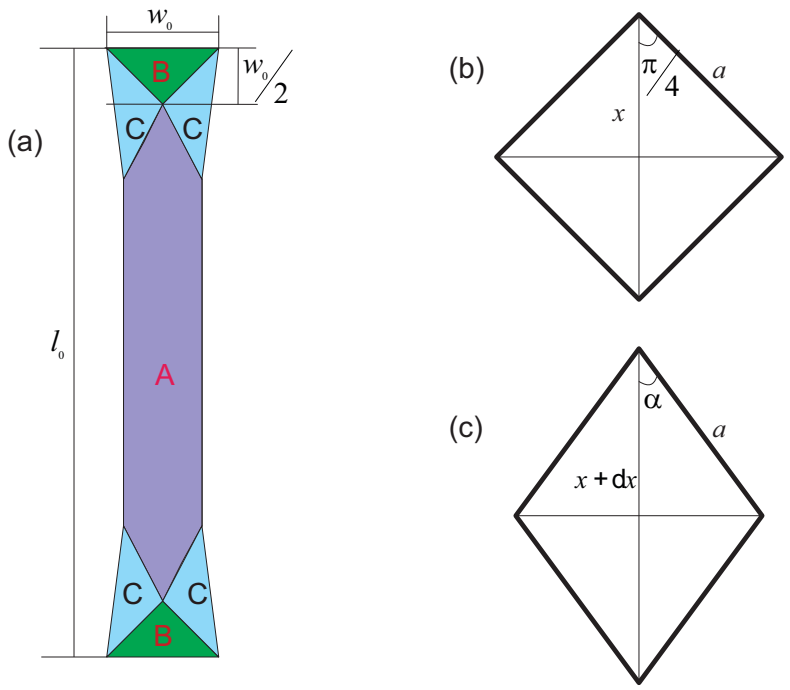

Figure 2.10: Illustration of the coated fabric under shear load: (a) different shear zones, (b) the initial configuration of zone A and (c) the deformed configuration of zone A.

where l_0 and w_0 are respectively the initial length and width of the coated fabric specimen. The shear angle θ is then calculated as:

$$\alpha = \cos^{-1}[(1+\epsilon^c)\cos(\frac{\pi}{4})];\ \theta = 90^\circ - 2\alpha. \tag{2.5}$$

Moreover, the shear stress τ is related to the stress σ in the loading direction as follows:

$$\tau = \frac{\sigma}{2 \cdot \cos(\alpha)}. \tag{2.6}$$

The converted shear stress-shear angle curve is plotted in fig. 2.11. Nevertheless, as shown in [25] the aforementioned calculation is only valid in the small strain regime when the shear angle is up to ca. 15°.

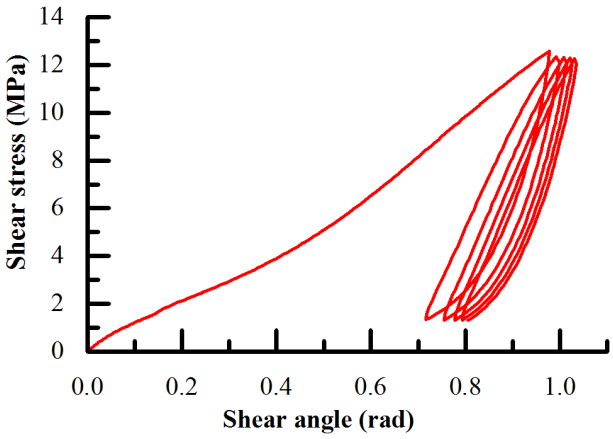

Figure 2.11: The shear stress- shear strain curve obtained from the uniaxial bias extension test.

2.5 Proposed material model for the PVC coated fabric

In this section, w and f are used to designate the warp and fill directions, respectively. Based on the obtained results from the uniaxial tensile tests, the linear hardening elasto-plastic models are separately proposed for the warp and fill directions (*cf.* fig. 2.12). In the warp direction, the relation between stress and strain is linear with the Young′s modulus E_{w1} when the stress in the warp direction is smaller than the yield stress. Once the yield stress $\sigma_{\mathrm{y}}^{\mathrm{w}}$ is reached the linear hardening occurs with plastic modulus H_{w}. Subsequently, if the coated fabric is unloaded, the relation between stress and strain is linear with the Young′s modulus E_{w3}, which is different from E_{w1}. A similar strategy is applied in the fill direction, but in this case, the relation between the stress and strain is nonlinear in the elastic regime. For the plastic regime, the piecewise linear hardening law governs the relation between stress and strain with different plastic moduli H_{f1} and H_{f2}, respectively. For unloading, the linear law is assumed with Young′s modulus E_{f4}. The material parameters mentioned by now are defined from the uniaxial tests. The interaction between warp and fill yarns is taken into account by means of two Poisson′s ratios ν_{12}

and ν_{21}, respectively. In addition, to capture the load ratio dependent characteristic of the coated fabric, $E_{\mathrm{w}4}$ and $E_{\mathrm{f}5}$ are introduced when the coated fabric passes on to the next load ratio and it is in loading stage. These parameters are identified from biaxial tests. The following is the definition of the proposed constitutive model for coated fabrics, *i.e.*, fabric plasticity model.

2.5.1 Orthotropic elasticity

In theory of plasticity, the strain can be decomposed into, *viz.*, elastic strain or recoverable strain and plastic strain or irreversible strain as follows:

$$\boldsymbol{\epsilon} = \boldsymbol{\epsilon}^{\mathrm{e}} + \boldsymbol{\epsilon}^{\mathrm{p}} \tag{2.7}$$

where $\boldsymbol{\epsilon} = [\epsilon^{\mathrm{w}}\ \epsilon^{\mathrm{f}}\ \epsilon^{\mathrm{wf}}]^T$ is the strain vector, $\boldsymbol{\epsilon}^{\mathrm{e}}$ is the elastic strain and $\boldsymbol{\epsilon}^{\mathrm{p}}$ is the plastic strain vector in case of plane stress.

The relation between the stress vector $\boldsymbol{\sigma}$ and the strain vectors is as follows:

$$\boldsymbol{\sigma} = \boldsymbol{K}\boldsymbol{\epsilon}^{\mathrm{e}} = \boldsymbol{K}(\boldsymbol{\epsilon} - \boldsymbol{\epsilon}^{\mathrm{p}}) \tag{2.8}$$

where $\boldsymbol{\sigma} = [\sigma^{\mathrm{w}}\ \sigma^{\mathrm{f}}\ \sigma^{\mathrm{wf}}]^T$ is the stress vector and $\boldsymbol{K}$ is the orthotropic stiffness matrix. This matrix can be defined as:

$$\boldsymbol{K} = \begin{bmatrix} \frac{E_{\mathrm{w}}}{1-\nu_{12}\nu_{21}} & \frac{E_{\mathrm{w}}\nu_{12}}{1-\nu_{12}\nu_{21}} & 0 \\ \frac{E_{\mathrm{f}}\nu_{21}}{1-\nu_{12}\nu_{21}} & \frac{E_{\mathrm{f}}}{1-\nu_{12}\nu_{21}} & 0 \\ 0 & 0 & G \end{bmatrix} \tag{2.9}$$

where E_{w} and E_{f} denote the Young′s moduli in the warp and fill directions, respectively and G is the shear stiffness.

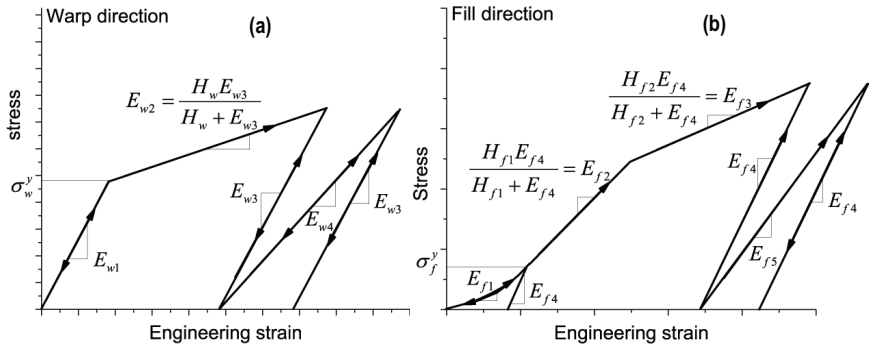

Figure 2.12: Hypothesis in the proposed model: (a) In the warp direction and (b) in the fill direction.

2.5.2 Yield functions

To check if the material is in the plastic regime, it is necessary to define the yield function. In this study, two different yield functions are respectively defined for the warp and fill directions.

$$f^{\mathrm{w}} = \sigma^{\mathrm{w}} - (\sigma_{\mathrm{y}}^{\mathrm{w}} + r_{\mathrm{n}}^{\mathrm{w}}), \tag{2.10}$$

$$f^{\mathrm{f}} = \sigma^{\mathrm{f}} - (\sigma_{\mathrm{y}}^{\mathrm{f}} + r_{\mathrm{n}}^{\mathrm{f}}). \tag{2.11}$$

Herein, f^{w} and f^{f} are the yield functions, σ^{w} and σ^{f} are the stresses that can be calculated from the strains in the warp and fill direction from eq. (2.8)[1], $\sigma_{\mathrm{y}}^{\mathrm{w}}$ and $\sigma_{\mathrm{y}}^{\mathrm{f}}$ are the yield stresses. r^{w} and r^{f} are the hardening terms and defined as follows:

$$r^{\mathrm{w}} = H_{\mathrm{w}} \epsilon^{\mathrm{p,w}}, \tag{2.12}$$

$$r^{\mathrm{f}} = H_{\mathrm{f}} \epsilon^{\mathrm{p,f}}, \tag{2.13}$$

where $\epsilon^{\mathrm{p,w}}$, $\epsilon^{\mathrm{p,f}}$ are the accumulated plastic strains and H_{w}, H_{f} are respectively the plastic moduli in the warp and fill directions.

Once the material is in the plasticity regime and the loading applied on it still continues to increase, the plastic increments in the warp and fill

1. From eq. (2.8), it can be seen that the mechanical behavior of the model in the warp and fill directions are indeed coupled. Therefore, the strain in the fill direction will also contribute to the yield function in the warp direction (*cf.* eq. (2.10)) and the strain in the warp direction will equally contribute to the yield function in the fill direction (*cf.* eq. (2.11))

directions can be obtained based on the normality hypothesis of plasticity [26] as follows:

$$\dot{\epsilon}^{\mathrm{p,w}} = \dot{\gamma}^{\mathrm{w}} \frac{\partial f^{\mathrm{w}}}{\partial \sigma^{\mathrm{w}}} = \dot{\gamma}^{\mathrm{w}} \mathrm{sign}(\sigma^{\mathrm{w}}), \tag{2.14}$$

$$\dot{\epsilon}^{\mathrm{p,f}} = \dot{\gamma}^{\mathrm{f}} \frac{\partial f^{\mathrm{f}}}{\partial \sigma^{\mathrm{f}}} = \dot{\gamma}^{\mathrm{f}} \mathrm{sign}(\sigma^{\mathrm{f}}). \tag{2.15}$$

The sign function is defined by

$$\mathrm{sign}(\sigma) = \begin{cases} +1 & \text{if } \sigma > 0 \\ -1 & \text{if } \sigma < 0 \end{cases} \tag{2.16}$$

and $\dot{\gamma}^{\mathrm{w}}$ and $\dot{\gamma}^{\mathrm{f}}$ represent the time derivative of the plastic multipliers. These multipliers have to be consistent with the classical loading/unloading conditions, *i.e.*, Kuhn-Tucker complementary conditions.

$$\dot{\gamma}^{\mathrm{w}} \geq 0, \quad f^{\mathrm{w}} \leq 0, \quad \dot{\gamma}^{\mathrm{w}} f^{\mathrm{w}} = 0, \tag{2.17}$$

$$\dot{\gamma}^{\mathrm{f}} \geq 0, \quad f^{\mathrm{f}} \leq 0, \quad \dot{\gamma}^{\mathrm{f}} f^{\mathrm{f}} = 0. \tag{2.18}$$

2.5.3 Integration algorithm

The fabric plasticity model is implemented in ABAQUS software by using the implicit return mapping method [26]. For convenience in implementation into the software, the model is presented in incremental form in the following subsections.

I. Elastic step

In this step, it is assumed that the material is in elastic regime and stresses are determined from strain increments by using plane stress formulas.

$$\sigma^{\mathrm{w,trial}}_{\mathrm{n+1}} = \sigma^{\mathrm{w}}_{\mathrm{n}} + k_{11}\Delta\epsilon^{\mathrm{w}}_{\mathrm{n+1}} + k_{12}\Delta\epsilon^{\mathrm{f}}_{\mathrm{n+1}}, \tag{2.19}$$

$$\sigma^{\mathrm{f,trial}}_{\mathrm{n+1}} = \sigma^{\mathrm{f}}_{\mathrm{n}} + k_{21}\Delta\epsilon^{\mathrm{w}}_{\mathrm{n+1}} + k_{22}\Delta\epsilon^{\mathrm{f}}_{\mathrm{n+1}}, \tag{2.20}$$

where $\sigma^{\mathrm{w}}_{\mathrm{n}}$, $\sigma^{\mathrm{f}}_{\mathrm{n}}$ are the stresses in the time step n, $\sigma^{\mathrm{w,trial}}_{\mathrm{n+1}}$, $\sigma^{\mathrm{f,trial}}_{\mathrm{n+1}}$ and $\Delta\epsilon^{\mathrm{w}}_{\mathrm{n+1}}$, $\Delta\epsilon^{\mathrm{f}}_{\mathrm{n+1}}$ are the trial stresses and the strain increments in the time step $\mathrm{n}+1$, respectively. k_{11}, k_{12}, k_{21}, k_{22} are the components in the stiffness

matrix $\boldsymbol{K}$ in eq. (2.9). For the sake of clarity, their formulas are repeated here as follows:

$$k_{11} = E_{\mathrm{w}}/(1-\nu_{12}\nu_{21}), \tag{2.21}$$
$$k_{12} = E_{\mathrm{w}}\nu_{12}/(1-\nu_{12}\nu_{21}), \tag{2.22}$$
$$k_{21} = E_{\mathrm{f}}\nu_{21}/(1-\nu_{12}\nu_{21}), \tag{2.23}$$
$$k_{22} = E_{\mathrm{f}}/(1-\nu_{12}\nu_{21}), \tag{2.24}$$

where E_{w} and E_{f} denote the Young′s moduli in the warp and fill directions, respectively. Moreover, to capture the stress ratio and stress history dependent characteristics of the coated fabric, the stress level $\alpha_{\mathrm{i}}(\mathrm{i}=\mathrm{w},\mathrm{f})$ and stress ratio β are introduced and defined as follows:

$$\alpha_{\mathrm{w}} = \sigma_{\mathrm{w}}/\sigma_{\mathrm{w}}^{\max}, \tag{2.25}$$
$$\alpha_{\mathrm{f}} = \sigma_{\mathrm{f}}/\sigma_{\mathrm{f}}^{\max}, \tag{2.26}$$
$$\beta = \sigma_{\mathrm{w}}/\sqrt{\sigma_{\mathrm{w}}^2+\sigma_{\mathrm{f}}^2}. \tag{2.27}$$

Herein $\sigma_{\mathrm{i}}^{\max}(\mathrm{i}=\mathrm{w},\mathrm{f})$ is respectively the maximum stress in the warp and fill directions that the material experienced in the first load cycle.

In case β is kept constant and once the stress level $\alpha_{\mathrm{i}}(\mathrm{i}=\mathrm{w},\mathrm{f})$ gets the value of 1, it will maintain this value. The Young′s moduli in the warp and fill directions are defined as follows:

$$E_{\mathrm{w}} = \begin{cases} E_{\mathrm{w1}}, & \text{if } \sigma_{\mathrm{w}} < \sigma_{\mathrm{w}}^{\mathrm{y}} \\ E_{\mathrm{w3}}, & \text{otherwise} \end{cases} \tag{2.28}$$

$$E_{\mathrm{f}} = \begin{cases} E_{\mathrm{f1}}, & \text{if } \sigma_{\mathrm{f}} < \sigma_{\mathrm{f}}^{\mathrm{y}} \\ E_{\mathrm{f4}}, & \text{otherwise} \end{cases} \tag{2.29}$$

where $\sigma_{\mathrm{w}}^{\mathrm{y}}$ and $\sigma_{\mathrm{f}}^{\mathrm{y}}$ are the yield stresses in the warp and fill directions, respectively.

In addition, if the material has been tensioned, the Young′s moduli in the warp and fill directions would be defined as follows (*cf.* fig. 2.13):

$$E_{\mathrm{w}} = E_{\mathrm{w4}}, \quad \alpha_{\mathrm{w}} < 1, \tag{2.30}$$
$$E_{\mathrm{f}} = E_{\mathrm{f5}}, \quad \alpha_{\mathrm{f}} < 1. \tag{2.31}$$

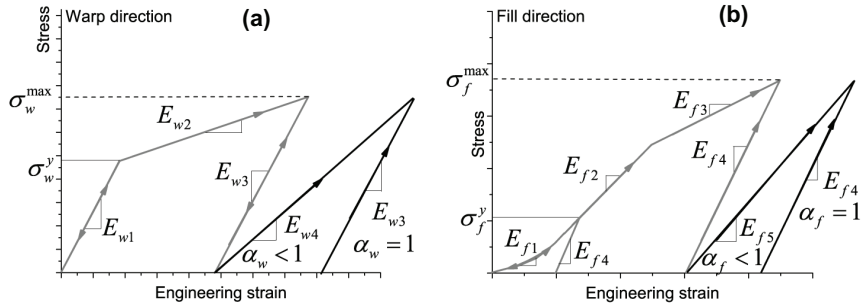

Figure 2.13: The behavior of the model after the first load cycle[2]: (a) In the warp direction and (b) in the fill direction.

II. Yield functions

The incremental forms of the yield functions can be expressed as follows:

$$f_{\mathrm{n+1}}^{\mathrm{w,trial}} = \sigma_{\mathrm{n+1}}^{\mathrm{w,trial}} - (\sigma_{\mathrm{y}}^{\mathrm{w}} + r_{\mathrm{n}}^{\mathrm{w}}), \tag{2.32}$$

$$f_{\mathrm{n+1}}^{\mathrm{f,trial}} = \sigma_{\mathrm{n+1}}^{\mathrm{f,trial}} - (\sigma_{\mathrm{y}}^{\mathrm{f}} + r_{\mathrm{n}}^{\mathrm{f}}). \tag{2.33}$$

Herein, $f_{\mathrm{n+1}}^{\mathrm{w,trial}}$ and $f_{\mathrm{n+1}}^{\mathrm{f,trial}}$ are the yield functions, $\sigma_{\mathrm{y}}^{\mathrm{w}}$ and $\sigma_{\mathrm{y}}^{\mathrm{f}}$ are the yield stresses. $r_{\mathrm{n}}^{\mathrm{w}}$ and $r_{\mathrm{n}}^{\mathrm{f}}$ are the hardening terms and defined as follows:

$$r_{\mathrm{n}}^{\mathrm{w}} = H_{\mathrm{w}}\epsilon^{\mathrm{p,w}}, \tag{2.34}$$

$$r_{\mathrm{n}}^{\mathrm{f}} = H_{\mathrm{f}}\epsilon^{\mathrm{p,f}}. \tag{2.35}$$

III. Return mapping

When the trial stress is outside the yield surface, the plastic correction is performed to bring it back to the yield surface. In this work, the return mapping algorithm in the plastic corrector step is used.

There are three cases that can occur:

- Plastic deformation only occurs in the warp direction

2. In case β is kept constant and once the stress level α_i (i=w, f) gets the value of 1, it will maintain this value.

Plastic strain increments can be calculated as follows:

$$\Delta\epsilon^{\mathrm{p,w}} = f_{\mathrm{n+1}}^{\mathrm{w,trial}}/(k_{11} + H_{\mathrm{w}}), \tag{2.36}$$

$$\Delta\epsilon^{\mathrm{p,f}} = 0. \tag{2.37}$$

Stresses are then updated as follows:

$$\sigma_{\mathrm{n+1}}^{\mathrm{w}} = \sigma_{\mathrm{n+1}}^{\mathrm{w,trial}} - k_{11}\Delta\epsilon_{\mathrm{n+1}}^{\mathrm{p,w}}, \tag{2.38}$$

$$\sigma_{\mathrm{n+1}}^{\mathrm{f}} = \sigma_{\mathrm{n+1}}^{\mathrm{f,trial}} - k_{21}\Delta\epsilon_{\mathrm{n+1}}^{\mathrm{p,w}}, \tag{2.39}$$

- Plastic deformation only occurs in the fill direction

  Plastic strain increments can be calculated as follows:

$$\Delta\epsilon^{\mathrm{p,w}} = 0, \tag{2.40}$$

$$\Delta\epsilon^{\mathrm{p,f}} = f_{\mathrm{n+1}}^{\mathrm{f,trial}}/(k_{22} + H_{\mathrm{f}}). \tag{2.41}$$

  Stresses are then updated as:

$$\sigma_{\mathrm{n+1}}^{\mathrm{w}} = \sigma_{\mathrm{n+1}}^{\mathrm{w,trial}} - k_{12}\Delta\epsilon_{\mathrm{n+1}}^{\mathrm{p,f}}, \tag{2.42}$$

$$\sigma_{\mathrm{n+1}}^{\mathrm{f}} = \sigma_{\mathrm{n+1}}^{\mathrm{f,trial}} - k_{22}\Delta\epsilon_{\mathrm{n+1}}^{\mathrm{p,f}}. \tag{2.43}$$

- Plastic deformation occurs in both the warp and fill directions

  By solving the following equations

$$\begin{cases} f_{\mathrm{n+1}}^{\mathrm{trial,w}} - (k_{11} + H_{\mathrm{w}})\Delta\epsilon^{\mathrm{p,w}} - k_{12}\Delta\epsilon^{\mathrm{p,f}} = 0, \\ f_{\mathrm{n+1}}^{\mathrm{trial,f}} - k_{21}\Delta\epsilon^{\mathrm{p,w}} - (k_{22} + H_{\mathrm{f}})\Delta\epsilon^{\mathrm{p,f}} = 0, \end{cases} \tag{2.44}$$

  plastic strain increments are obtained as:

$$\begin{cases} \Delta\epsilon^{\mathrm{p,w}} = \frac{-f_{\mathrm{n+1}}^{\mathrm{f,trial}}k_{12} + f_{\mathrm{n+1}}^{\mathrm{w,trial}}(k_{22}+H_{\mathrm{f}})}{(H_{\mathrm{f}}+k_{22})(H_{\mathrm{w}}+k_{11}) - k_{12}k_{21}}, \\ \Delta\epsilon^{\mathrm{p,f}} = \frac{-f_{\mathrm{n+1}}^{\mathrm{w,trial}}k_{21} + f_{\mathrm{n+1}}^{\mathrm{f,trial}}(k_{11}+H_{\mathrm{w}})}{(H_{\mathrm{w}}+k_{11})(H_{\mathrm{f}}+k_{22}) - k_{12}k_{21}}, \end{cases} \tag{2.45}$$

  Stresses are then updated as follows:

$$\sigma_{\mathrm{n+1}}^{\mathrm{w}} = \sigma_{\mathrm{n+1}}^{\mathrm{w,trial}} - k_{11}\Delta\epsilon^{\mathrm{p,w}} - k_{12}\Delta\epsilon^{\mathrm{p,f}}, \tag{2.46}$$

$$\sigma_{\mathrm{n+1}}^{\mathrm{f}} = \sigma_{\mathrm{n+1}}^{\mathrm{f,trial}} - k_{21}\Delta\epsilon^{\mathrm{p,w}} - k_{22}\Delta\epsilon^{\mathrm{p,f}}. \tag{2.47}$$

Moreover, in this model we assume that the shear behavior is linear and independent of the tensile behavior. By considering the data from the bias extension test within the small shear angle regime, a shear modulus of 11.5 MPa is deduced (*cf.* fig. 2.11). The implementation of the fabric plasticity model in ABAQUS is summarized in table 2.1.

Table 2.1: Algorithm for implementation of the fabric plasticity model for the PVC coated fabric.

(i) **Elastic step** (predictor step). Given $\Delta\epsilon$ and state variables at t_{n}

Calculate the trial stresses

$\sigma^{\mathrm{w,trial}}_{\mathrm{n+1}} = \sigma^{\mathrm{w}}_{\mathrm{n}} + k_{11}\Delta\epsilon^{\mathrm{w}}_{\mathrm{n+1}} + k_{12}\Delta\epsilon^{\mathrm{f}}_{\mathrm{n+1}}$

$\sigma^{\mathrm{f,trial}}_{\mathrm{n+1}} = \sigma^{\mathrm{f}}_{\mathrm{n}} + k_{21}\Delta\epsilon^{\mathrm{w}}_{\mathrm{n+1}} + k_{22}\Delta\epsilon^{\mathrm{f}}_{\mathrm{n+1}}$

(ii) **Plastic step** (corrector step)

If $f^{\mathrm{trial,w}}_{\mathrm{n+1}} \leq 0$ and $f^{\mathrm{trial,f}}_{\mathrm{n+1}} \leq 0$, *trial state is admissible*:

$\sigma^{\mathrm{w}}_{\mathrm{n+1}} = \sigma^{\mathrm{w,trial}}_{\mathrm{n+1}}$, $\sigma^{\mathrm{f}}_{\mathrm{n+1}} = \sigma^{\mathrm{f,trial}}_{\mathrm{n+1}}$

$\epsilon^{\mathrm{p,w}}_{\mathrm{n+1}} = \epsilon^{\mathrm{p,w}}_{\mathrm{n}}$, $\epsilon^{\mathrm{p,f}}_{\mathrm{n+1}} = \epsilon^{\mathrm{p,f}}_{\mathrm{n}}$, $r^{\mathrm{p,w}}_{\mathrm{n+1}} = r^{\mathrm{p,w}}_{\mathrm{n}}$, $r^{\mathrm{p,f}}_{\mathrm{n+1}} = r^{\mathrm{p,f}}_{\mathrm{n}}$

Else If $f^{\mathrm{trial,w}}_{\mathrm{n+1}} > 0$ and $f^{\mathrm{trial,f}}_{\mathrm{n+1}} \leq 0$

plastic deformation only occurs in the warp direction:

1. Calculate the plastic increment in the warp direction

   $\Delta\epsilon^{\mathrm{p,w}} = \frac{f^{\mathrm{w,trial}}_{\mathrm{n+1}}}{k_{11}+H_{\mathrm{w}}}$

2. Correct the stresses

   $\sigma^{\mathrm{w}}_{\mathrm{n+1}} = \sigma^{\mathrm{w,trial}}_{\mathrm{n+1}} - k_{11}\Delta\epsilon^{\mathrm{p,w}}_{\mathrm{n+1}}$

   $\sigma^{\mathrm{f}}_{\mathrm{n+1}} = \sigma^{\mathrm{f,trial}}_{\mathrm{n+1}} - k_{21}\Delta\epsilon^{\mathrm{p,w}}_{\mathrm{n+1}}$

3. Update the plastic strains and hardening terms

   $\epsilon^{\mathrm{p,w}}_{\mathrm{n+1}} = \epsilon^{\mathrm{p,w}}_{\mathrm{n}} + \Delta\epsilon^{\mathrm{p,w}}_{\mathrm{n+1}}, \epsilon^{\mathrm{p,f}}_{\mathrm{n+1}} = \epsilon^{\mathrm{p,f}}_{\mathrm{n}}, r^{\mathrm{p,w}}_{\mathrm{n+1}} = r^{\mathrm{p,w}}_{\mathrm{n}} + H_{\mathrm{w}}\Delta\epsilon^{\mathrm{p,w}}, r^{\mathrm{p,f}}_{\mathrm{n+1}} = r^{\mathrm{p,f}}_{\mathrm{n}}$

Else If $f^{\mathrm{trial,w}}_{\mathrm{n+1}} \leq 0$ and $f^{\mathrm{trial,f}}_{\mathrm{n+1}} > 0$

plastic deformation only occurs in the fill direction:

1. Calculate the plastic increment in the fill direction

   $\Delta\epsilon^{\mathrm{p,f}} = \frac{f^{\mathrm{f,trial}}_{\mathrm{n+1}}}{k_{22}+H_{\mathrm{f}}}$

2. Correct the stresses

   $\sigma^{\mathrm{w}}_{\mathrm{n+1}} = \sigma^{\mathrm{w,trial}}_{\mathrm{n+1}} - k_{12}\Delta\epsilon^{\mathrm{p,f}}_{\mathrm{n+1}}$

   $\sigma^{\mathrm{f}}_{\mathrm{n+1}} = \sigma^{\mathrm{f,trial}}_{\mathrm{n+1}} - k_{22}\Delta\epsilon^{\mathrm{p,f}}_{\mathrm{n+1}}$

3. Update the plastic strains and hardening terms

   $\epsilon^{\mathrm{p,w}}_{\mathrm{n+1}} = \epsilon^{\mathrm{p,w}}_{\mathrm{n}}, \epsilon^{\mathrm{p,f}}_{\mathrm{n+1}} = \epsilon^{\mathrm{p,f}}_{\mathrm{n}} + \Delta\epsilon^{\mathrm{p,f}}_{\mathrm{n+1}}, r^{\mathrm{p,w}}_{\mathrm{n+1}} = r^{\mathrm{p,w}}_{\mathrm{n}}, r^{\mathrm{p,f}}_{\mathrm{n+1}} = r^{\mathrm{p,f}}_{\mathrm{n}} + H_{\mathrm{f}}\Delta\epsilon^{\mathrm{p,f}}$

Else

plastic deformation occurs in both the warp and fill directions:

1. Calculate the plastic increment in the warp and fill directions

   $\Delta\epsilon^{\mathrm{p,w}} = \frac{-f^{\mathrm{f,trial}}_{\mathrm{n+1}}k_{12}+f^{\mathrm{w,trial}}_{\mathrm{n+1}}(k_{22}+H_{\mathrm{f}})}{(H_{\mathrm{f}}+k_{22})(H_{\mathrm{w}}+k_{11})-k_{12}k_{21}}$

   $\Delta\epsilon^{\mathrm{p,f}} = \frac{-f^{\mathrm{w,trial}}_{\mathrm{n+1}}k_{21}+f^{\mathrm{f,trial}}_{\mathrm{n+1}}(k_{11}+H_{\mathrm{w}})}{(H_{\mathrm{w}}+k_{11})(H_{\mathrm{f}}+k_{22})-k_{12}k_{21}}$

2. Correct the stresses

   $\sigma^{\mathrm{w}}_{\mathrm{n+1}} = \sigma^{\mathrm{w,trial}}_{\mathrm{n+1}} - k_{11}\Delta\epsilon^{\mathrm{p,w}} - k_{12}\Delta\epsilon^{\mathrm{p,f}}$

   $\sigma^{\mathrm{f}}_{\mathrm{n+1}} = \sigma^{\mathrm{f,trial}}_{\mathrm{n+1}} - k_{21}\Delta\epsilon^{\mathrm{p,w}} - k_{22}\Delta\epsilon^{\mathrm{p,f}}$

3. Update the plastic strains and hardening terms

   $\epsilon^{\mathrm{p,w}}_{\mathrm{n+1}} = \epsilon^{\mathrm{p,w}}_{\mathrm{n}} + \Delta\epsilon^{\mathrm{p,w}}_{\mathrm{n+1}}, \epsilon^{\mathrm{p,f}}_{\mathrm{n+1}} = \epsilon^{\mathrm{p,f}}_{\mathrm{n}} + \Delta\epsilon^{\mathrm{p,f}}_{\mathrm{n+1}}$

   $r^{\mathrm{p,w}}_{\mathrm{n+1}} = r^{\mathrm{p,w}}_{\mathrm{n}} + H_{\mathrm{w}}\Delta\epsilon^{\mathrm{p,w}}, r^{\mathrm{p,f}}_{\mathrm{n+1}} = r^{\mathrm{p,f}}_{\mathrm{n}} + H_{\mathrm{f}}\Delta\epsilon^{\mathrm{p,f}}$

2.6 Implementation of the fabric plasticity model in large deformations

During the course of deformation of the tensioned fabric membrane structures, the displacements and rigid body rotations of the fabric membrane can be very large, while the strains are only in the range of small to moderate. Therefore, the fabric plasticity model developed in this chapter can still be used in simulations within the finite deformation framework if the rigid body rotation can be excluded in every stress update increment, *i.e.*, the stress-strain relation has to be defined in a so-called objective or co-rotational frame [26]. Before the user material subroutine (UMAT) in ABAQUS is called, the strain and stress tensors have been rotated to account for rigid body motion in every increment. Thus, the implementation algorithm mentioned in table 2.1 is still valid in large deformations.

2.7 Verifications

The proposed model is implemented in ABAQUS/Standard as a user material subroutine (UMAT). In order to verify this UMAT, the numerical simulations of the uniaxial tests and biaxial tests are performed. The numerical results are then compared with the experimental data.

2.7.1 Uniaxial tests

By fitting with the experimental data obtained from the uniaxial tensile tests (*cf.* figs. 2.5 and 2.6), the following parameters are determined:

- In the warp direction

$$\begin{cases} E_{\mathrm{w}1} = 1364 \text{ MPa}, & \text{if} \quad \sigma_{\mathrm{w}} < 15 \text{ MPa} \\ E_{\mathrm{w}2} = \frac{E_{\mathrm{w}3} H_{\mathrm{w}}}{H_{\mathrm{w}} + E_{\mathrm{w}3}}, & \text{if} \quad \sigma_{\mathrm{w}} > 15 \text{ MPa} \quad \text{and} \quad \Delta\sigma_{\mathrm{w}} > 0 \\ E_{\mathrm{w}3} = 1130 \text{ MPa}, & \text{otherwise}, \end{cases} \tag{2.48}$$

  and the plastic modulus in the warp direction $H_{\mathrm{w}} = 448$ MPa.

- In the fill direction, we have

$$\begin{cases} E_{\mathrm{f1}} = 10^4(14.1309(\epsilon_f)^2 + 0.04\epsilon_f + 0.0115) \text{ MPa}, & \sigma_{\mathrm{f}} < 5 \text{ MPa} \\ E_{\mathrm{f2}} = \frac{H_{\mathrm{f1}}E_{\mathrm{f4}}}{H_{\mathrm{f1}}+E_{\mathrm{f4}}} \text{ MPa}, & 5 \text{ MPa} \leq \sigma_{\mathrm{f}} < 15 \text{ MPa and } \Delta\sigma_{\mathrm{f}} \geq 0 \\ E_{\mathrm{f3}} = \frac{H_{\mathrm{f2}}E_{\mathrm{f4}}}{H_{\mathrm{f2}}+E_{\mathrm{f4}}} \text{ MPa}, & \sigma_{\mathrm{f}} \geq 15 \text{ MPa and } \Delta\sigma_{\mathrm{f}} \geq 0 \\ E_{\mathrm{f4}} = 825 \text{ MPa}, & \text{otherwise} \end{cases} \tag{2.49}$$

  and the plastic moduli in the fill direction can be defined as:

$$\begin{cases} H_{\mathrm{f1}} = 593 \text{ MPa}, & 5 \text{ MPa} \leq \sigma_{\mathrm{f}} < 15 \text{ MPa} \\ H_{\mathrm{f2}} = 236.82 \text{ MPa}, & \sigma_{\mathrm{f}} \geq 15 \text{ MPa} \end{cases} \tag{2.50}$$

The stress-strain curves obtained from the FEM model and experimental data are plotted in fig. 2.14. As can be seen from the figure, good agreement is observed between FEM results and experimental data.

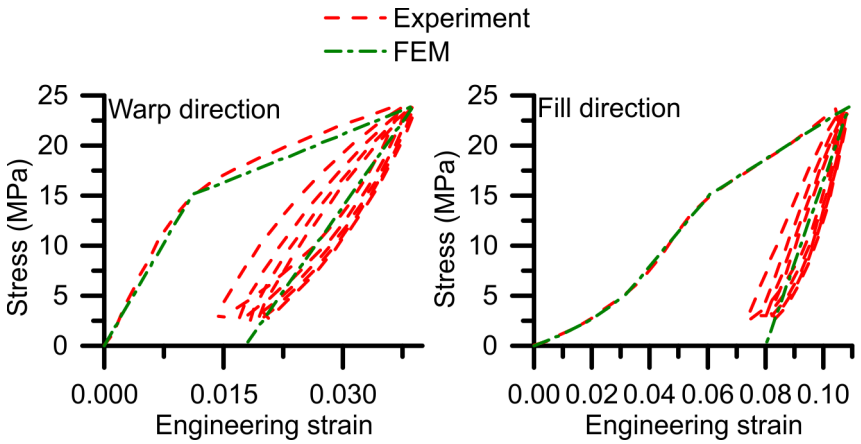

Figure 2.14: Comparison the stress-strain curves between the experimental data obtained from the uniaxial tensile tests and their counterparts obtained from the simulations.

2.7.2 Biaxial tests

At this point, the numerical correctness of the model has been checked. In the next step, the model is validated by the experimental data obtained from the biaxial tensile tests. Due to the symmetric properties of the problem, the finite element analysis for the biaxial test can be performed on

a quarter of the cruciform. Figures 2.15 and 2.16 show the geometry and finite element description of the model. The mesh is composed by 5041 quadrilateral membrane elements (M3D4). As mentioned in section II., in order to take into account the interaction between yarns as well as the stress ratio dependence, two Poisson's ratios and two Young's moduli are needed.

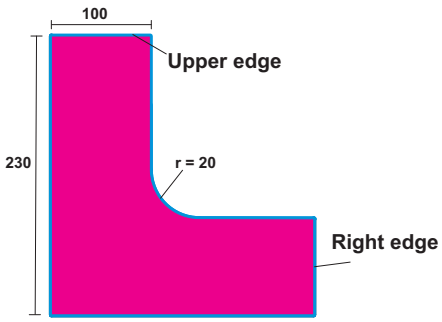

Figure 2.15: The geometry of a quarter of the cruciform.

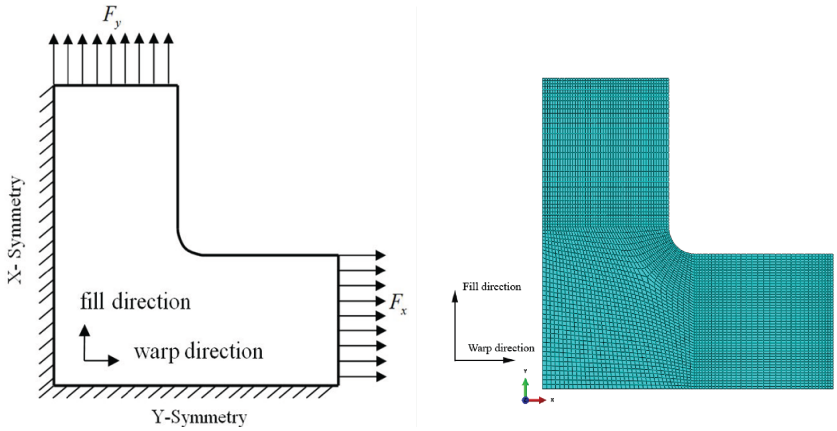

Figure 2.16: The finite element model for the biaxial test: (a) boundary conditions and (b) meshing.

While the extracted parameters from the uniaxial tests are identified straightforwardly, the ones from the biaxial tests are not easy to determine. In order to minimize the discrepancies between the numerical simulations and the experimental data, a parameter identification method is implemented. In this method the boundary value problem in ABAQUS is combined with

the built-in multi-objective genetic algorithm routine in MATLAB [27]. However, in the experimental data obtained from the biaxial tests (*cf.* fig. 2.8) there is a non-unique value of the strain with a given stress and vice versa in the warp and fill directions. Therefore, the parameter identification procedure is carried out in two steps. Firstly, the distance between a point, which is characterized by the stress and strain obtained from the simulation, and the counterpart from the experiment is minimized. Subsequently, the least square problems are solved. The parameter identification attempts to find ν_{12}, ν_{21}, E_{w4} and E_{f5} that can yield the best fit to the given stress-strain history. To obtain this target, the following objective functions should be minimized:

$$f_1(\nu_{12}, \nu_{21}, E_{\mathrm{w4}}, E_{\mathrm{f5}}) = \sum_{i=1}^{N} [(\epsilon_{11_i}^{\mathrm{ex}} - \epsilon_{11_i}^{\mathrm{sim}})^2 + (\sigma_{11_i}^{\mathrm{ex}} - \sigma_{11_i}^{\mathrm{sim}})^2], \quad (2.51)$$

$$f_2(\nu_{12}, \nu_{21}, E_{\mathrm{w4}}, E_{\mathrm{f5}}) = \sum_{i=1}^{N} [(\epsilon_{22_i}^{\mathrm{ex}} - \epsilon_{22_i}^{\mathrm{sim}})^2 + (\sigma_{22_i}^{\mathrm{ex}} - \sigma_{22_i}^{\mathrm{sim}})^2], \quad (2.52)$$

where N is the number of data points from the simulation, $\epsilon_{11_i}^{\mathrm{ex}}$, $\epsilon_{11_i}^{\mathrm{sim}}$, $\sigma_{11_i}^{\mathrm{ex}}$ and $\sigma_{11_i}^{\mathrm{sim}}$ are respectively the strains and stresses in the warp direction in the experiment and the simulation and $\epsilon_{22_i}^{\mathrm{ex}}$, $\epsilon_{22_i}^{\mathrm{sim}}$, $\sigma_{22_i}^{\mathrm{ex}}$ and $\sigma_{22_i}^{\mathrm{sim}}$ are the counterparts in the fill direction. The state variables in these objective functions are subjected to the below linear constraints

$$\begin{cases} 0 \leq \nu_{12} \leq 1 \\ 0 \leq \nu_{21} \leq 1 \\ 0 \leq E_{\mathrm{w4}} \leq E_{\mathrm{w3}} = 1130 \text{ MPa} \\ 0 \leq E_{\mathrm{f5}} \leq E_{\mathrm{f4}} = 825 \text{ MPa} \end{cases} \quad (2.53)$$

From this identification parameter procedure, $\nu_{12} = 0.09076$, $\nu_{21} = 0.46923$, E_{w4} =852.241 MPa and E_{f5} =618.402 MPa are determined.

Figures 2.17 and 2.18 present the strain field when the coated fabric is subjected to the load ratio (1:1) with the applied force of 24.1 MPa in each direction. While the strain in the center of the model is extracted, the stresses in the right edge and upper edge (*cf.* fig. 2.15) are averaged to obtain the applied stresses in the warp and fill directions, respectively. In fig. 2.19, the stress-strain curves in the warp and fill direction extracted from the numerical simulations and the experiments are plotted. Good agreement between them can be seen. Especially, the proposed model

can successfully capture nonlinearities in the warp and fill directions as well as the orthotropic effect. Moreover, the permanent strains and load ratio dependence are captured quite precisely in both directions. Nevertheless, the model is not yet validated with different combinations of load ratios. This issue requires additional biaxial experiments, which will be considered in the next step of this work.

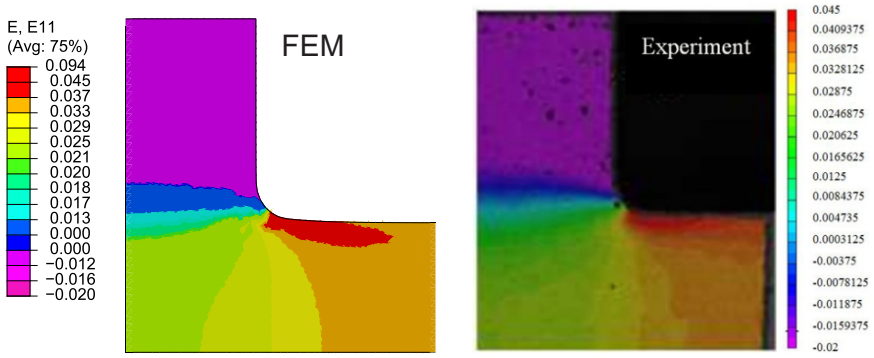

Figure 2.17: The strain field in the warp direction (the DIC measurement was done at VUB [19, 20]).

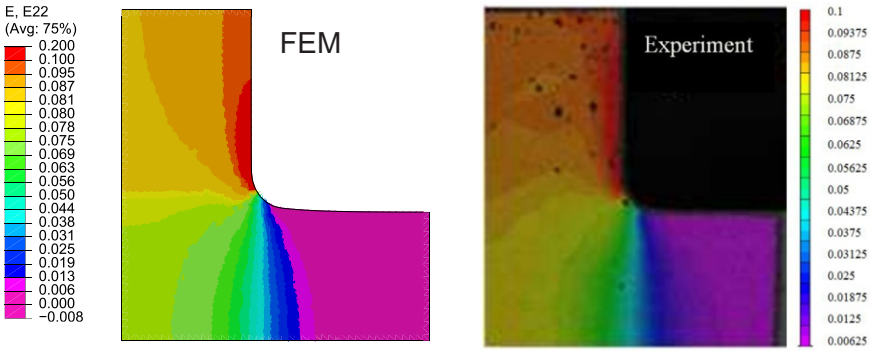

Figure 2.18: The strain field in the fill direction (the DIC measurement was done at VUB [19, 20]).

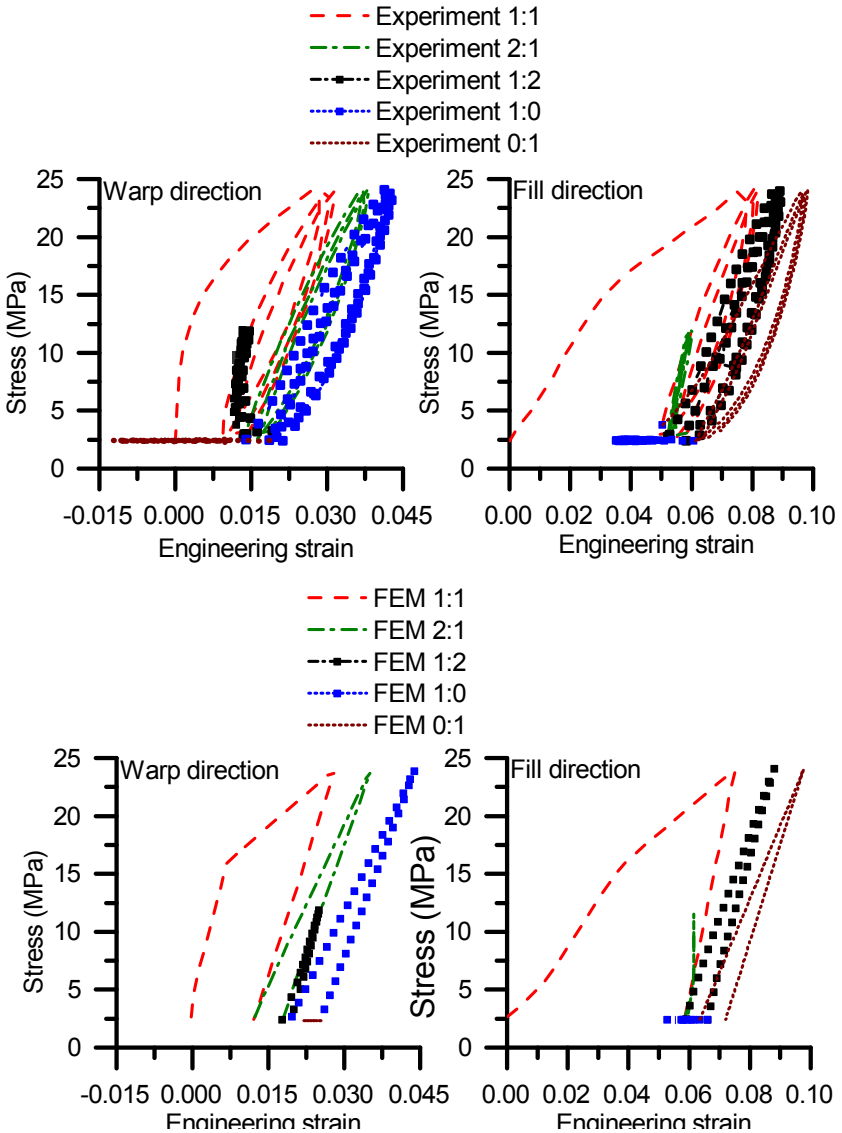

Figure 2.19: Comparisons of the stress-strain curves between the FEM and experiments obtained from the biaxial test.

2.8 Case study

As mentioned in section 2.2, one of the most important features in the mechanical behavior of coated fabric is the crimp interchange. This salient feature is dominant in the first load cycle; therefore, it leads to an initial slack. In practice, the linear orthotropic elasticity model is widely used for coated fabrics [28], the initial slack is excluded in the numerical calculations and its effect on the structure is compensated in the patterning stage. However, the method for this compensation is not well-documented in the literature. In this part, the proposed material model and the linear orthotropic elastic model are used to simulate the deformed shape of a hypar membrane structure. The final configurations of the membrane obtained from the two models are compared to evaluate the role of the mechanical model as well as the effect of the initial slack in deformation of coated fabric membrane structures. Moreover, the calculation time for the two models is also compared. From that, the performance of the proposed model can be evaluated.

In this study the material parameters for orthotropic elasticity can be defined using the least squares method mentioned in the standard MSAJ/M-02-1995 [29]. According to this standard, the elastic constants are determined based on the experimental data in the range of 2 kN/m and the maximum load of each ratio. Since the initial slack is excluded, only stabilized behavior is considered and all subsequent calculations are carried out based on the data of the last cycle of each load ratio (*cf.* fig. 2.20). In the assumption of plane stress, the relation between strains and stresses can be expressed as:

$$\begin{cases} \sigma_{\mathrm{w}} = k_{11}\epsilon_{\mathrm{w}} + k_{12}\epsilon_{\mathrm{f}} \\ \sigma_{\mathrm{f}} = k_{21}\epsilon_{\mathrm{w}} + k_{22}\epsilon_{\mathrm{f}}, \end{cases} \tag{2.54}$$

where k_{11}, k_{12}, k_{21} and k_{22} are defined in eqs. (2.21) to (2.24) and σ_{w}, ϵ_{w}, σ_{f} and ϵ_{f} are stresses and strains in the warp and fill directions, respectively. Moreover, in [29] it is assumed that the reciprocal condition is fulfilled, which results in $k_{12} = k_{21}$.

By substituting the values of strain and stress in the warp and fill directions for each load ratio in eq. (2.54), the system of equations can be

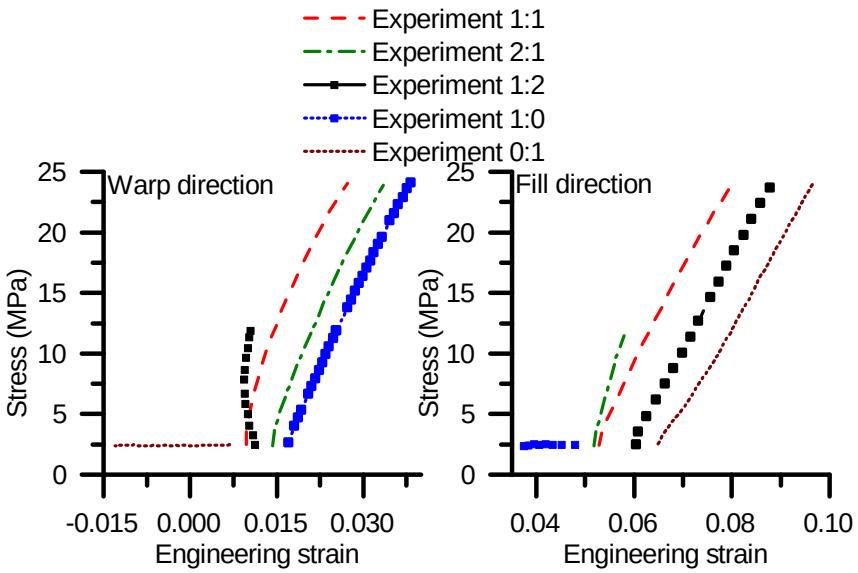

Figure 2.20: The stress-strain curve in the last cycles in the biaxial test.

expressed in matrix form as follows:

$$\begin{bmatrix} \sigma_{\mathrm{w}}^{1:1} \\ \sigma_{\mathrm{f}}^{1:1} \\ \sigma_{\mathrm{w}}^{2:1} \\ \sigma_{\mathrm{f}}^{2:1} \\ \sigma_{\mathrm{w}}^{1:2} \\ \sigma_{\mathrm{f}}^{1:2} \\ \sigma_{\mathrm{w}}^{1:0} \\ \sigma_{\mathrm{f}}^{1:0} \\ \sigma_{\mathrm{w}}^{0:1} \\ \sigma_{\mathrm{f}}^{0:1} \end{bmatrix} = \begin{bmatrix} \epsilon_{\mathrm{w}}^{1:1} & \epsilon_{\mathrm{f}}^{1:1} & 0 \\ 0 & \epsilon_{\mathrm{w}}^{1:1} & \epsilon_{\mathrm{f}}^{1:1} \\ \epsilon_{\mathrm{w}}^{2:1} & \epsilon_{\mathrm{f}}^{2:1} & 0 \\ 0 & \epsilon_{\mathrm{w}}^{2:1} & \epsilon_{\mathrm{f}}^{2:1} \\ \epsilon_{\mathrm{w}}^{1:2} & \epsilon_{\mathrm{f}}^{1:2} & 0 \\ 0 & \epsilon_{\mathrm{w}}^{1:2} & \epsilon_{\mathrm{f}}^{1:2} \\ \epsilon_{\mathrm{w}}^{1:0} & \epsilon_{\mathrm{f}}^{1:0} & 0 \\ 0 & \epsilon_{\mathrm{w}}^{1:0} & \epsilon_{\mathrm{f}}^{1:0} \\ \epsilon_{\mathrm{w}}^{0:1} & \epsilon_{\mathrm{f}}^{0:1} & 0 \\ 0 & \epsilon_{\mathrm{w}}^{0:1} & \epsilon_{\mathrm{f}}^{0:1} \end{bmatrix} \cdot \begin{bmatrix} k_{11} \\ k_{12} \\ k_{22} \end{bmatrix} \tag{2.55}$$

This over-determined system can be solved by using Moore-Penrose pseudo-inverse routine in MATLAB so that the sum of squares of strain terms

$$S = \sum [(k_{11}\epsilon_{\mathrm{w}}^{\mathrm{i:j}} + k_{12}\epsilon_{\mathrm{f}}^{\mathrm{i:j}} - \sigma_{\mathrm{w}}^{\mathrm{i:j}})^2 + (k_{12}\epsilon_{\mathrm{w}}^{\mathrm{i:j}} + k_{22}\epsilon_{\mathrm{f}}^{\mathrm{i:j}} - \sigma_{\mathrm{f}}^{\mathrm{i:j}})^2] \tag{2.56}$$

is minimized. Herein $\epsilon_{\mathrm{w}}^{\mathrm{i:j}}, \epsilon_{\mathrm{f}}^{\mathrm{i:j}}, \sigma_{\mathrm{w}}^{\mathrm{i:j}}$ and $\sigma_{\mathrm{f}}^{\mathrm{i:j}}$ are strains and stresses in the

warp and fill directions for load ratio i:j. As a result, we obtain:

$$\begin{cases} E_{\mathrm{w}} = 975.6 \text{ MPa}, & \nu_{12} = 0.23 \\ E_{\mathrm{f}} = 716.1 \text{ MPa}, & \nu_{21} = 0.17 \end{cases} \tag{2.57}$$

Since the standard [29] assumes a stabilized behavior for the membrane, we also consider the stabilized effective Young′s modulus E_{xx} for the bias extension test; this effective Young′s modulus can be calculated as (*cf.* fig. 2.9):

$$E_{\mathrm{xx}} = \frac{\Delta\sigma}{\Delta\epsilon} \approx \frac{13.05 - 2.44}{0.28016 - 0.24481} = 300 \text{ MPa}. \tag{2.58}$$

Now, in order to identify the shear modulus G_{xy} for the membrane so that the effective Young′s modulus E_{xx} from the uniaxial bias extension test can be reproduced, a parametric study of the shear modulus is performed. After this parametric study (*cf.* fig. 2.21), the shear modulus of 87.714 MPa is obtained. This value is used in the subsequent calculations. In fig. 2.22

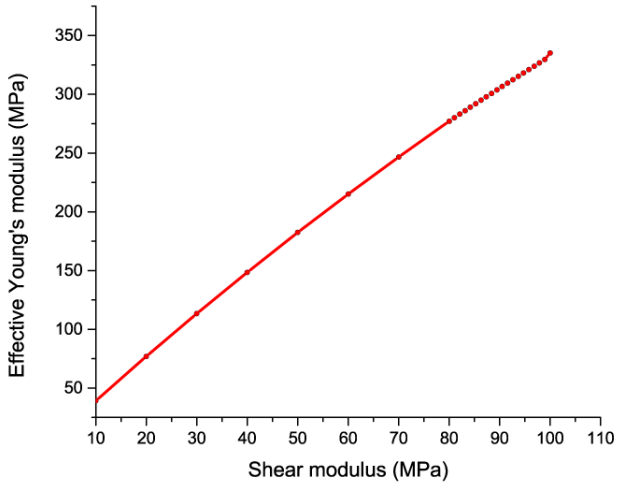

Figure 2.21: Correlation between in-plane shear stiffness and effective Young′s modulus.

the dimensions of the squared membrane are shown. While nodes 1 and 2 move upward 1 m in z direction, nodes 3 and 4 move downward 1 m in z direction.

The finite element analysis is performed by using ABAQUS/Standard 6.12. The mesh is composed by 2496 M3D4 and 8 M3D3 (triangular membrane)

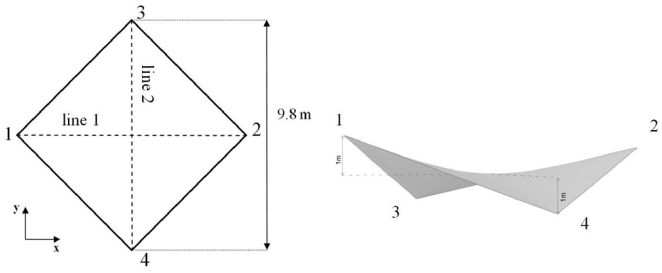

Figure 2.22: Model description: (a) initial configuration and (b) final configuration.

elements (*cf.* fig. 2.23). Figure 2.24 shows the contour plot of displacement of the membrane in the final configuration when we use the proposed material model for the coated fabric. The simulation was done on an Intel Core i7-2760Qm processor 2.4 GHz. It takes 87 s for the simulation when the linear elasticity is used for the membrane, while in case of the proposed model it takes 206 s. The displacements in z direction in the two models are extracted along the diagonal lines of the membrane (*cf.* fig. 2.22). The considerable discrepancies of the obtained results (*cf.* fig. 2.25) emphasize the vital role of the material model and the profound effect of the initial slack in the final shape of the tension fabric structure.

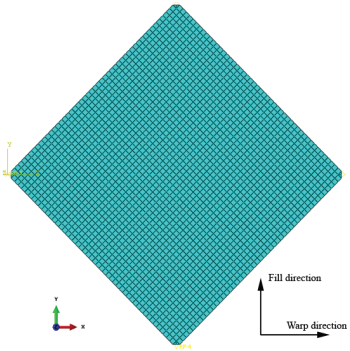

Figure 2.23: Finite element mesh for the hypar structure.

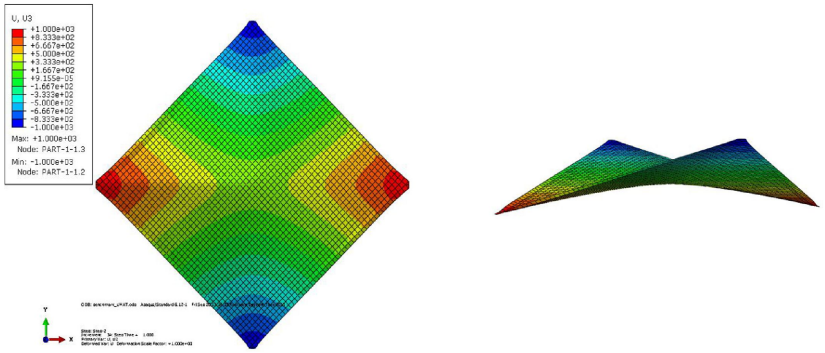

Figure 2.24: Contour plot of the displacement field in the membrane.

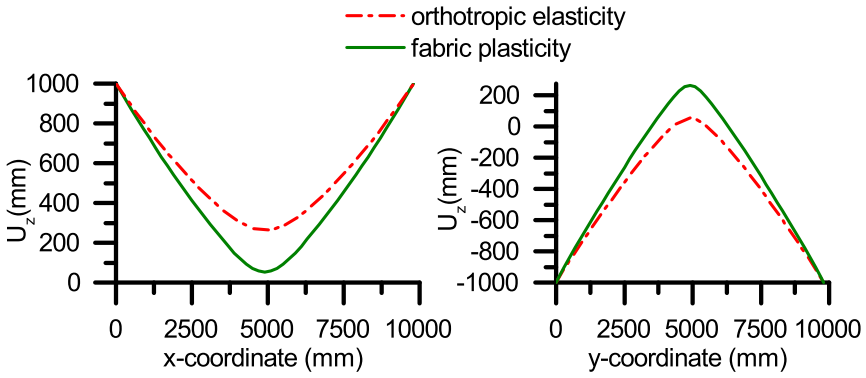

Figure 2.25: The displacement in z direction in the final configuration: (a) displacement along line 1 and (b) displacement along line 2

2.9 Conclusions

In this chapter, an elasto-plastic model for coated fabrics is proposed based on the experimental data obtained from uniaxial tensile tests. The interaction between the warp and fill yarns as well as between yarns and coating are taken into account by using Poisson's ratios. The model is subsequently verified by the experimental data from the uniaxial and biaxial tests. From the obtained results, it can be seen that the proposed model can capture the nonlinear, orthotropic and load ratio dependent behavior as well as permanent strains. Therefore, by using the proposed model in tension membrane structure design, it can be possible to reduce

the safety factor that is used to compensate for aforementioned features in mechanical behavior of coated fabrics, which cannot be captured when using linear orthotropic elasticity models. Consequently, we can reduce the uncertainties in design and create more ambitious structures. In addition, during the course of numerical simulations, good performance in computation is observed. From this point, this model is eligible for simulation of the whole large scale structure. Nevertheless, in this model time dependent behavior and nonlinear shear are not considered. These characteristics will be considered in further developments of this model.

Bibliography

[1] T. D. Dinh, A. Rezaei, L. De Laet, M. Mollaert, D. Van Hemelrijck, W. Van Paepegem, A new elasto-plastic material model for coated fabric, Engineering Structures 71 (2014) 222–233. doi:10.1016/j.engstruct.2014.04.027.

[2] C. Galliot, R. H. Luchsinger, A simple model describing the non-linear biaxial tensile behaviour of PVC-coated polyester fabrics for use in finite element analysis, Composite Structures 90 (4) (2009) 438–447. doi:10.1016/j.compstruct.2009.04.016.

[3] J. B. Pargana, D. Lloyd-Smith, B. A. Izzuddin, Advanced material model for coated fabrics used in tensioned fabric structures, Engineering Structures 29 (7) (2007) 1323–1336. doi:10.1016/j.engstruct.2006.09.001.

[4] Y. Zhang, Q. Zhang, H. Lv, Mechanical properties of polyvinylchloride-coated fabrics processed with Precontraint® technology, Journal of Reinforced Plastics and Composites 31 (23) (2012) 1670–1684. doi:10.1177/0731684412459898.

[5] S. Chen, X. Ding, R. Fangueiro, H. Yi, J. Ni, Tensile behavior of PVC-coated woven membrane materials under uni- and bi-axial loads, Journal of Applied Polymer Science 107 (3) (2008) 2038–2044. doi:10.1002/app.27303.

[6] R. B. Testa, W. R. Spillers, N. Stubbs, Bilinear model for coated square fabrics, Journal of The Engineering Mechanics Division 104 (5) (1978) 1027–1042.

[7] F. T. Peirce, The Geometry of Cloth Structure, Journal of the Textile Institute Transactions 28 (3) (1937) T45–T96. doi:10.1080/19447023708658809.

[8] S. Kawabata, M. Niwa, H. Kawai, The Finite-Deformation Theory of Plain-Weave Fabrics Part I: The Biaxial-Deformation Theory, The Journal of The Textile Institute 64 (1) (1973) 21–46. doi:10.1080/00405007308630416.

[9] N. Stubbs, H. Fluss, A space-truss model for plain-weave coated fabrics, Applied Mathematical Modelling 4 (1) (1980) 51–58. doi:10.1016/0307-904X(80)90213-9.

[10] N. Stubbs, S. Thomas, A nonlinear elastic constitutive model for coated fabrics, Mechanics of Materials 3 (2) (1984) 157–168. doi:10.1016/0167-6636(84)90006-1.

[11] S. Kato, T. Yoshino, H. Minami, Formulation of constitutive equations for fabric membranes based on the concept of fabric lattice model, Engineering Structures 21 (8) (1999) 691–708. doi:10.1016/S0141-0296(98)00024-8.

[12] B. N. Bridgens, P. D. Gosling, Direct stress–strain representation for coated woven fabrics, Computers & Structures 82 (23–26) (2004) 1913–1927. doi:10.1016/j.compstruc.2003.07.005.

[13] T. R., Y. L., Stress-strain relation for coated fabrics, Journal of Engineering Mechanics 113 (11) (1987) 1631–1646. doi:10.1061/(ASCE)0733-9399(1987)113:11(1631).

[14] M. Kageyama, S. Kawabata, M. Niwa, The Validity of a "Linearizing Method" for Predicting the Biaxial-extension Properties of Fabrics, The Journal of The Textile Institute 79 (4) (1988) 543–567. doi:10.1080/00405008808659163.

[15] H. Minami, A Multi-Step Linear Approximation Method for Nonlinear Analysis of Stress and Deformation of Coated Plain-Weave Fabric, Journal of Textile Engineering 52 (5) (2006) 189–195. doi:10.4188/jte.52.189.

[16] S. Thomas, N. Stubbs, An Inelastic Biaxial Constitutive Model for Fabric-Reinforced Composites, Journal of Industrial Textiles 13 (3) (1984) 144–160. doi:10.1177/152808378401300303.

[17] J. B. Pargana, V. M. A. Leitão, A simplified stress–strain model for coated plain-weave fabrics used in Tensioned Fabric Structures, Engineering Structures 84 (2015) 439–450. doi:10.1016/j.engstruct.2014.12.002.

[18] R. J. Bassett, R. Postle, N. Pan, Experimental Methods for Measuring Fabric Mechanical Properties: A Review and Analysis, Textile Research Journal 69 (11) (1999) 866–875. doi:10.1177/004051759906901111.

[19] Tapali P., Tensile behaviour of PVC coated fabrics under biaxial load: determination of the test procedure., Master's thesis, Vrij Universiteit Brussel (2012).

[20] M. VAN CRAENENBROECK, S. PUYSTIENS, L. DE LAET, D. VAN HEMELRIJCK, M. MOLLAERT, Biaxial testing of fabric materials and deriving their material properties–A quantitative study, in: Proceedings of the international association for shell and spatial structures (IASS) symposium, 2015.

[21] Vandenboer K., Numerical assessment of material models for coated fabrics in foldable tent structures., Master's thesis, Ghent University (2012).

[22] B. N. Bridgens, P. D. Gosling, M. J. S. Birchall, Membrane material behaviour: concepts, practice & developments, Structural Engineer 82 (14) (2004) 28–33.

[23] M. Van Craenenbroeck, S. Puystiens, L. De Laet, D. Van Hemelrijck, M. Mollaert, Quantitative Study of the Impact of Biaxial Test Protocols on the Derived Material Parameters for a PVC Coated Polyester Fabric, Procedia Engineering 155 (2016) 220–229. doi:10.1016/j.proeng.2016.08.023.

[24] C. Galliot, R. H. Luchsinger, The shear ramp: A new test method for the investigation of coated fabric shear behaviour – Part I: Theory, Composites Part A: Applied Science and Manufacturing 41 (12) (2010) 1743–1749. doi:10.1016/j.compositesa.2010.08.008.

[25] P. Potluri, D. A. Perez Ciurezu, R. B. Ramgulam, Measurement of meso-scale shear deformations for modelling textile composites, Composites Part A: Applied Science and Manufacturing 37 (2) (2006) 303–314. doi:10.1016/j.compositesa.2005.03.032.

[26] Dunne, F, Petrinic, N., Introduction to Computational Plasticity, Oxford University Press, 2005.

[27] T. Mathworks, Matlab Optimization Toolbox User's Guide.
URL http://www.mathworks.co.uk/access/helpdesk/help/pdf_doc/optim/optim_tb.pdf

[28] T. Nouri-Baranger, Computational methods for tension-loaded structures, Archives of Computational Methods in Engineering 11 (2) (2004) 143–186. doi:10.1007/BF02905937.

[29] MSAJ Testing Method for Elastic Constants with commentary (Feb. 1995).

Chapter 3

A Study of Tension Fabric Membrane Structures Under In-plane Loading: Nonlinear Finite Element Analysis and Validation

Analysis of tension fabric structures exhibits severe nonlinearities because of the large deformation of the fabric membrane and its peculiar material behavior. At this moment, there is limited literature on analysis and design of this kind of structures. This chapter presents a nonlinear finite element analysis of a tension fabric membrane structure used in foldable architectural applications. The aim of this analysis is twofold: validate the fabric elasto-plastic model proposed in chapter 2 and propose a benchmark for numerical simulations in the research field of tension fabric membrane structure. The results of this chapter were presented in [1].

3.1 Introduction

The membranes used in tensioned fabric membrane structures are very thin and flexible. Actually the flexural stiffness of these membranes is

negligible and hence it is difficult to pre-assign the shape of a tension fabric membrane structure [2, 3]. Indeed, there is a tight interconnection between the membrane's shape and the stress state in the membrane. In this interconnection, the membrane configuration, the applied loads on the structure and the internal stresses interact in a nonlinear manner to satisfy the equilibrium conditions [4]. Even though the pioneering work in tension fabric membrane structures was proposed by Otto et al. [5] fifty years ago, the development of this kind of structures has been hampered because of limitations in analysis methodologies [6]. Therefore, the urgent need for a unifying code and consistent methodology for design and analysis was mentioned in the work of Gosling et al. [7]. Moreover, a lack of proper benchmarks for verifications of membrane structure analyses, leaves numerical simulations of these structures in dubiety [7].

Within the framework of the EU-funded Integrated Project Context-T, a dome-like structure was designed (*cf.* fig. 3.1). Its skin is an assembly of flat triangular PVC coated membrane parts, which are welded together. By adjusting the belts, the whole structure is in tension [8–10]. The purposes of the project is to verify whether the Context-T structure can be stable in intermediate configurations between fully open and closed positions. To find a proper answer to this issue, knowledge about how the tension membrane behaves is required. Therefore, to gain a better assessment of the feasibility of the design concept, a single tension membrane unit is analyzed first. Moreover, through this analysis the material constitutive model, which we have developed for coated fabrics in the previous chapter, is further validated for a different load case. Because of these reasons, the success of this analysis will thus be the premise for further investigation of the feasibility of this design concept. In this chapter, a two-dimensional membrane that is subjected to in-plane loads is considered, both numerically and experimentally [1]. Moreover, due to the fact that there is no benchmark for membrane analysis yet [7], the model used in this chapter can serve as the first benchmark for future studies in this research field.

The outline of this chapter is as follows. The next section explains the experimental set-up. Afterward, the details of the finite element model are presented. Finally, the obtained results from the finite element sim-

1. The experimental tests were done at *the architectural engineering research laboratory (ae-lab) of the department of Architectural Engineering and the department of Mechanics of Materials and Constructions at Vrije Universiteit Brussel.*

ulations are validated with the experimental data and then general conclusions are drawn.

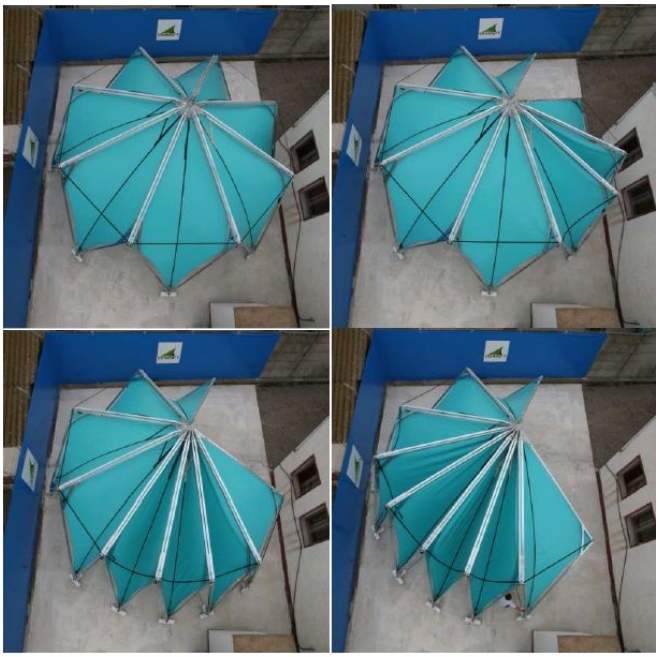

Figure 3.1: The real scale model of the Context-T structure in different configurations [8].

3.2 Details of the experiments[2]

3.2.1 Geometry of the experimental model

The PVC coated fabric used in this study is the same as the one considered in chapter 2. It has a thickness of 0.83 mm and a surface mass density of 1050 $\mathrm{g/m^2}$. Densities of the fabric are respectively 12 yarns/cm and 13 yarns/cm in the warp and fill directions. For the sake of convenience in the model descriptions, the most important parts of the model are named as shown in fig. 3.2. In this figure, the following notations are used:

2. The experimental tests were done at *the architectural engineering research laboratory (ae-lab) of the department of Architectural Engineering and the department of Mechanics of Materials and Constructions at Vrije Universiteit Brussel.*

- A and B are the lower and upper edges.
- C and D are the side edges.
- A′, C′ and D′ are the edges of the triangle from which the membrane geometry is derived. The length of A′ is equal to 6 m while the lengths of C′ and D′ are *ca.* 3.3 m (fig. 3.3).
- RP1, RP2 and RP3 are the reference points at the corners of the membrane. Through these reference points, the loads L_1, L_2 and L_3 are applied to the membrane.

The membrane is cut from a coated fabric roll, so that the fill direction is perpendicular to the edge A′ of the triangle. In order to prevent high stress concentrations when the membrane is under tension, the edges are cut with a sag of 5%. Moreover, in each corner of the membrane, an extra layer of the fabric is welded. Along the membrane′s edges, polyester

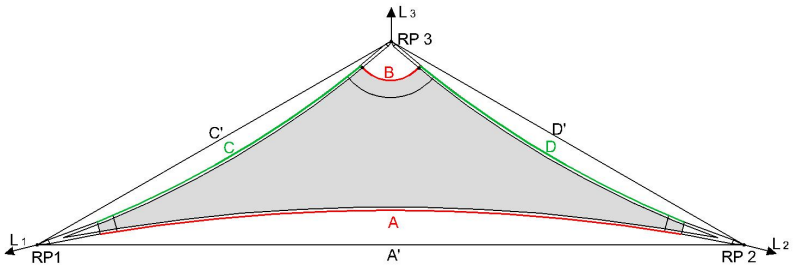

Figure 3.2: Naming convention of the model.

belts of 2.5 mm thickness and 25 mm width are stitched. These belts are used to reinforce the membrane′s edges as well as to transfer the load to the membrane. The parts of the belts, which are not tied to the membrane, are duplicated to provide sleeves where the metal clamps are attached to connect the belts with the supports (*cf.* fig. 3.4). To start from a visually flat configuration, the membrane is slightly tensioned. The hook of the crane is pulled up until the turnbuckles at the corners are positioned alongside the belts. At this stage, the reaction forces L_1 and L_2 are equal to 0.18 kN and L_3 is ca. 0.04 kN.

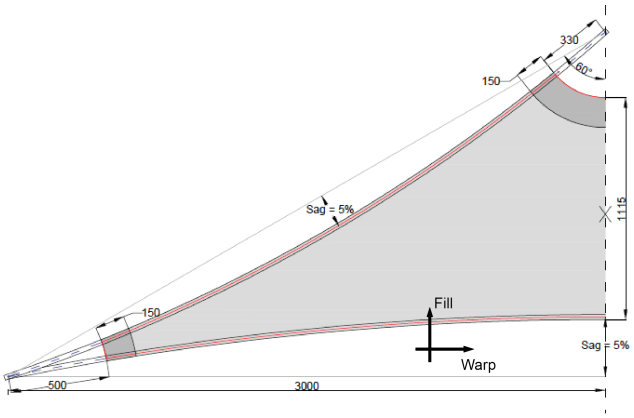

Figure 3.3: Design dimensions (mm) of the model, fully symmetric about the dashed line.

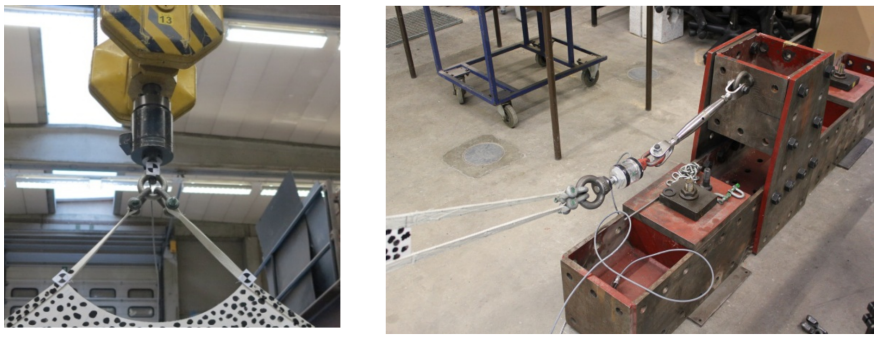

(a) (b)

Figure 3.4: Connection details of (a) top connection and (b) bottom connection (courtesy of the ae-lab and MeMC, VUB).

3.2.2 Digital image correlation (DIC) measurements[3]

This measurement technique uses two cameras that take a series of pictures of the speckle pattern on the membrane during the course of the experiment (*cf.* fig. 3.5). By this way, the displacement of the speckles can be traced based on comparisons among images taken at different load steps. Subsequently, the strain fields in the membrane are obtained by derivation of the displacement field. By using the two cameras, not only the in-plane, but also the out-of-plane displacement can be measured.

Figure 3.5: The overview of the membrane that was used in the experiment (courtesy of the ae-lab and MeMC, VUB).

3. The experimental tests were done at *the architectural engineering research laboratory (ae-lab) of the department of Architectural Engineering and the department of Mechanics of Materials and Constructions at Vrije Universiteit Brussel.*

3.3 The finite element model

3.3.1 Geometry and the membrane lay-up

The geometry and dimensions of the numerical model are based on the cutting pattern of the experimental set-up. As mentioned in section 3.2.1, some parts of the model consist of two layers (membrane-membrane, membrane-belt and belt-belt) or even three layers (membrane-belt-membrane). These coupled regions are modeled by using the tie-constraint [11] in order to couple all displacement degrees of freedom at every node on a slave surface to the counterparts of the corresponding nodes on a master surface. Details for the membrane lay-up can be seen in fig. 3.6.

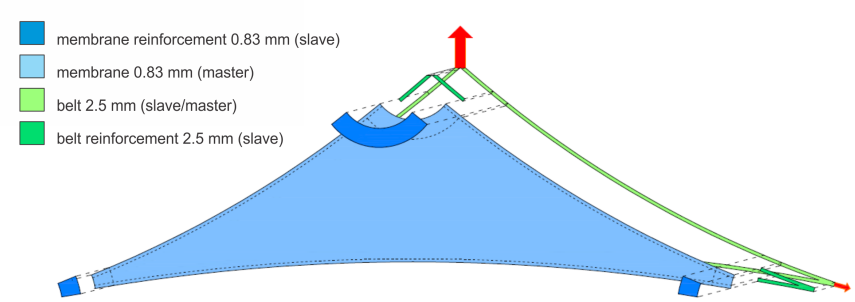

Figure 3.6: The illustration of membrane lay-up.

3.3.2 Boundary conditions

In the experiment, the loads are applied to the rings that are used to connect the ends of the belts. For simplicity, the rings are not modeled but replaced by the reference points. There are RP1, RP2 and RP3 in fig. 3.2. The nodes at the ends of the belts are kinematically coupled with the closest reference point so that they have the same displacement degrees of freedom with the corresponding reference point (*cf.* fig. 3.7). However, there is no coupling between the reference points and the nodes at the ends of the belts with respect to the rotational degrees of freedom. The load applied to the membrane can be divided into two steps. In the first step, reference point RP3 is fixed, while reference points RP1 and RP2 are moved 15.55 mm away from the membrane in the direction of the

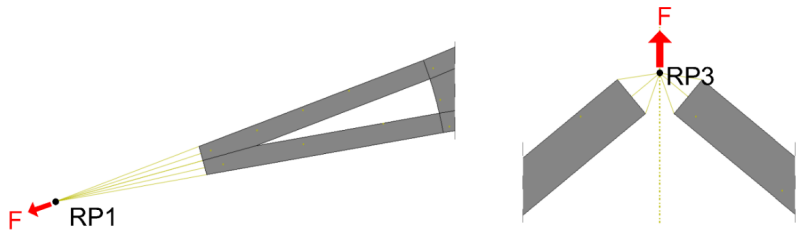

Figure 3.7: Applied load in a reference point (a) at a bottom corner and (b) at the top.

bisectors of the angles that are formed by the belts at the corners. These displacements cause reaction forces $L_1 = L_2 = 0.18$ kN, which is the value obtained in the load cells in the prestress stage of the membrane. In the second step, reference point RP3 is displaced upward while reference points RP1 and RP2 are fixed. The displacement at reference point RP3 is stopped when the reaction force L_3 reaches the value of 7.81 kN, which corresponds to the maximum force that is applied in the experiment.

3.3.3 Spatial discretization

In this analysis, membrane elements [11] are chosen to model the coated fabric, as well as the belts. There are 11,923 linear quadrilateral elements (M3D4) and 154 linear triangular elements (M3D3) in the model (*cf.* fig. 3.8).

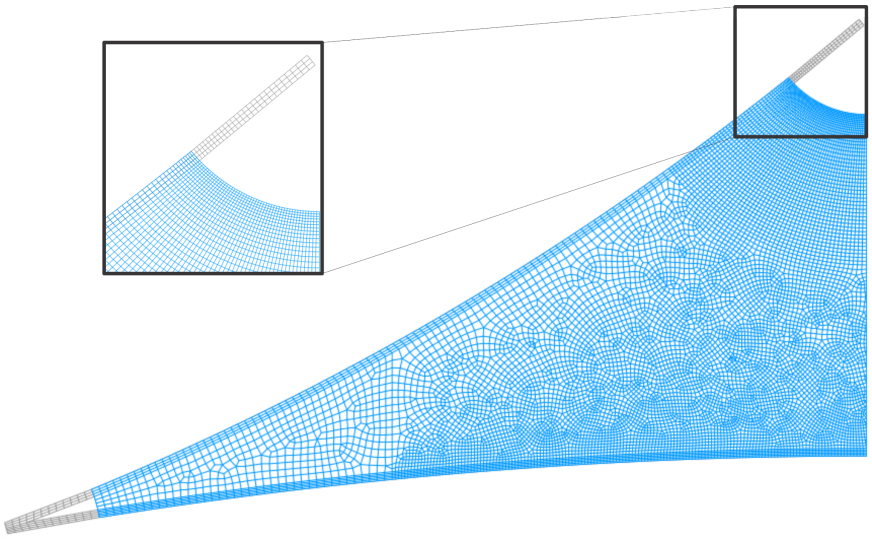

Figure 3.8: The finite element mesh used in the simulation.

3.3.4 Material models

I. The PVC coated fabric

In fact, there is an interconnection between the behavior of the membrane′s material and its configuration. It implies that in order to have a realistic simulation of tension membrane structures, an accurate material model plays a crucial role. Moreover, membrane structures are typically large-scale structures and the numerical analyses are usually expensive from a computational viewpoint. Thus, the material model used for the PVC coated fabric should be computationally inexpensive. In chapter 2, the elasto-plastic model for coated fabrics has been proposed, that model has proved to capture the salient features of mechanical behavior of coated fabrics. As mentioned in chapter 2, even though that material model has been developed within the small deformation framework, it can also applied to large deformation problems in ABAQUS. Indeed, before the user material subroutine (UMAT) is called, the strain and stress tensors have been rotated to account for rigid body motion in every increment. Therefore, this material model has been used here for the numerical simulations, which have been carried out within finite deformation framework. Moreover, because the assumption of orthotropic elasticity has been widely used in practice for fabric membranes [12], therefore, for the

sake of comparison the orthotropic elasticity, whose material parameters are derived based on the Japanese standard MSAJ/M-02-1995 [13], is also used for the fabric membrane in the simulations.

II. The polyester belts

The polyester belts used in this work are fabricated by the company Load-Lok, England. Following the provided data from the manufacturer, the Young's modulus and Poisson's ratio are respectively equal to 2398 MPa and 0.31.

3.4 Numerical results and their validation

In this section, the results of the numerical simulation for the membrane and their validation are presented. Firstly, these numerical results and the experiment are compared qualitatively by means of contour plots of strains. For quantitative comparison, the strain fields in the membrane obtained from the numerical simulation are extracted along three paths (*cf.* fig. 3.9) and then compared with their counterparts from the experiment. The origin that was used to identify the paths on the membrane is the middle point of the lower edge A (*cf.* fig. 3.2) and all coordinates of the endpoints of the paths are identified in the prestress stage. Based on the distances between the origin point and the end points, the paths are defined as can be seen in fig. 3.9. However, the paths in the simulation are defined based on the positions of nodes, but the points on the membrane in the experiment on which the paths are defined are not coincident to the nodes in the numerical model. As a consequence, there are some differences in the paths of the numerical model and their counterparts from the experiment. Nevertheless, the differences are very small (from 4 to 12 mm) compared to the size of the membrane.

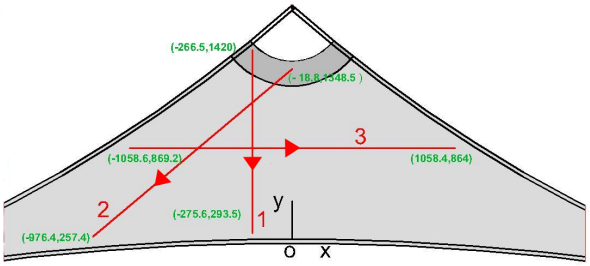

Figure 3.9: Schematic of three paths along which the strains are extracted.

3.4.1 Qualitative comparison

The strain fields obtained from the numerical simulation in which the fabric elasto-plastic model is used for the membrane are shown. As can be seen from figs. 3.10 to 3.12, the numerical simulation can capture the strain patterns in the membrane in every load stage. Especially, the agreement between the numerical simulation results and the experimental data tends to be better when the load increases. Moreover, we can observe from the graphs that in the numerical simulation, the model is perfectly symmetric with respect to the vertical direction. However, there is a small eccentricity in the experiment. It affects the strain field in the warp direction (*cf.* fig. 3.10).

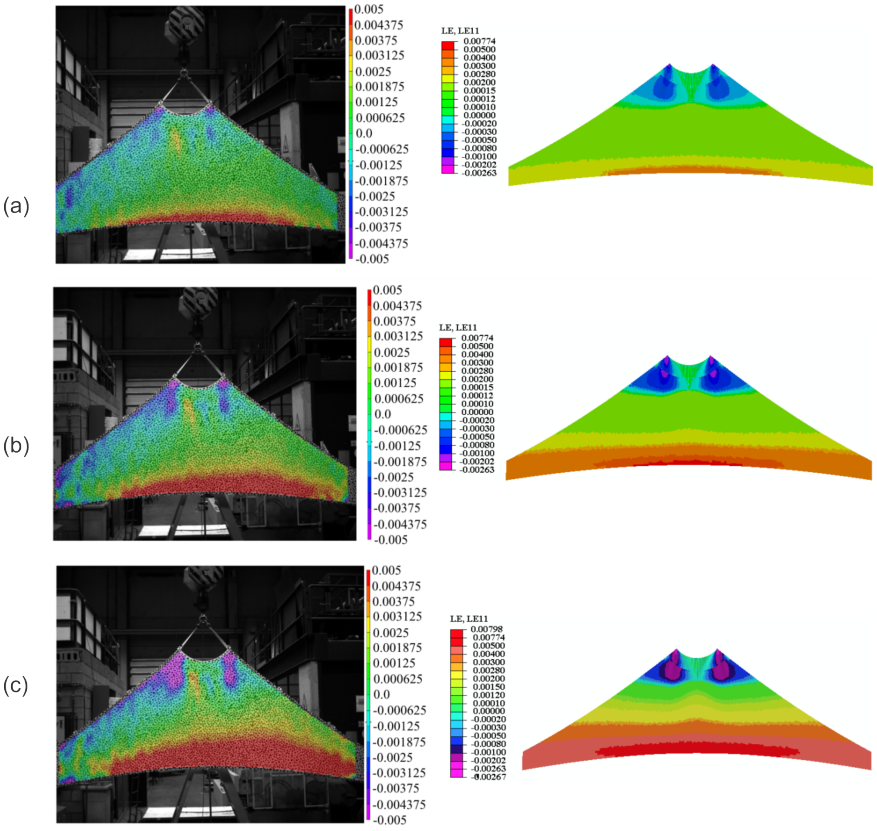

Figure 3.10: Strain in the warp direction ϵ_{xx} on the membrane from the experiment (left column) and the simulation (right column) when the load L_3 respectively equals 1.73 kN (a), 5.45 kN (b) and 7.81 kN (c).

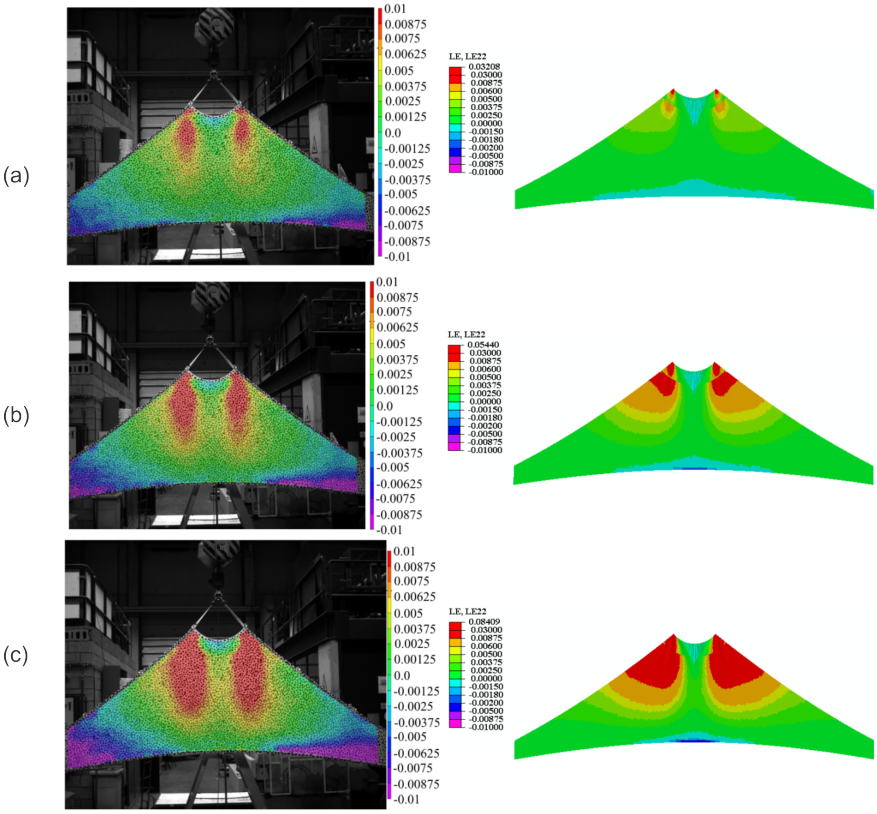

Figure 3.11: Strain in the fill direction ϵ_{yy} on the membrane from the experiment (left column) and the simulation (right column) when the load L_3 respectively equals 1.73 kN (a), 5.45 kN (b) and 7.81 kN (c).

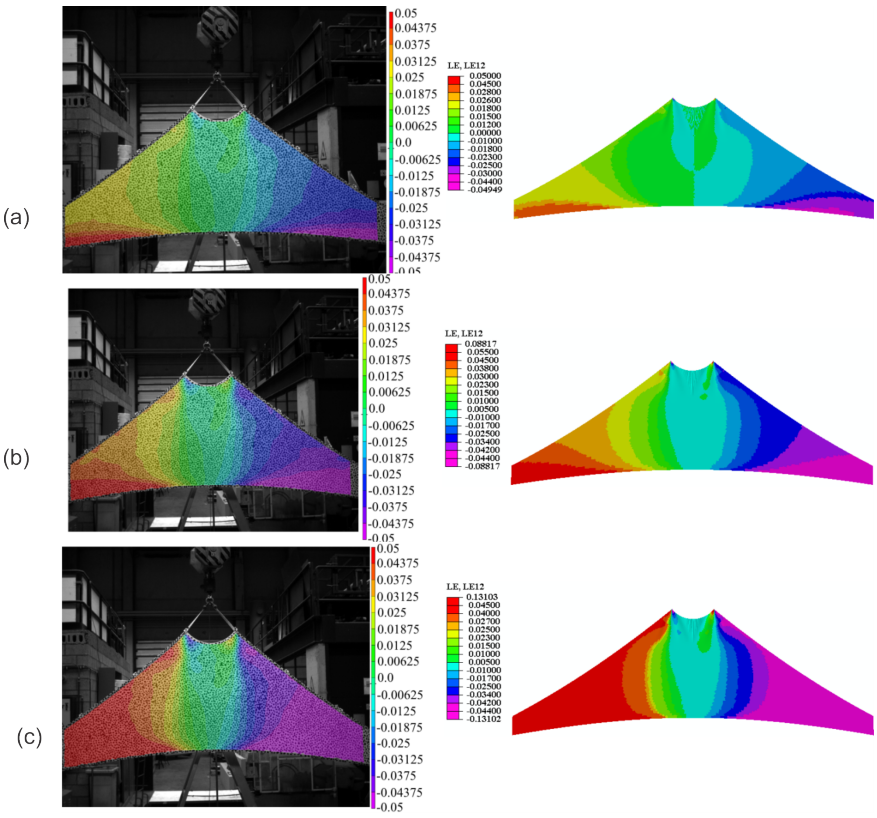

Figure 3.12: Shear strain ϵ_{xy} on the membrane from the experiment (left column) and the simulation (right column) when the load L_3 respectively equals 1.73 kN (a), 5.45 kN (b) and 7.81 kN (c).

3.4.2 Quantitative comparison

In figs. 3.13 to 3.21 , the strains in the warp and the fill directions as well as the shear strain in the membrane are extracted along the three paths, as illustrated in fig. 3.9. From these graphs, the fabric plasticity model provides a satisfactory strain prediction. In most of the figures, the predicted strains from this model have the same tendencies and their values are in the same order of magnitude as their counterparts from the experiment. It can be observed from these graphs that the higher the applied load, the better the correlation between the simulation results and the experimental data. Especially, the results for the strain in the warp direction along path 1 are in very good agreement with the experiment. It is also worth mentioning that the correlation in the strain in the fill direction and the shear strain is in higher level than those in the strain in the warp direction. This phenomenon can be explained by the fact that the strain values in the warp direction are rather small along path 2 and path 3 (maximum strains in the warp direction in these paths are *ca.* 0.004 and 0.002, respectively) and there is a lot of noise in the obtained experimental data (*cf.* figs. 3.16 and 3.19), while the other strains are much larger. Once, the strain value in the warp direction is larger, that is the case for the data in path 1 (*cf.* fig. 3.16), a very good correlation between the fabric plasticity model and the experimental data can also be seen. Therefore, it cannot be concluded that the fabric plasticity model cannot provide good prediction in the strain in the warp direction because of the deviations observed in figs. 3.16 and 3.19. Nevertheless, a large deviation can be seen in the top area of the membrane (close to edge B in fig. 3.2). The main reason for this discrepancy is that the fabric elasto-plastic model developed in chapter 2 was based on the experimental data in which only the most common stress ratios in the design stage of the membrane structure were considered. However, during the course of loading, the local stress ratio in a certain material point in the membrane can be different from the considered stress ratios. This is the case for the material points in the top area of the membrane, which experienced highly different stress ratios in the warp and fill directions. Furthermore, the problem related to the eccentricity (mentioned in section 3.4.1) causes larger discrepancies in the strains prediction along path 3. In addition, it can be observed from the results that using the orthotropic elasticity for modeling the fabric membrane leads to the poor strains prediction in all directions at every load stage and the discrepancies are more visible when the load increases.

The aforementioned discrepancies between the numerical results and the experiment are due to the following reasons:

- The material parameters for the orthotropic elasticity are derived based on [13]. This standard excludes the nonlinear behavior of the membrane in the first loading cycle and only considers the stable behavior. From experimental tests, it is clear that the stiffness in the fill direction and the shear stiffness derived from [13] are far stiffer than those in the first loading cycle (*cf.* chapter 2), while the stiffness in the warp direction is less stiff than the counterpart in the first loading cycle (*cf.* chapter 2). This reason explains why the results from the orthotropic elasticity do not match with the experimental data.
- As mentioned at the beginning of this section, there are some differences in the paths of the numerical model and the ones from the experiment. As a consequence, they contribute to the discrepancies in the results.
- The belt is also a kind of woven fabric and its mechanical behavior can be also nonlinear. Therefore, using the linear elasticity model for the belt can also contribute to the discrepancies in the results.
- There are some errors arisen from DIC measurements, e.g., the camera resolution, the noise of gray values, the different illumination conditions for the two cameras, the image contrast and the speckle pattern on the specimen surface [14].

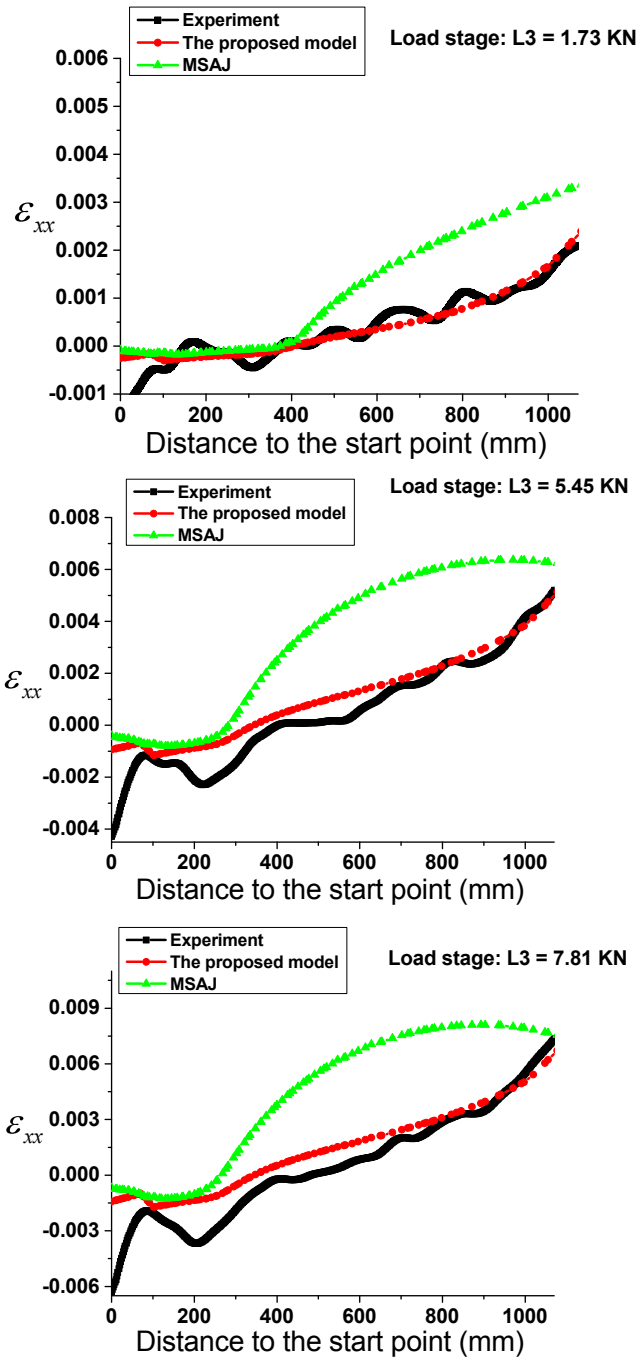

Figure 3.13: The strain in the warp direction ϵ_{xx} are extracted along path 1 in different load stages.

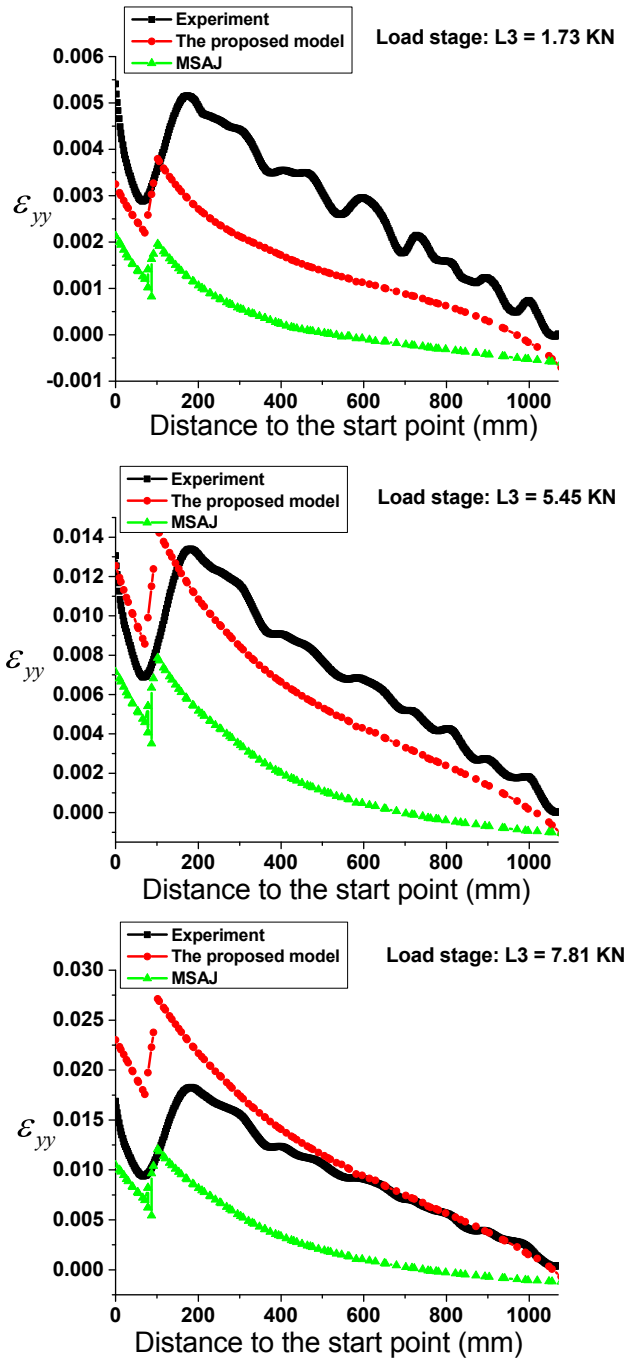

Figure 3.14: The strain in the fill direction ϵ_{yy} are extracted along path 1 in different load stages.

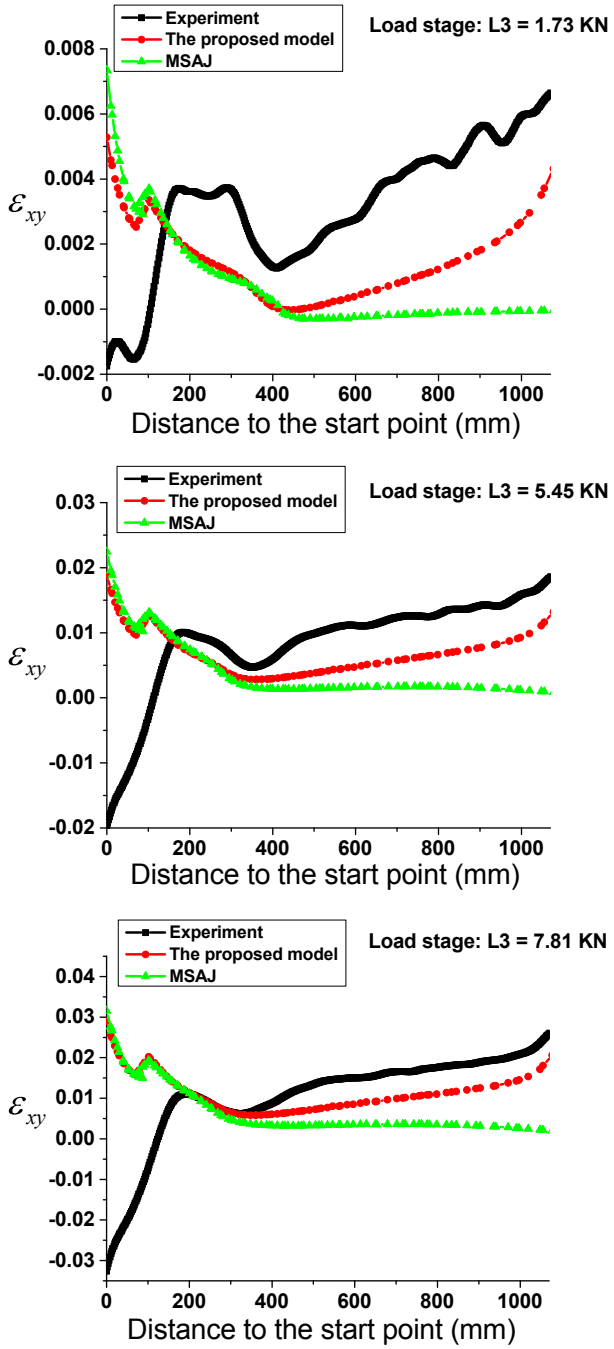

Figure 3.15: The shear strain ϵ_{xy} are extracted along path 1 in different load stages.

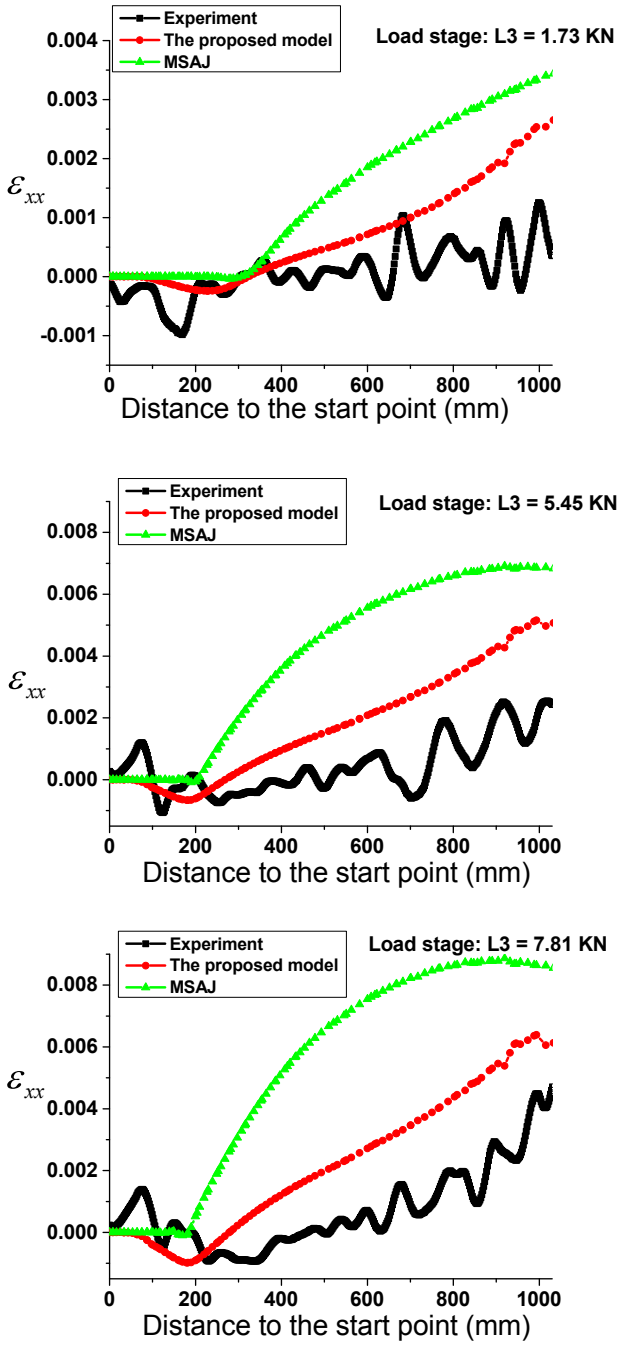

Figure 3.16: The strain in the warp direction ϵ_{xx} are extracted along path 2 in different load stages.

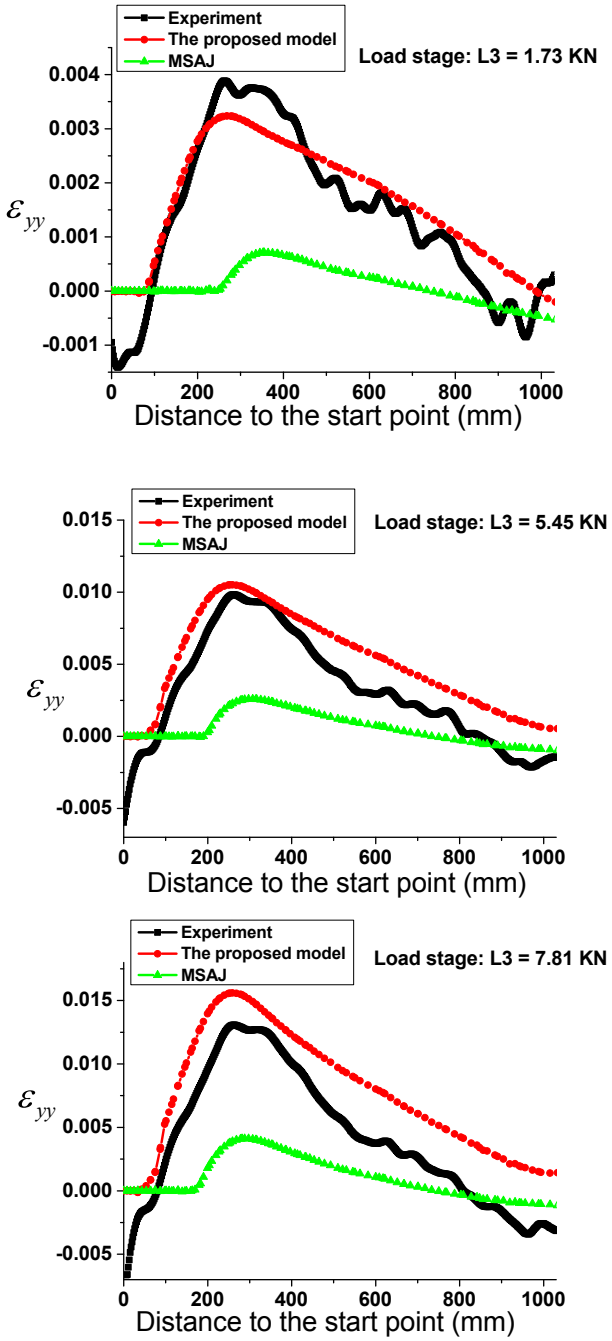

Figure 3.17: The strain in the fill direction ϵ_{yy} are extracted along path 2 in different load stages.

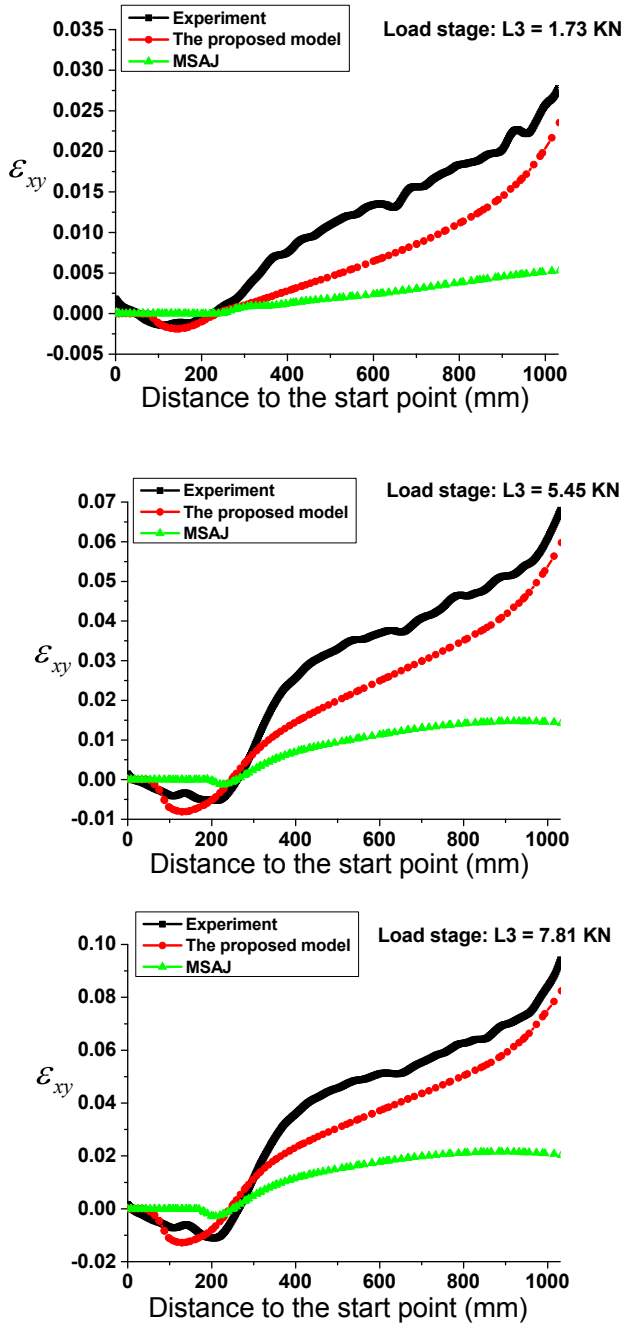

Figure 3.18: The shear strain ϵ_{xy} are extracted along path 2 in different load stages.

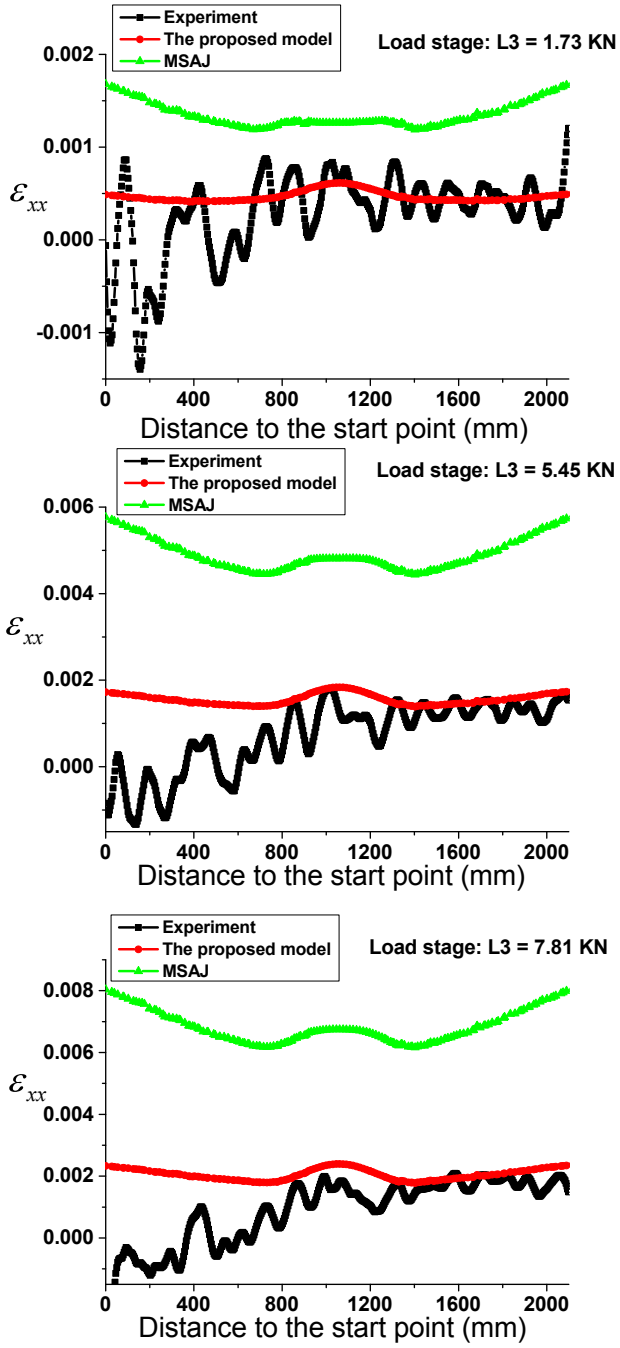

Figure 3.19: The strain in the warp direction ϵ_{xx} are extracted along path 3 in different load stages.

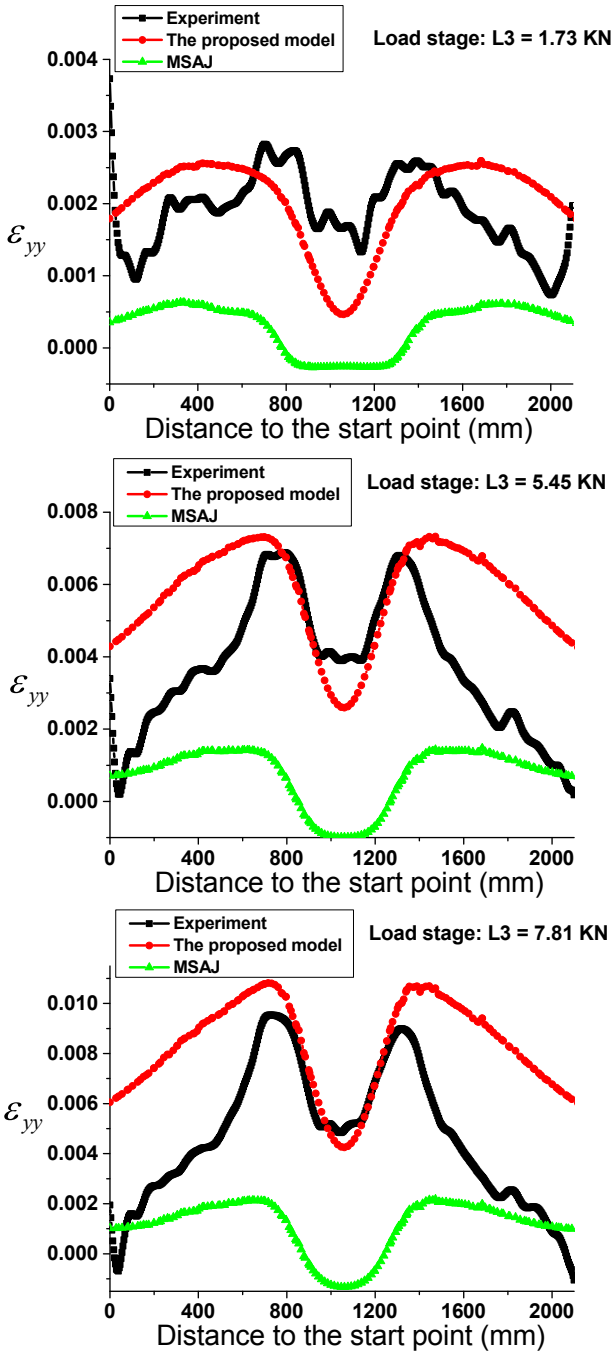

Figure 3.20: The strain in the fill direction ϵ_{yy} are extracted along path 3 in different load stages.

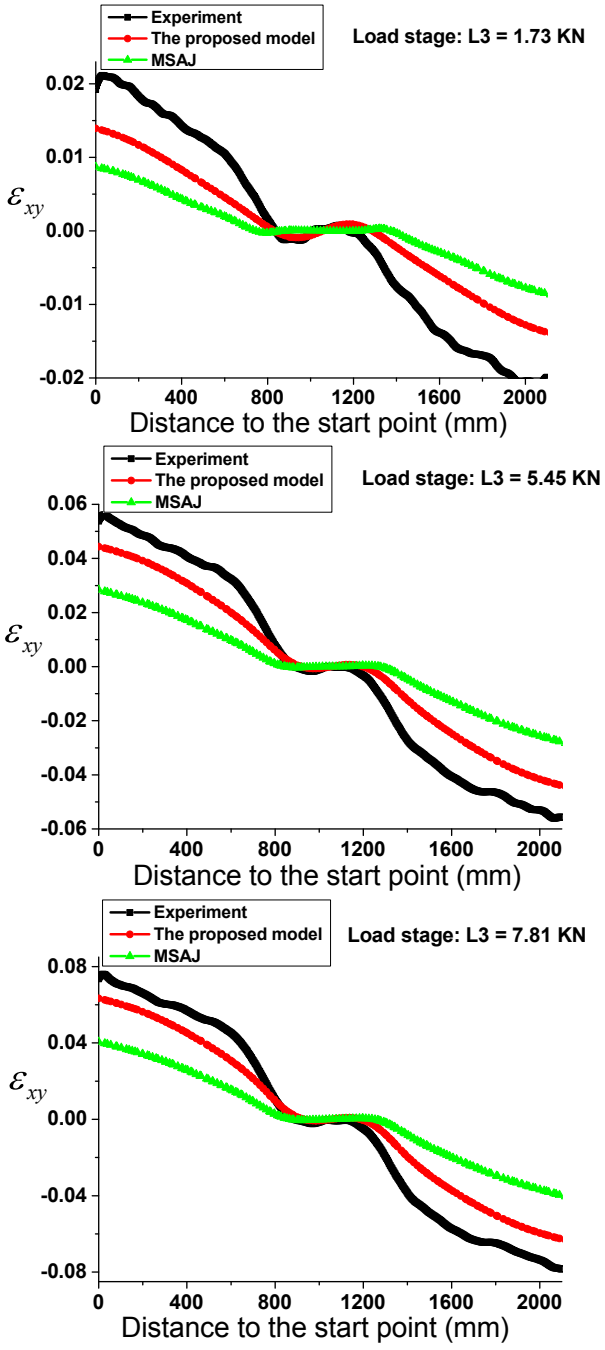

Figure 3.21: The shear strain ϵ_{xy} are extracted along path 3 in different load stages.

3.5 Conclusions

In this chapter, a nonlinear analysis of a tension fabric membrane structure is presented. From the results, the fabric elasto-plastic model shows good improvements in strains prediction compared with the orthotropic elasticity model, that has been widely used in the research field. The success of this study is the premise for further investigation of the feasibility of the design concept of the Context-T structure. Moreover, there are few benchmarks to validate numerical results in the research field, the case study considered in this chapter can serve as a benchmark for numerical simulations. In this way, this work can contribute to the development of consistent methodologies for design and analysis of tension membrane structures.

Bibliography

[1] T. D. Dinh, A. Rezaei, S. Puystiens, M. Van Craenenbroeck, K. Carbonez, L. De Laet, M. Mollaert, D. Van Hemelrijck, W. Van Paepegem, A study of tension fabric membrane structures under in-plane loading: Nonlinear finite element analysis and validation, Composite Structures 128 (2015) 10–20. doi:10.1016/j.compstruct.2015.03.055.

[2] K.-U. Bletzinger, E. Ramm, Structural optimization and form finding of light weight structures, Computers & Structures 79 (22) (2001) 2053–2062.

[3] K.-U. Bletzinger, M. Firl, J. Linhard, R. Wüchner, Optimal shapes of mechanically motivated surfaces, Computer Methods in Applied Mechanics and Engineering 199 (5–8) (2010) 324–333. doi:10.1016/j.cma.2008.09.009.

[4] P. P. Véron, P. Trompette, P. J. C. Léon, Integrated design and collaborative engineering of fabric structures, Engineering with Computers 14 (1) (1998) 23–35. doi:10.1007/BF01198972.

[5] F. Otto, Tensile Structures; Design, Structure, and Calculation of Buildings of Cables, Nets, and Membranes, M.I.T. Press, 1967.

[6] J. B. Pargana, D. Lloyd-Smith, B. A. Izzuddin, Fully integrated design and analysis of Tensioned Fabric Structures: Finite elements and case studies, Engineering Structures 32 (4) (2010) 1054–1068. doi:10.1016/j.engstruct.2009.12.032.

[7] P. Gosling, B. Bridgens, A. Albrecht, H. Alpermann, A. Angeleri, M. Barnes, N. Bartle, R. Canobbio, F. Dieringer, S. Gellin, W. Lewis, N. Mageau, R. Mahadevan, J.-M. Marion, P. Marsden, E. Milligan, Y. Phang, K. Sahlin, B. Stimpfle, O. Suire, J. Uhlemann, Analysis and design of membrane structures: Results of a round robin exercise, Engineering Structures 48 (2013) 313–328. doi:10.1016/j.engstruct.2012.10.008.

[8] M. Mollaert, L. D. Laet, J. Roekens, B. Belkassem, (un)folding the membrane in the deployable demonstrator of context-t, in: E. Onate, B. Kroplin, K. Bletzinger (Eds.), Textile Composites and Inflatable Structures V (STRUCTURAL MEMBRANES 2011), 2011, pp. 41–50.

[9] M. Van Craenenbroeck, S. Puystiens, L. De Laet, D. Van Hemelrijck, W. Van Paepegem, M. Mollaert, Integrated analysis of kinematic form active structures for architectural applications: Experimental verification, Engineering Structures 123 (2016) 59–70. doi:10.1016/j.engstruct.2016.05.032.

[10] S. Puystiens, M. Van Craenenbroeck, L. De Laet, D. Van Hemelrijck, W. Van Paepegem, M. Mollaert, Integrated analysis of kinematic form active structures for architectural applications: Design of a representative case study, Engineering Structures 124 (2016) 376–387. doi:10.1016/j.engstruct.2016.06.038.

[11] Hibbit, Karlsson, Sorensen, ABAQUS/Standard Analysis User's Manual, Hibbit, Karlsson, Sorensen Inc., 2014.

[12] T. Nouri-Baranger, Computational methods for tension-loaded structures, Archives of Computational Methods in Engineering 11 (2) (2004) 143–186.

[13] MSAJ Testing Method for Elastic Constants with commentary (Feb. 1995).

[14] K. Carbonez, Finite element simulation of tensioned membrane structures in deployable systems, Master's thesis, Ghent University (2013).

Chapter 4

A Shape Optimization Approach to Integrated Design and Nonlinear Analysis of Tensioned Fabric Membrane Structures with Boundary Cables

In the previous chapter (*cf.* chapter 3), it has been shown that the fabric elasto-plastic material constitutive law can provide better results in the fabric membrane structure analysis. However, in order to use this material model in a 3-D structure analysis we need to have a dedicated design and analysis method. In this chapter, such method is developed within the framework of shape optimization. This method is then applied to design and analysis of a hypar structure with boundary cables. The content of this chapter has been published in [1].

4.1 Introduction

Typically, the fabric membrane is tensioned by using the supporting structures and the prestressed cables [2–5]. Generally, there are two design

methods, *viz*., a conventional design method and an integrated one. In the conventional one, the design process of the membrane structures can be divided into three steps, *viz*., form-finding, structural analysis and cutting pattern generation [6–14]. Comprehensive studies for this design method can be found in the monographs of Lewis [15] and Forster and Mollaert [16]. In the integrated design method, the above three steps are combined into one single step [13, 17–25]. A literature study of these design methods is presented in the following subsections.

4.1.1 Conventional method in design and analysis of tension membrane structures

Different from conventional structures, the shape of a fabric membrane structure is a priori unknown. In order to find this shape, form-finding has to be performed. In the form-finding stage, the layout of the boundary cables and kinematic boundary conditions are specified. The prestress distribution in the membrane, which is supposed to be uniform and isotropic or orthotropic, is prescribed and not dependent on the deformation. The shape of the membrane is formed such that the membrane is in equilibrium with the given prestress fields [2, 19]. Because the stress field is supposed to be given regardless of how it has been generated, it is therefore not necessary to specify precisely the material model at this stage. However, to avoid the numerical singularities, some authors have used a very small value, but different from zero for Young′s moduli of the fabric membrane and the cables. They referred to the material models in this stage as fictitious materials [2, 13]. In Ref. [26], the most common form-finding methods, such as the force density method, the dynamic relaxation method and the updated reference strategy are presented and discussed in details. Nevertheless, in Ref. [20] the authors argued that the stress fields in the membrane cannot be imposed and are unknown in many cases. Moreover, a feasible shape that can be found from this approach is limited to a surface with homogeneous stress, but from an engineering viewpoint prestress fields should deviate from a homogeneous and isotropic distribution in order to fully exploit the mechanical capacity of the membrane materials to resist the structural effects of loadings [19].

The form-finding is followed by a materialization stage. In this stage, the actual material properties of the fabric membrane and the boundary cables are used and the support locations are held fixed [13, 27]. Once the

equilibrium shape of the membrane structure is found, the three dimensional geometry of the membrane structure with its associated stress state is provided. Subsequently, the structural analysis is conducted in which the membrane structure is subjected to environmental loads. As shown in Ref. [28], material nonlinearities should be included in this step. However, the characterization of the mechanical properties of architectural fabrics demands data from uniaxial tests, biaxial tests and a shear test. It is time-consuming, expensive and even when these data are available, how to interpret and use them is not well-established [6, 19]. Thus far, the only standard for interpreting biaxial test data is still the Japanese MSAJ/M-02-1995 standard [29]. Due to these difficulties, the linear orthotropic elasticity is widely used in common practice [6, 27, 30]. To compensate for this oversimplification, designers have to use a very high safety factor [31].

Moreover, the fabric membranes are supplied in rolls of 1-5 m widths and have planar shapes, so a cutting pattern generation is needed to determine the geometry of the unstressed fabric membrane panels that can be welded together to make up the complicated curved three dimensional surface resulting from form-finding [10, 13, 23]. Indeed, the cutting pattern generation is an inverse mechanical problem and to solve it, the deformation process needs to be traced back. In conventional cutting pattern generation, the three dimensional surface with its associated stress is divided into subsurfaces using the geodesic line technique. Subsequently, the linear orthotropic elastic material law is used in an unloading step to determine the stress-free panels. Because the membrane material used for the cutting pattern has never been loaded before, the first stress-strain curve of the biaxial test of the membrane material should be used [10]. As can be seen in [32–34], fabric membrane materials behave strongly nonlinear, especially, irreversible deformation can occur very early in the loading stage. Thus, using linear orthotropic elasticity, designers exclude all of the nonlinear effects. Aware of this weakness in the method, designers have to apply compensation for the cutting patterns. However, the method for applying compensation has not been well-documented yet and many problems associated with cutting pattern generation still occur, especially when the structure has a high curvature shape [23].

4.1.2 Integrated approach for design and analysis of tension membrane structures

Three-dimensional curved membrane structures are undevelopable, thus the planar membrane panels cannot form these curved surfaces without deformation [10, 13, 19]. Due to the fact that in the conventional method, the form-finding and patterning generation stages are decoupled, additional stresses that arise in the planar membrane panels are not taken into account. However, these stresses are not so small and cannot be neglected [18, 19, 22, 25]. As a consequence, wrinkles can appear in the structure and the final shape, which is formed by assembling the planar membrane panels, might be very different from the one determined in the form-finding stage. The use of advanced material models for architectural fabrics is difficult in the conventional design method, because in these material models [18, 33, 34], the mechanical behavior of these fabrics is path-dependent. In other words, for a given stress value, there is no unique value for the strain. There are different material parameters for a material point in the fabric. The values assigned to these parameters for the material point depend on the load level, the load history as well as the stress ratio it has experienced. In the conventional approach, we do not start the structural analyses with stress-free fabric panels, but with a 3D curved surface and its associated prestresses. After materialization stage, the prestresses in the membrane are not uniform, but different from point to point. As a consequence, it is impossible to assign proper material parameters for the membrane.

In order to overcome the aforementioned drawbacks of the conventional method, the integrated design procedure was proposed by Haber et al. [21]. Further developments can be found in [18–20, 22–25, 35]. In this method, the influence of the cutting pattern can be integrated in the form-finding and structural analysis steps based on correct nonlinear continuum mechanics, which can provide a reliable analysis of tension fabric membrane structures [18, 19]. Concisely, shapes of the cutting patterns are iteratively adjusted in this approach in such a way that the resulting structure assembled by these patterns has a permissible stress distribution and the difference between the actual stresses on the membrane and the designed prestresses is minimized. Different methods have been proposed within this framework. In the work of Kim and Lee [22], the authors used the finite element method for analyses and proposed a method to determine optimum cutting patterns. Firstly, a form-finding was carried

out to find the reference 3D shape and it was followed by initial cutting patterns. In this step, the geometric projection technique was used. Elements in the resulting 2D panels were assumed to have the same stress values as the ones in the corresponding elements in 3D. Then, the initial stress-free cutting patterns were determined by unloading. Subsequently, kinematic boundary conditions are imposed on these patterns to form the 3D shape found in the first step. The stress differences were treated as residual stresses for the previous cutting patterns. To achieve stress free panels, unloading was carried out and new cutting patterns were generated. In the works of Ohsaki and Fujiwara [25] and Ohsaki and Uetani [24], the authors used 3D displacements as principal variables. They developed so-called developability conditions to convert 3D membrane surfaces with their associated prestress into stress-free panels. In the work of Bletzinger et al. [19], the authors proposed two different methods to find the optimum cutting patterns, *viz.*, least square optimization and minimization of stress difference energy. In both methods, the weak forms of objective functions were derived and discretized by finite element method. By solving the equations that are resulting from setting Gateux-derivatives of the objective functions equal to zero, the nodal coordinates of the cutting patterns were identified. As a consequence, the planar cutting patterns were determined. Recently, Punurai et al. [23] proposed a method in which they also considered the displacements of the 3D membrane surface as principal variables and used genetic algorithms to obtain the optimum cutting patterns. In these works, the authors have claimed that the methods could be applicable for nonlinear material models, but in their numerical examples, linear elasticity was used for the fabric membrane. Moreover, the interaction between the boundary cables and the membrane was not considered. This interaction and the nonlinear material model were taken into consideration in the work of Pargana et al. [18]. In that article, the authors presented nonlinear finite element formulations of a quadratic membrane element and a quadratic sliding cable element. The nonlinear material model developed in Ref. [32] was also used. However, in their work, adjustments of the membrane′s shape and the cables′s length were done manually.

The work presented in this chapter can be considered as a continuing study of the integrated design method in tension fabric membrane structures. In this work it is assumed that the membrane is initially flat and stress-free. It means that cutting pattern generation is not considered, since any size of the flat membrane can be assembled, as long as the weld-

ing respects the assumptions of a flat and stress-free panel. At first, the lengths of the boundary cables and shape of the planar fabric membrane, which can be obtained from welding different fabric panels, are estimated. Then, a deployed shape of the membrane structure is formed by imposing kinematic boundary conditions. During these steps, the fabric elasto-plastic material model, which has been proposed in chapter 2, is used for the membrane. The interaction between the membrane and the boundary cables is also taken into account. In order to evaluate the quality of the structure, the stresses in the structure are compared with the reference prestresses, which are the values designers choose to provide stiffness for the structure. The sum of differences between the current stresses in the membrane and the reference prestresses is used as a target function for the optimization procedure. The procedure is iterated to find the minimum value for the target function. In each iteration, the lengths of the boundary cables and the shape of the planar fabric membrane are adjusted. At the end of the procedure, the stresses in the three-dimensional membrane structure should be very close to the reference ones and the planar fabric membrane used to form the three-dimensional structure can be determined.

The outline of this chapter is as follows. In the next section, details of the shape optimization of tension membrane structures are presented. Subsequently, numerical results with shape optimization are presented to design and analyze a hypar structure. The chapter ends with some conclusions.

4.2 Shape optimization of a planar fabric membrane

This section commences with a description of the implementation of the boundary cable elements. Then, details of the shape optimization procedure are provided.

4.2.1 Sliding cable elements

In tension membrane structures, prestresses are introduced in the membrane by stretching the boundary cables at the edges of the membrane.

These cables may fit within fabric sleeves and may slide when the membrane structure is loaded [3, 18]. In common practice, the cable is modeled as a sequence of truss elements that share the nodes with the membrane. By doing this, it is assumed that there is no sliding movement between the cable and the membrane. As a consequence, the nonlinear interaction, referred to as boundary nonlinearity in Ref. [36], between these structural elements is excluded. It can substantially affect the response of the membrane under loads [3, 17, 18]. In this work, the sliding cable is modeled by using slip-ring element in ABAQUS [37]. This kind of element can be used to model material flow and stretching between two points of a cable system (*cf.* fig. 4.1). When using this element at both nodes of the connector, an additional degree of freedom, so-called material flow is activated. By attaching slip-ring elements to each other, the whole cable system can be modeled (*cf.* fig. 4.2). The following assumptions are used in this work for this kind of element: (i) the sliding cable behaves elastic, (ii) the cross section of the cable is constant during the course of deformation and (iii) there is no frictional sliding between two integrated elements.

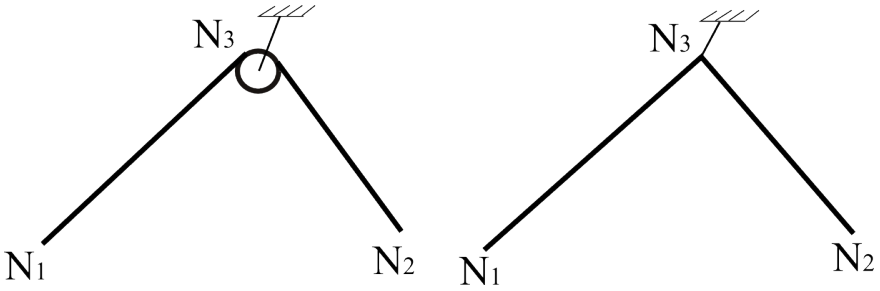

Figure 4.1: The slip-ring element used to simulate the sliding cable (left: reality; right: modeling) [37].

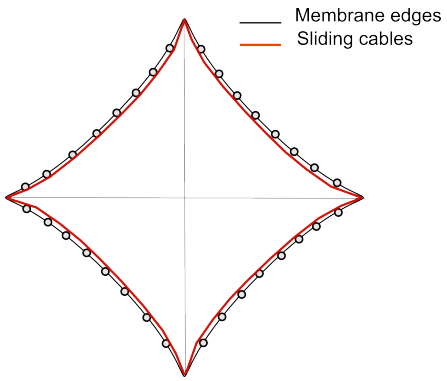

Figure 4.2: Sliding cables are implemented at the edges of a hypar structure. In this case, nodes that lay on the edge of the membrane are considered as pulleys.

4.2.2 Shape optimization

In this work, the shape of a planar and stress-free fabric panel is optimized such that the total stress deviations in the resulting 3D membrane and the reference one is minimized. As mentioned in [38–40], the way chosen to describe the shape plays a vital role in shape optimization and substantially affects the reliability of the results. In the finite element framework, there are three methods currently used to describe the shape of a structure, *viz.*, (i) the boundary nodes, (ii) the boundary shape is described by polynomials and (iii) the boundary shape is described by spline or spline blending functions. To avoid computational expenses as well as numerical instabilities, which have been mentioned in Ref. [38], we have chosen spline functions, which are composed of low order polynomial pieces that are combined to maximize smoothness, to describe the boundary shapes of the fabric patterns. The positions of the control points are the design variables for this optimization problem. The optimization is formulated as follows:

Objective function:

$$W(\mathbf{P}) = w_1 \int_a (\boldsymbol{\sigma}^{\text{membrane}} - \boldsymbol{\sigma}^{\text{membrane}}_{\text{ref}}) : (\boldsymbol{\sigma}^{\text{membrane}} - \boldsymbol{\sigma}^{\text{membrane}}_{\text{ref}}) \mathrm{d}a + w_2 \int_l (\boldsymbol{\sigma}^{\text{cable}} - \boldsymbol{\sigma}^{\text{cable}}_{\text{ref}}) : (\boldsymbol{\sigma}^{\text{cable}} - \boldsymbol{\sigma}^{\text{cable}}_{\text{ref}}) \mathrm{d}l. \tag{4.1}$$

Constraints:

$$\mathbf{P}_l \leq \mathbf{P} \leq \mathbf{P}_u \tag{4.2}$$

where the vector $\mathbf{P}$ contains displacements of the control points, $\mathbf{P}_l$ and $\mathbf{P}_u$ are respectively their lower and upper values. $\boldsymbol{\sigma}^{\diamond}$ is the Cauchy stress tensor on the 3D structure and $\boldsymbol{\sigma}^{\diamond}_{\text{ref}}$ is the reference stress tensor. a is the area of the 3D surface and l is the length of the deformed cable. w_1 and w_2 are the weights whose values reflect the importance of the associated components in the target function. $' : '$ is the tensor contraction operator.

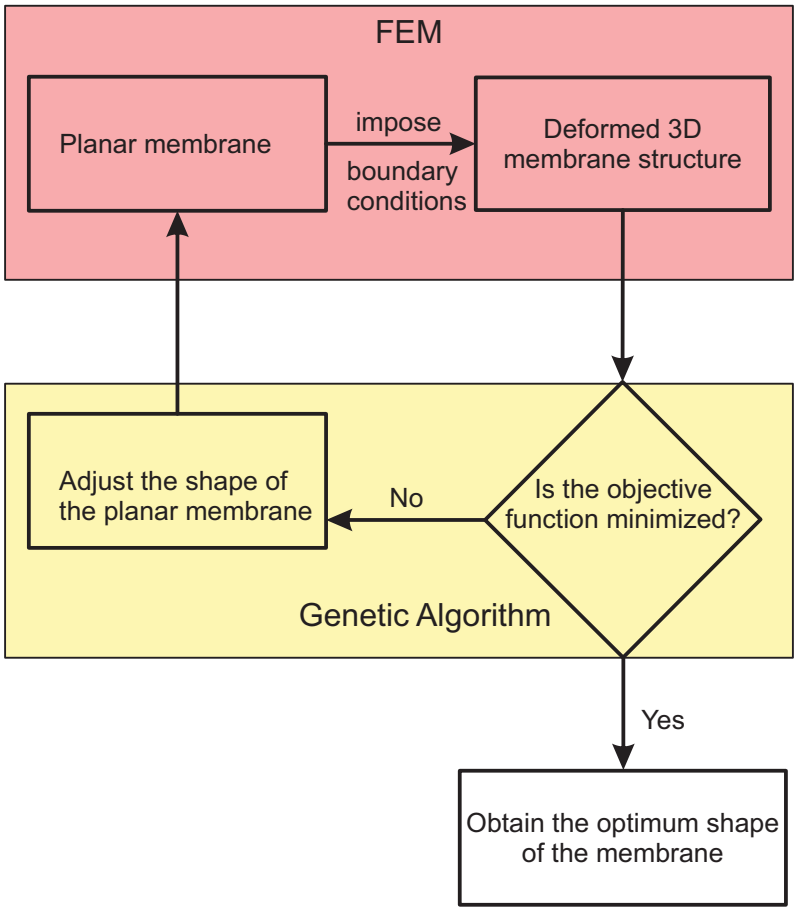

Figure 4.3: The shape optimization procedure used to determine the optimum cutting pattern

The objective function is here calculated by using the finite element results obtained from ABAQUS/Standard [37]. Although the objective func-

tion is formulated in stress deviations, when we do post-processing, the output for the boundary cables is the force, not the stress. Thus, the unit of the objective function in the simulation is not consistent. However, the cross-sectional area of the cable does not change during the simulation. Therefore, it does not affect the result. Moreover, in the work of Punurai et al. [23], those authors have recognized that using the gradient based optimization algorithms for finding the optimum shape of the fabric panels led to poor results because the optimization algorithm was trapped at local minima. To overcome that problem, those authors have used genetic algorithms. Therefore, in this study the genetic algorithm (GA) in MATLAB [41] is also chosen as an optimizer (*cf.* fig. 4.3). GA is a method to solve optimization problems based on the principles of evolution and natural selection process. This method is especially well-suited for problems in which the objective function is discontinuous and highly nonlinear. In this algorithm, a population of individual solutions is modified in iterated steps. The performance of each individual is evaluated by means of a fitness function. In our case, the fitness function is the objective function W and an individual is a tuple of the position vector of the control points on the boundary edges of the membrane. At each step, individuals are selected and recombined randomly through genetic operators, *viz.*, reproduction, crossover and mutation [23], to produce the children for the next generation. The individuals who perform well are copied directly to the next generation while the ones with poor performance are replaced by new members. The implementation of the shape optimization is summarized in table 4.1 and fig. 4.4.

Table 4.1: Algorithm for implementation of the shape optimization for tension fabric membrane structures.

(i)	**Pre-processing**. Given initial values for design variables $\boldsymbol{P}$, the weight factors w_i in the objective function W and the reference stresses in the cable and in the membrane $\rightarrow$ Create an input file for ABAQUS/Standard
(ii)	**Finite Element Analysis** Running the analysis in ABAQUS/Standard and check if the simulation can go to the end of the load step
(iii)	**Post-processing**. If the simulation is prematurely terminated because of divergence $\rightarrow$ assign the penalty factor for the objective function Else $\rightarrow$ calculate the objective function using the formula eq. (4.1)
(iv)	**Optimization** If terminated conditions for optimization are reached, the optimization process stops. Otherwise, new values for the design variables are created and go to step (i)

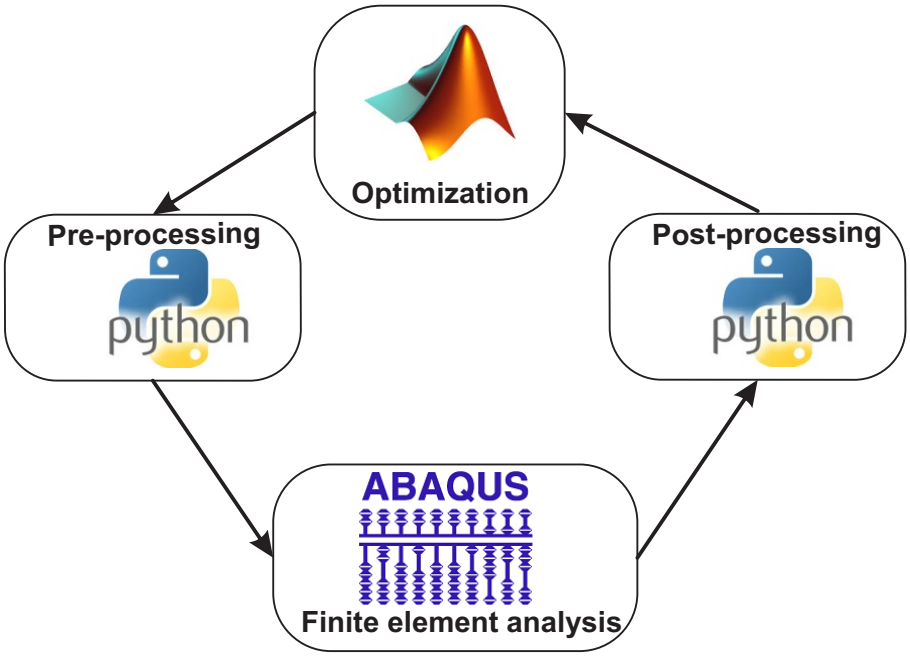

Figure 4.4: Software implementation of the shape optimization.

4.3 Numerical results

In Ref. [6], the authors studied the importance of the material properties and structural geometry in tension membrane structures. From that work, the hypar structure exhibits more complex structural behavior under loading and is very sensitive to changes in material properties, especially when it has high curvature. For these reasons, design and analysis of a hypar structure tensioned by cables around the perimeters is considered as a case study in this chapter.

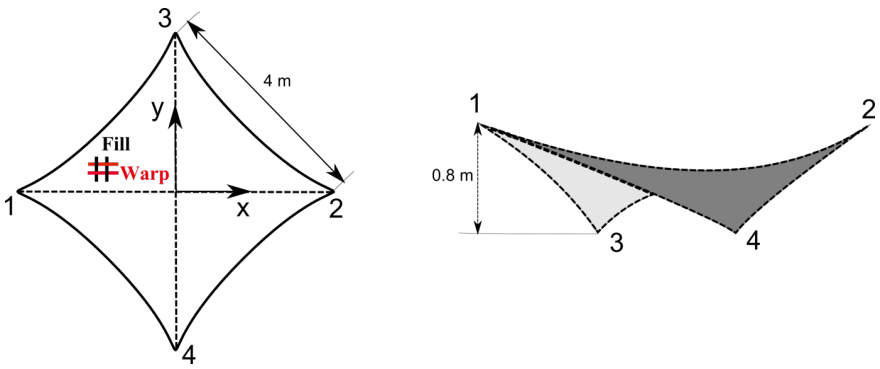

Figure 4.5: Schematic configuration of the simulated hypar structure.

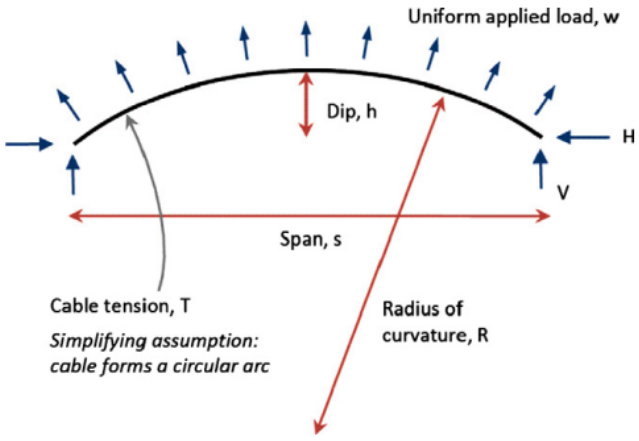

Figure 4.6: Relation between cable curvature and cable tension force (reprinted from [6]).

Figure 4.5 shows the dimensions of the membrane. The material used for this membrane is the same PVC-coated fabric studied in the previous chapters (*cf.* chapter 2, chapter 3). The design objective is to achieve a stress field as uniform as possible and close to 5 MPa in the membrane. The design tension force in the cable is 20 kN. These prestress values are chosen in such a way that the dip to span ratio (*cf.* fig. 4.6) is *ca.* 1:6. This ratio is considered as a rule of thumb for efficient and aesthetically pleasing design [6]. In this case study, the fabric elasto-plastic material model is used for the membrane. Moreover, for the sake of comparison, the orthotropic elasticity is also used for the membrane. Material parameters of these models can be seen in chapter 2, thus for the sake of brevity, they are not presented here. In addition, the effective stiffness [1] (*i.e.*, Young′s modulus multiplied by cross sectional area) of each cable is 2000 kN. Moreover, the following assumptions are used in the case study:

- The simulation is performed in a large deformation framework, but the strains are only in the range of small to moderate. This assumption is used because the fabric elasto-plastic model developed in chapter 2 is not designed for large strains.
- The membrane welded (tied) from different fabric panels is assumed to be flat and stress-free.
- The welded membrane is assumed to be seamless.

Following the second and the third assumptions, we can optimize the welded membrane instead of individual fabric panels to achieve the design objective. There is no need for cutting pattern optimization, since the optimized flat shape of the membrane is stress-free and can be cut into smaller panels.

During the shape optimization procedure, the positions of the control points on the boundary edges are changed. The distribution and the directions of the in-plane movement of these points are presented in fig. 4.7. For each edge, several control points are required to govern the sag of the edge as well as the compensations in the warp and fill directions. Here it is assumed that the initial shape of the flat membrane is symmetric with respect to the x and y axes. Therefore, the number of design variables is reduced to three. $P_i(i = \overline{1,3})$ in fig. 4.7 are denoted for the displacements

1. This terminology was also used in [27].

of the control points at the boundary edges with the associated directions visualized by the arrows. While the sign convention for P_2 and P_3 is based on the mentioned coordinate in fig. 4.7, P_1 always receives a non-negative value. In order to identify the initial estimate for these variables, the following formula is used to correlate the cable curvature and cable tension force [6, 42]:

$$T = \sqrt{(\frac{ws^2}{8h})^2 + (\frac{ws}{2})^2}. \tag{4.3}$$

The explanation of these notations can be seen in fig. 4.6. Here, T is the

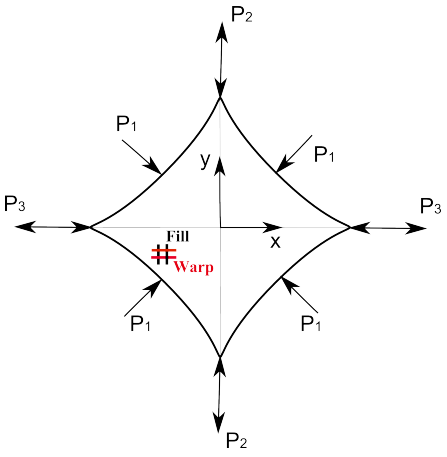

Figure 4.7: Chosen design variables for the shape optimization (left: distribution of control points; right: movement directions of control points).

tension force in the cable (kN), w is a uniform load that comes from the pretension force in the membrane (kN/m), s is the span of the membrane (m) and h is the sag of the membrane (m). Following eq. (4.3), the values of $P_i (i = \overline{1,3})$ are determined (*cf.* table 4.2).

Table 4.2: Initial values for optimum parameters

P_1(m)	P_2(m)	P_3(m)
0.577	0.0	0.0

Moreover, it is assumed that the fabric is cut in such a way that the warp and fill directions are respectively aligned with the x and y axes

(*cf.* fig. 4.5). The aforementioned design variables are bounded as follows:

$$\begin{aligned} 0 \leq P_1 &\leq \frac{a\sqrt{2}}{2}, \\ \frac{-a}{4} \leq P_2 &\leq \frac{a}{4}, \\ \frac{-a}{4} \leq P_3 &\leq \frac{a}{4}, \end{aligned} \tag{4.4}$$

where a=4 m.

During the course of simulations, it is recognized that a certain combination of the values of the design variables can lead to numerical divergence. When this happens, the objective function cannot be evaluated by using eq. (4.1) and a great number has to be assigned to the objective function. The value for this great number is judicious. By experimenting with different values, the one of 6000 can provide a good result in the present case study. Moreover, we use w_1=0.3 and w_2=0.7 for the weight factors in the objective function. Regarding the MATLAB/GA toolbox, the parameters are set as follows: the number of generations is equal to 250 and in each generation there are 50 individuals. The initial population is created by the *gacreationlinearfeasible* function. To create crossover children, the *crossoverintermediate* function is used. The proportion of crossover is set to 0.6 and the elite count, which specifies how many individuals in the current generation are guaranteed to survive to the next generation, is set to 3. The *fitscalingrank* function is used to scale the values of the objective function. The migration direction, fraction and interval are, respectively, set to *forward*, 0.2 and 20. The *selectionstochunif* function is used to select parents of crossover and mutation children. Moreover, the objective function is evaluated in parallel.

In order to gain a better understanding of how sliding cables affect the stress distribution in the membrane, the two following simulations without shape optimization are carried out first. In the first simulation, the sliding cables are attached to the edges of the membrane, in the second one the sliding cables are replaced by truss elements tied to the membrane. In fig. 4.8, the stress distributions in the membrane obtained from these simulations are shown, respectively. The results highlight big differences in the stress fields when the nonlinear interaction between the cable and the membrane is excluded from the structural analysis by using truss elements. When the sliding cables are used, the stresses in the membrane are more uniform compared with the counterparts when the

truss elements are used. In addition, the maximum stress values in the latter case are also higher.

In the aforementioned simulations the initial shape of the membrane is identified by using the empirical formula, *cf.* eq. (4.3). However, as can be seen from fig. 4.9 (the color band is now limited at 10 MPa), the stresses in the membrane are very different from the target stress (5 MPa) even when sliding cables are used. Thus, it is necessary to perform shape optimization to have a better performance structure in this case.

In figs. 4.10 and 4.11, convergences of the GA are shown. In these figures, the black markers denote the best fitness values, while the green ones denote the averages of the fitness values in each generation. As can be seen from these figures, the best fitness converges very fast, *i.e.*, after 30 generations in the case of orthotropic elasticity and 120 generations in the case of fabric elasto-plasticity.

The optimum parameters for $P_i(i = \overline{1,3})$ for the linear orthotropic elasticity and fabric elasto-plasticity models are summarized in table 4.3.

Table 4.3: Values of the design variables obtained from: column 1, initial estimate; column 2, optimization when linear orthotropic elasticity is used for the membrane; column 3, optimization when the fabric elasto-plasticity is used for the membrane.

	Initial estimate	Orthotropic elasticity	Fabric plasticity
P_1 (m)	0.577	0.350	0.482
P_2 (m)	0.0	0.020	-0.011
P_3 (m)	0.0	0.021	0.032

The influence of the material model that is chosen to model the fabric is highlighted in fig. 4.12. The optimum shapes of the membrane with the linear orthotropic elasticity and the fabric elasto-plasticity are shown respectively in the figure. A visible discrepancy between these shapes is also exposed. Moreover, as can be seen from table 4.3 the compensations in the warp and fill directions are almost the same in case of linear orthotropic elasticity. This is due to the difference between the stiffness in these directions not being large in that case. However, these values are quite different in case of the fabric elasto-plasticity because of the strong orthotropy of the coated fabric. In figs. 4.13 and 4.14, the evolution of the force in the cable versus time and the stress distributions in the

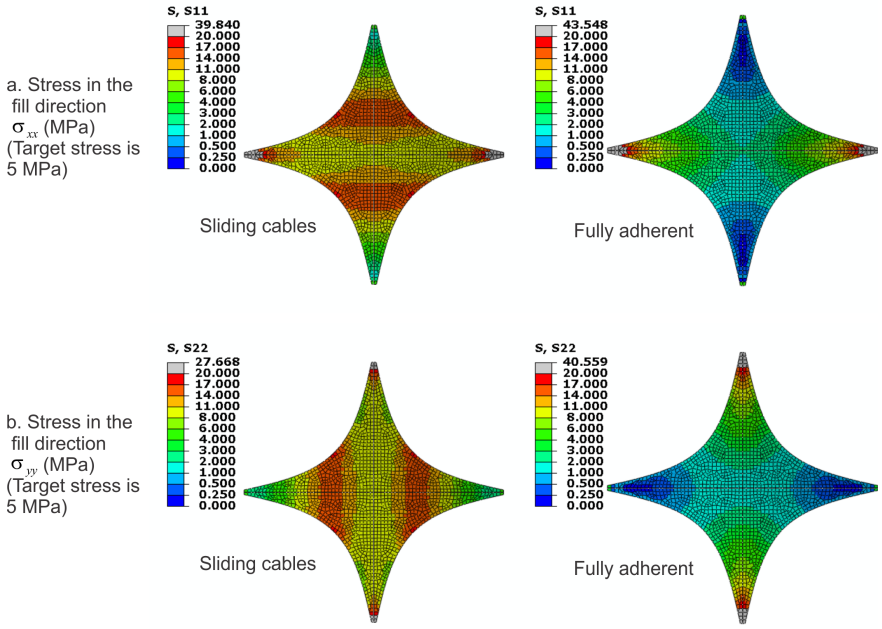

Figure 4.8: The influence of the sliding cable on the stress distributions of the fabric membrane: (a) stress in the warp direction; (b) stress in the fill direction.

initial and optimum membranes with the linear orthotropic elasticity and the fabric elasto-plasticity model are presented, respectively. In general, the stress distributions in the optimum membrane are more uniform and closer to the target prestresses compared with their counterparts in the initial membrane. In the optimum shapes, the stresses range from 2 MPa to 10 MPa except for a small area at the corners where stress concentrations occur. Especially, in the center of the membrane the stresses are very close to the target stress. Moreover, the force in the cable is much higher than the target one when the shape of the membrane is obtained based on the empirical formula (*cf.* eq. (4.3)). Table 4.4 shows the quantitative deviations of the stress and force components. It is shown that not only the force in the cable but also the stress components in the membrane obtained from the empirical formula are very different from the target prestress values when either the elasticity or the fabric elasto-

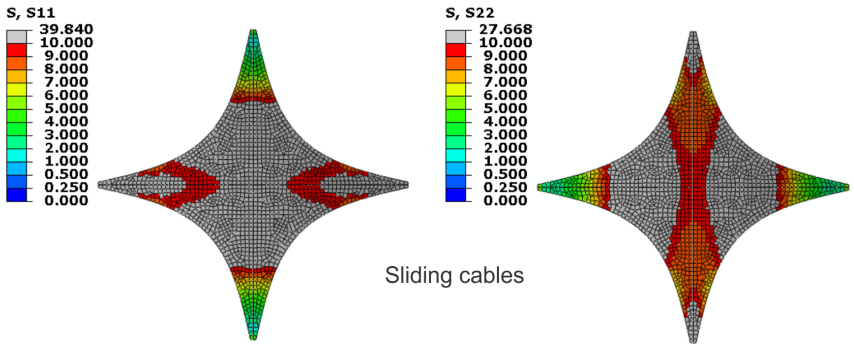

Figure 4.9: Stress distribution in the membrane whose shape is identified based on the empirical formula (left: the stress in the warp direction; right: the stress distribution in the fill direction). In this case, the legend is cut off at 10 MPa for the sake of clarity.

plasticity model is used for the membrane. These results point to the systematic problem of the assumption of uniform stress in the membrane in the conventional design method. On the contrary, the stresses in the optimum shapes are sizeable and bounded in the admissible range of stress states of the coated fabric (less than 24.1 MPa as mentioned in [33]).

Table 4.4: Average (Arithmetic Mean) deviations between the stress and force components of the final structures and the reference ones when linear orthotropic elasticity (Orth. elasticity) and fabric elasto-plasticity are respectively used for the membrane.

		$\overline{\Delta\sigma_{11}}$(MPa)	$\overline{\Delta\sigma_{22}}$(MPa)	$\overline{\Delta F}$(kN)
Orth. elasticity	Initial shape	6.864	5.939	10.210
	Optimum shape	1.130	1.218	0.090
Fabric plasticity	Initial shape	4.765	3.015	4.056
	Optimum shape	1.829	1.715	0.045

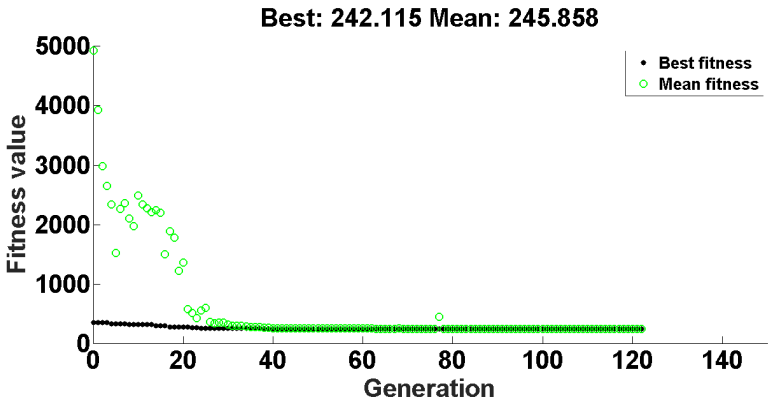

Figure 4.10: The evolution of the best fitness and the averages of the fitness values over generations when the orthotropic elasticity model is used for the membrane.

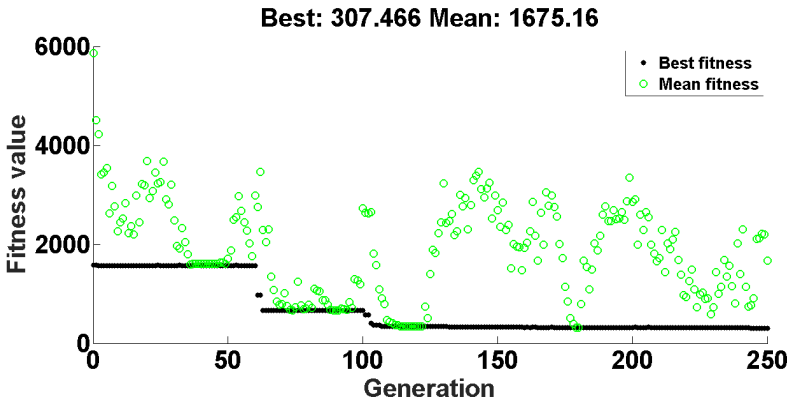

Figure 4.11: The evolution of the best fitness and the averages of the fitness values over generations when the fabric elasto-plastic model is used for the membrane.

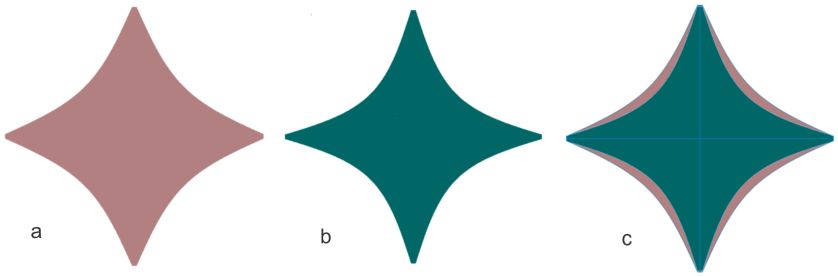

Figure 4.12: Influence of the material model on the resulting optimum shape: (a) linear orthotropic elasticity, (b) fabric elasto-plasticity, and (c) difference between two resulted shapes.

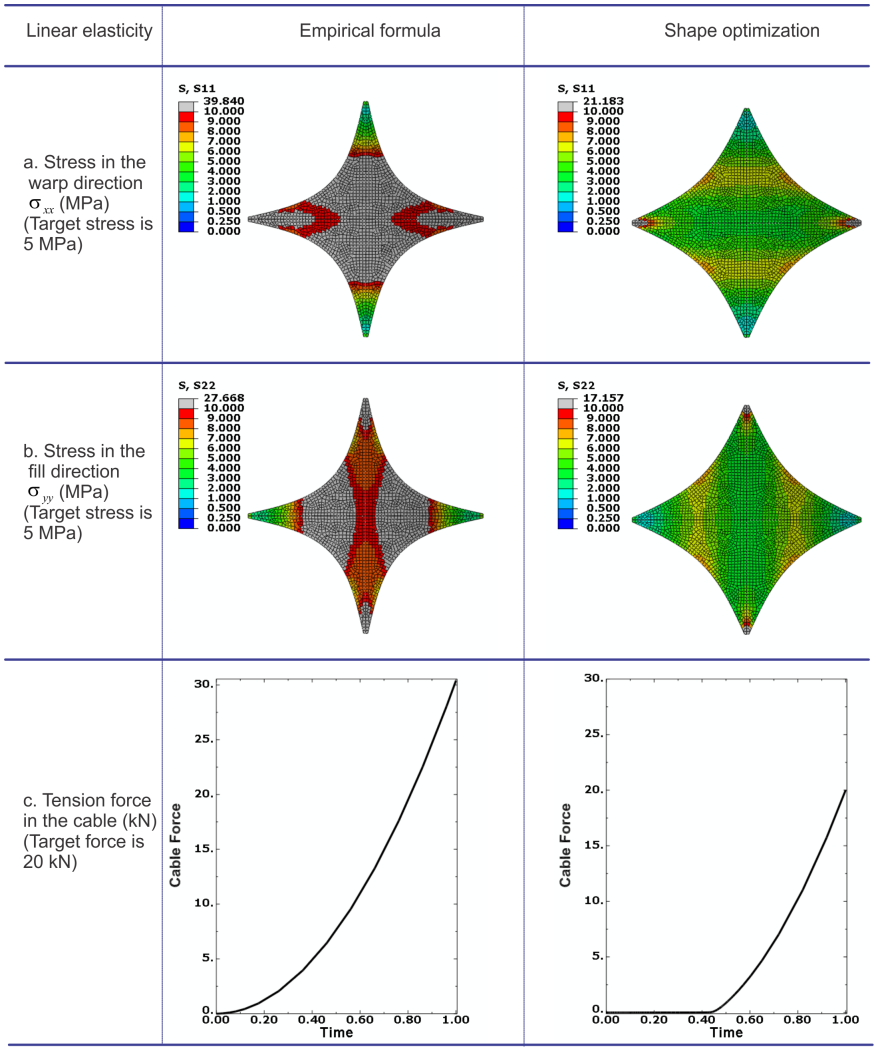

Figure 4.13: Distribution of stresses in the warp and fill directions as well as the force in the sliding cable when linear orthotropic elasticity is used for the membrane (in the first column, the shape of the membrane is identified from the empirical formula; in the second column, the shape of the membrane is identified from the shape optimization procedure).

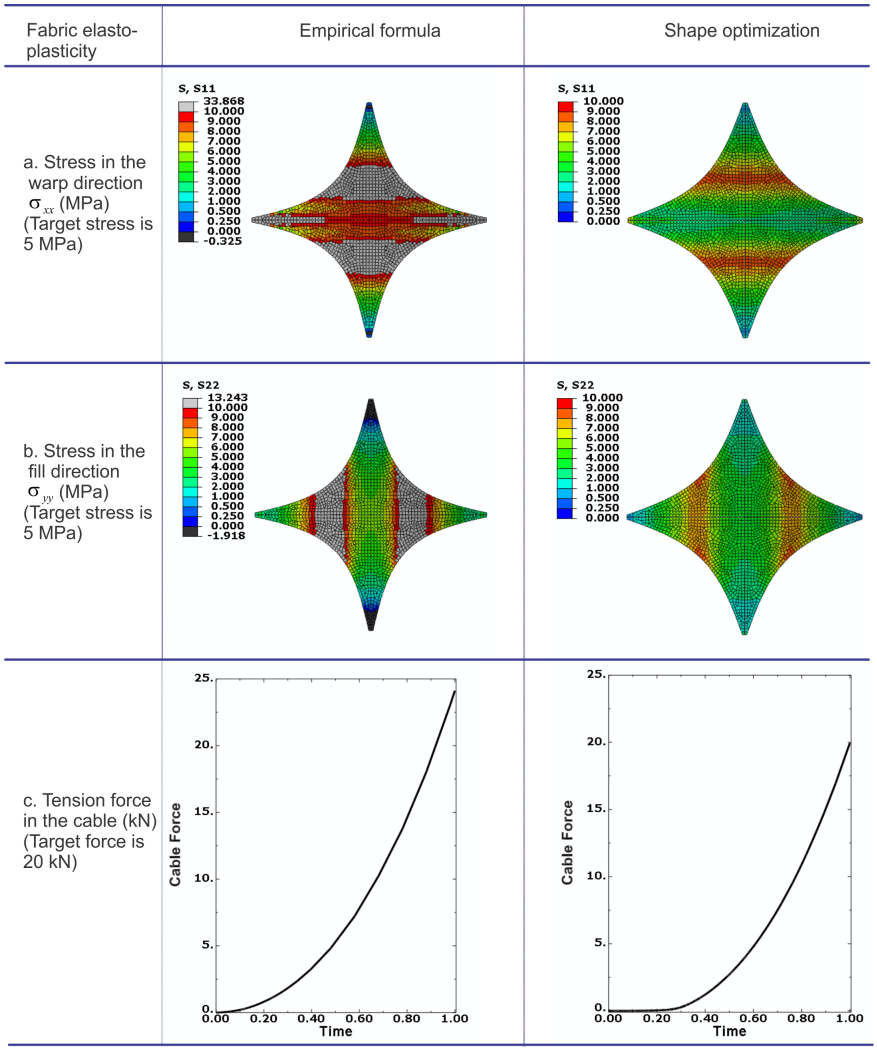

Figure 4.14: Distribution of stresses in the warp and fill directions as well as the force in the sliding cable when fabric elasto-plasticity is used for the membrane (in the first column, the shape of the membrane is identified from the empirical formula; in the second column, the shape of the membrane is identified from the shape optimization procedure).

4.4 Conclusions

The primary goal of this study is to combine all stages in the design and analysis of fabric membrane structures in a unified step. This has been achieved in the framework of shape optimization, shown in this chapter. In each iteration of the optimization loop, a nonlinear analysis is provided by using the fabric elasto-plasticity material model for the membrane and taking into account the interaction between the boundary cable and the membrane. It hence enhances the reliability of the overall optimization. Two conclusions can be drawn from the results of the numerical example. Firstly, a proper material model for the fabric membrane plays a crucial role as well as the need to consider the effect from the boundary cables in the analysis and design of this kind of structures. Secondly, in the numerical example only a single panel is used, but the stresses on the membrane are still permissible. It can enable the designers to use a lower number of panels in their design.

Further research will apply the approach in this chapter to design and analyze a large-scale highly-curved membrane structure in which the effect of undevelopability of the fabric membrane is more pronounced.

Bibliography

[1] T. Dinh, A. Rezaei, W. Punurai, L. De Laet, M. Mollaert, D. Van Hemelrijck, W. Van Paepegem, A shape optimization approach to integrated design and nonlinear analysis of tensioned fabric membrane structures with boundary cables, International Journal of Solids and Structures 83 (2016) 114–125. doi:10.1016/j.ijsolstr.2016.01.004.

[2] F. Masahisa, K. Osamu, F. Seiichiro, Analysis of fabric tension structures, Computers & Structures 32 (3) (1989) 537–547.

[3] R. M. PAULETTI, D. M. GUIRARDI, S. GOUVEIA, Modeling sliding cables and geodesic lines through dynamic relaxation, in: Symposium of the International Association for Shell and Spatial Structures (50th. 2009. Valencia). Evolution and Trends in Design, Analysis and Construction of Shell and Spatial Structures: Proceedings, Editorial de la Universitat Politécnica de Valencia., 2010.

[4] W. R. Spillers, R. B. Testa, N. Stubbs, Analysis of Fabric Structures, Journal of the Franklin Institute 306 (5) (1978) 341–353. doi:10.1016/0016-0032(78)90026-1.

[5] P. P. Véron, P. Trompette, P. J. C. Léon, Integrated design and collaborative engineering of fabric structures, Engineering with Computers 14 (1) (1998) 23–35. doi:10.1007/BF01198972.

[6] B. Bridgens, M. Birchall, Form and function: The significance of material properties in the design of tensile fabric structures, Engineering Structures 44 (2012) 1–12. doi:10.1016/j.engstruct.2012.05.044.

[7] M. R. Barnes, Form-finding and analysis of prestressed nets and membranes, Computers & Structures 30 (3) (1988) 685–695. doi:10.1016/0045-7949(88)90304-5.

[8] K.-U. Bletzinger, R. Wüchner, F. Daoud, N. Camprubí, Computational methods for form finding and optimization of shells and membranes, Computer Methods in Applied Mechanics and Engineering 194 (30-33) (2005) 3438–3452. doi:10.1016/j.cma.2004.12.026.

[9] M. Hashimoto, N. Kishimoto, Y. Miyazaki, M. C. Natori, Numerical Analysis on Deployment Behaviors of Membrane Structure Systems, in: ASME 2006 International Mechanical Engineering Congress and Exposition, American Society of Mechanical Engineers, 2006, pp. 453–458.

[10] K. Ishii, Form finding analysis in consideration of cutting patterns of membrane structures, International Journal of Space Structures 14 (2) (1999) 105–119.

[11] R. M. O. Pauletti, P. M. Pimenta, The natural force density method for the shape finding of taut structures, Computer Methods in Applied Mechanics and Engineering 197 (49–50) (2008) 4419–4428. doi:10.1016/j.cma.2008.05.017.

[12] J. Sánchez, M. n. Serna, P. Morer, A multi-step force–density method and surface-fitting approach for the preliminary shape design of tensile structures, Engineering Structures 29 (8) (2007) 1966–1976. doi:10.1016/j.engstruct.2006.10.015.

[13] B. Tabarrok, Z. Qin, Form finding and cutting pattern generation for fabric tension structures, Computer-Aided Civil and Infrastructure Engineering 8 (5) (1993) 377–384.

[14] D. S. Wakefield, Engineering analysis of tension structures: theory and practice, Engineering Structures 21 (8) (1999) 680–690. doi:10.1016/S0141-0296(98)00023-6.

[15] W. J. Lewis, Tension structures: form and behaviour, Thomas Telford, 2003.

[16] B. Forster, The European Design Guide for Tensile Surface Structures, Tensinet, 2004.

[17] J.-J. Li, S.-L. Chan, An integrated analysis of membrane structures with flexible supporting frames, Finite Elements in Analysis and Design 40 (5–6) (2004) 529–540. doi:10.1016/S0168-874X(03)00076-3.

[18] J. B. Pargana, D. Lloyd-Smith, B. A. Izzuddin, Fully integrated design and analysis of Tensioned Fabric Structures: Finite elements and case studies, Engineering Structures 32 (4) (2010) 1054–1068. doi:10.1016/j.engstruct.2009.12.032.

[19] K.-U. Bletzinger, J. Linhard, R. Wüchner, EXTENDED AND INTEGRATED NUMERICAL FORM FINDING AND PATTERNING OF MEMBRANE STRUCTURES, Journal of the International Association for Shell and Spatial Structures 50 (1) (2009) 35–49.

[20] R. B. Haber, J. F. Abel, Initial equilibrium solution methods for cable reinforced membranes part I—formulations, Computer Methods in Applied Mechanics and Engineering 30 (3) (1982) 263–284. doi:10.1016/0045-7825(82)90080-9.

[21] R. B. Haber, J. F. Abel, D. P. Greenberg, An integrated design system for cable reinforced membranes using interactive computer graphics, Computers & Structures 14 (3–4) (1981) 261–280. doi:10.1016/0045-7949(81)90012-2.

[22] J.-Y. Kim, J.-B. Lee, A new technique for optimum cutting pattern generation of membrane structures, Engineering Structures 24 (6) (2002) 745–756. doi:10.1016/S0141-0296(02)00003-2.

[23] W. Punurai, W. Tongpool, J. Héctor Morales, Implementation of genetic algorithm for optimum cutting pattern generation of wrinkle free finishing membrane structures, Finite Elements in Analysis and Design 58 (2012) 84–90. doi:10.1016/j.finel.2012.04.008.

[24] M. Ohsaki, K. Uetani, Shape-stress trade-off design of membrane structures for specified sequence of boundary shapes, Computer Methods in Applied Mechanics and Engineering 182 (1–2) (2000) 73–88. doi:10.1016/S0045-7825(99)00086-9.

[25] M. Ohsaki, J. Fujiwara, Developability conditions for prestress optimization of a curved surface, Computer Methods in Applied Mechanics and Engineering 192 (1–2) (2003) 77–94. doi:10.1016/S0045-7825(02)00523-6.

[26] D. Veenendaal, P. Block, An overview and comparison of structural form finding methods for general networks, International Journal of Solids and Structures 49 (26) (2012) 3741–3753. doi:10.1016/j.ijsolstr.2012.08.008.

[27] P. Gosling, B. Bridgens, A. Albrecht, H. Alpermann, A. Angeleri, M. Barnes, N. Bartle, R. Canobbio, F. Dieringer, S. Gellin, W. Lewis,

N. Mageau, R. Mahadevan, J.-M. Marion, P. Marsden, E. Milligan, Y. Phang, K. Sahlin, B. Stimpfle, O. Suire, J. Uhlemann, Analysis and design of membrane structures: Results of a round robin exercise, Engineering Structures 48 (2013) 313–328. doi:10.1016/j.engstruct.2012.10.008.

[28] T. D. Dinh, A. Rezaei, S. Puystiens, M. Van Craenenbroeck, K. Carbonez, L. De Laet, M. Mollaert, D. Van Hemelrijck, W. Van Paepegem, A study of tension fabric membrane structures under in-plane loading: Nonlinear finite element analysis and validation, Composite Structures 128 (2015) 10–20. doi:10.1016/j.compstruct.2015.03.055.

[29] MSAJ/M-02-1995. Testing method for elastic constants of membrane materials, 1995.

[30] T. Nouri-Baranger, Computational methods for tension-loaded structures, Archives of Computational Methods in Engineering 11 (2) (2004) 143–186.

[31] Z. Yingying, Z. Qilin, L. Ke, K. Bei-lei, Experimental analysis of tensile behaviors of polytetrafluoroethylene-coated fabrics subjected to monotonous and cyclic loading, Textile Research Journal 84 (3) (2014) 231–245. doi:10.1177/0040517513494259.

[32] J. B. Pargana, D. Lloyd-Smith, B. A. Izzuddin, Advanced material model for coated fabrics used in tensioned fabric structures, Engineering Structures 29 (7) (2007) 1323–1336. doi:10.1016/j.engstruct.2006.09.001.

[33] T. D. Dinh, A. Rezaei, L. De Laet, M. Mollaert, D. Van Hemelrijck, W. Van Paepegem, A new elasto-plastic material model for coated fabric, Engineering Structures 71 (2014) 222–233. doi:10.1016/j.engstruct.2014.04.027.

[34] S. Kato, T. Yoshino, H. Minami, Formulation of constitutive equations for fabric membranes based on the concept of fabric lattice model, Engineering Structures 21 (8) (1999) 691–708. doi:10.1016/S0141-0296(98)00024-8.

[35] J. F. Abel, R. B. Haber, D. C. Salmon, M. L. Brown, Development of computer aided-design of cable-reinforced membrane structures in

the USA. Shells, membrane and space frames, in: Proceedings IASS symposium, Vol. 2, 1986, pp. 111–8.

[36] P. Wriggers, Nonlinear Finite Element Methods, Springer Berlin Heidelberg, Berlin, Heidelberg, 2008.

[37] Hibbit, Karlsson, Sorensen, ABAQUS/Standard Analysis User's Manual, Hibbit, Karlsson, Sorensen Inc., 2014.

[38] Y. Ding, Shape optimization of structures: a literature survey, Computers & Structures 24 (6) (1986) 985–1004. doi:10.1016/0045-7949(86)90307-X.

[39] U. Schramm, W. D. Pilkey, The coupling of geometric descriptions and finite elements using NURBs — A study in shape optimization, Finite Elements in Analysis and Design 15 (1) (1993) 11–34. doi:10.1016/0168-874X(93)90067-Z.

[40] W. A. Wall, M. A. Frenzel, C. Cyron, Isogeometric structural shape optimization, Computer Methods in Applied Mechanics and Engineering 197 (33–40) (2008) 2976–2988. doi:10.1016/j.cma.2008.01.025.

[41] T. Mathworks, Matlab Optimization Toolbox User's Guide.
URL http://www.mathworks.co.uk/access/helpdesk/help/pdf_doc/optim/optim_tb.pdf

[42] A. Borgart, An Approximate Calculation Method for Air Inflated Cushion Structures for Design Purposes, International Journal of Space Structures 25 (2) (2010) 83–92. doi:10.1260/0266-3511.25.2.83.

Chapter 5

A Computational Compensation Method for Fabric Panels of Tensioned Membrane Structures Using A Shape Optimization Method Based on Gradientless Algorithms

In the previous chapter, we have proposed a method to combine different stages in design and analysis of tensioned membrane structures within the shape optimization framework. The proposed method facilitates the incorporation of various sources of nonlinearities in the analysis of tensioned membrane structures. Especially, the amount of fabric panels compensation when using a simple material model for the coated fabric, *i.e.*, linear orthotropic elasticity, as is widely used in practice, was presented. However, in that chapter, we assumed that the membrane, which has been assembled from different fabric panels, had been flat. That assumption is rather oversimplified for a highly curved membrane structure. In this chapter, that proposed method is further developed. The novelty lies in the postulation of a stress-free 3-D intermediate configuration, which is

built from flat fabric panels. The goal is to find an optimum shape of this 3-D intermediate configuration such that the stress distribution in the resulting structure, which is formed by deforming the 3-D intermediate configuration, remains at desired stress levels. A nonlinear finite element analysis is employed to identify these stress fields in the resulting structures. In this analysis, material and geometrical nonlinearities are taken into account. Moreover, the nonlinear kinematical interaction between the boundary cables and the membrane is also considered. Hence the stress fields on the resulting structures are expected to be reliable and close to the physical ones. Moreover, in this chapter, different gradient-less optimization algorithms, *viz.*, genetic algorithm, pattern search, and Bayesian, are considered.

5.1 Introduction

As can be seen from the previous chapters, design and analysis of tensioned fabric membrane structures are very complicated, in which different sources of nonlinearities, *i.e.*, geometrical, material and boundary nonlinearities, are involved. In the literature, one can find numerous numerical works related to the research field, but only a few of them have covered these kinds of nonlinearities [1–3].

In this chapter, a novel approach in design and analysis of tensioned fabric membrane structures is proposed. The core idea of this method is to postulate a stress-free 3-D intermediate configuration of the structure, which is formed by assembling different flat fabric panels. Afterward, the intermediate configuration is deformed into the final shape, and the stress fields on the resulting structure are obtained through a FEM analysis. In this analysis, all sources of nonlinearities are considered. The obtained stress fields are then compared to the counterparts that are put-forward by designers. If the stress fields are not converged to the targeted ones, the geometry of the 3-D intermediate configuration will be adjusted. This process continues till the stress fields in the resulting structure are close to the design ones. Indeed, the reason to introduce the 3-D intermediate configuration is two-fold: (i) by starting with the stress-free configuration, the nonlinear material model can be used; (ii) we optimize the 3-D shape instead of optimizing different flat fabric panels, as other researchers have proposed [1, 4–6], thus the problem related to fabric panels compatibility

can be avoided. The present author considers this work as a continuation of the work presented in the previous chapter (*cf.* chapter 4).

The outline of this chapter is as follows. In the next section, a brief overview of design and analysis methods for tensioned membrane structures is presented. Deficiencies of the current method are exposed and how the proposed method can tackle these issues are mentioned. In the subsequent section, the main ingredients of the FEM analysis, *viz.*, material models, a kinematical interaction between the cables and the membrane, and the elements of the shape optimization, *viz.*, the objective function and optimization algorithms are presented. This section is then followed by numerical results. The chapter ends with some concluding remarks.

5.2 Design and analysis of tensioned fabric membrane structures

5.2.1 Motivation

As mentioned in the chapter 4, the design and analysis method of tensioned fabric membrane structures can be divided into two methods, *viz.*, conventional and integrated ones. To overcome the deficiencies of the conventional method, the integrated design and analysis method was proposed by Haber et al. [7]. Further developments of this approach can be found in [3, 8] and the previous chapter (*cf.* chapter 4). In this method, different stages of design and analysis of tensioned membrane structures are combined in a single loop. Thus, the influence of the cutting pattern can be integrated into the form-finding and load analysis steps based on correct nonlinear continuum mechanics, which can provide a reliable analysis of tension fabric membrane structures. In these works, the planar shape of the fabric panels was iteratively adjusted such that the stress fields in the membrane either obtained by assembling these panels [8, 9] or in the deformed configuration after the load analysis [3] are at desired levels. These works are distinguished by sources of nonlinearities that were considered in the finite element analysis and in the way the shape of the fabric panels is adjusted. In the works of Pargana et al. [8] and Dinh et al. [9], the authors both used nonlinear material models for the fabric membrane and took into account the interaction between the cable and the membrane. While in [8], the shape of the planar fabric panel

was adjusted manually, in [9] the authors employed the genetic algorithm to adjust this shape. However, in these works, the authors assumed that the intermediate configuration, *i.e.*, the unstressed membrane that is formed by assembling different fabric panels (*cf.* fig. 5.1), was flat. This assumption is generally not true because the membrane structures must be doubly curved to resist external loads and the doubly curved surface cannot be formed from a flat fabric without distortion [10]. To reduce this distortion, the fabric panels are cut in such a way that the unstressed assembled fabric membrane, *i.e.*, the intermediate configuration, has a certain curvature instead of flat, as is assumed in [8, 9].

Figure 5.1: Different configurations of a tensioned membrane structure: (a) flat fabric panels, (b) 3D- intermediate configuration, which is formed by assembling the fabric panels, and (c) the resulting structure, which is formed by deforming the intermediate membrane (reprinted from [3]).

5.2.2 Principles of the proposed method

The proposed method in this present chapter can be considered as a continuation of the work presented in the previous chapter. This time, the target is to find an optimum stress-free 3-D intermediate membrane such that the stress fields in the resulting structure are in desired levels. Similar

to the previous work, geometrical and material nonlinearities, as well as nonlinear interaction between the cable and the membrane, are considered in the FEM analysis. It thus ensures that the obtained stress fields in the membrane are reliable. Once the optimum 3-D intermediate membrane is obtained, cutting patterns generation is carried out. At this stage, the stress-free assumption in the 3-D intermediate membrane is verified. If the strains in the resulting fabric panels obtained from the cutting patterns generation stage are negligible, the obtained results are deemed to be valid. Overview of the proposed method can be found in fig. 5.2.

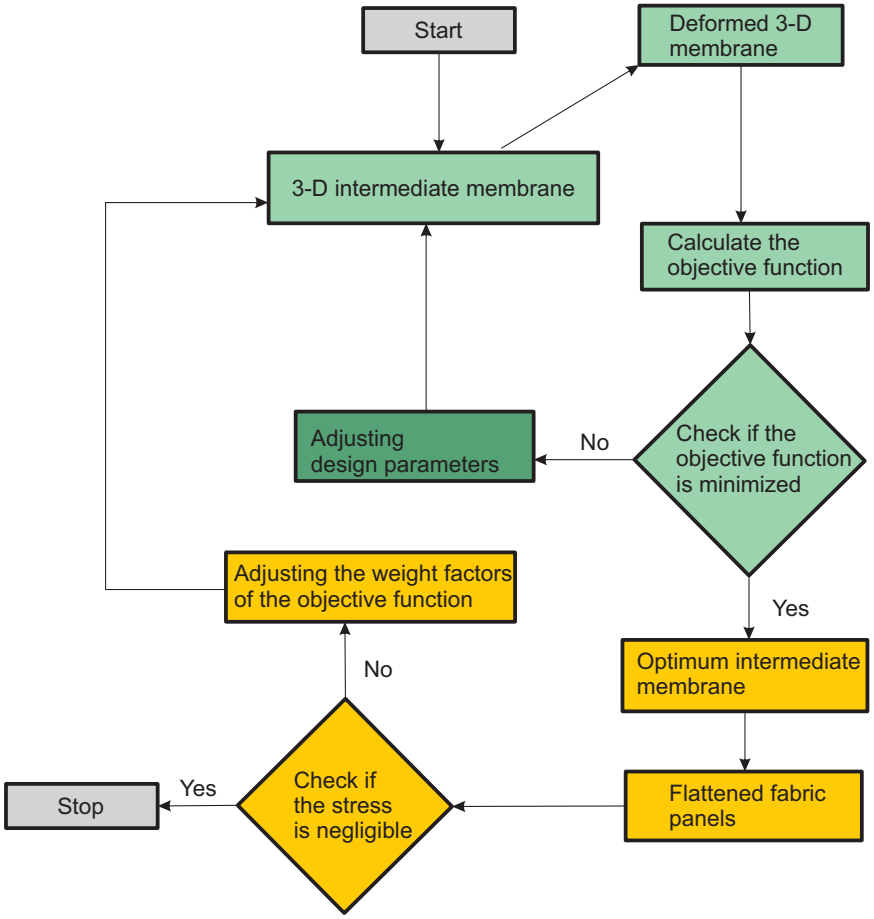

Figure 5.2: Flowchart of the proposed method.

5.3 Nonlinear finite element analysis of tensioned fabric membrane structures

5.3.1 Material models

The coated fabric considered in this work is the polyester fiber woven fabric with PVC coating, which is manufactured by Sioen Industry, Belgium. This kind of coated fabric is ubiquitously used now in tension membrane structures. The present author has proposed a material constitutive law, *viz.*, fabric-plasticity model, for this material, details of this model can be found in chapter 2. This material model has shown a good performance in capturing the nonlinear behavior of the coated fabric when we used it for a load analysis of a large-scale membrane (*cf.* chapter 3). Therefore, in this chapter, we also use it to simulate the mechanical behavior of the fabric membrane. Moreover, in practice, the linear orthotropic elasticity model is widely used. Thus, for the sake of comparison this material model is also used for the fabric in our simulation. Comparison of the obtained results when we use different material models for the membrane, *i.e.*, fabric-plasticity and orthotropic elasticity, will bring us insight into the amount of fabric compensation that designers should apply to their fabric panels when the elasticity model is used in their computation. This information is of paramount importance for practitioners, but rarely reported in the literature.

5.3.2 Nonlinear interaction between the boundary cable and the membrane

As mentioned in the previous chapter, in tensioned fabric membrane structures, the prestresses are introduced in the membrane by stretching the boundary cables at the edges of the membrane. These cables may fit within the fabric sleeves and may slide when the membrane structure is loaded [8, 11]. This interaction is referred to as boundary nonlinearity [12]. In chapter 4, it has been shown that this kind of nonlinearity had a profound effect on the stress distribution in the membrane and could not be ignored. That conclusion was also in line with the ones presented in [8, 11, 13]. In the present work, the sliding cable is also modeled by using the slip-ring elements in ABAQUS [14].

5.4 Shape optimization

Structural shape optimization is concerned with finding an optimal geometry of the structure, such that a certain structural behavior is fulfilled at best within certain constraints [15]. As a whole, there are three steps in shape optimization, *viz.*, (i) parameterized geometry description: the structural geometry is described by a number of design variables, (ii) structural analysis: the results from this step are used to calculate the objective function, and (iii) optimization: an optimization algorithm regularizes the new values for design variables such that the optimum value for the objective function can be achieved. In this study, design and analysis of a hypar structure, which has also been considered in chapter 4, is chosen to verify the proposed method. The size of the membrane and material orientations are illustrated in fig. 5.3. At the edges of the membrane, cables are implemented. The effective stiffness (Young's modulus multiplied by cross-sectional area) of each cable is 2000 kN. The design objective is to achieve a stress field as uniform as possible and close to 5 MPa in the membrane and the tension force in the cable is 20 kN. Indeed, these prestress values are chosen so that the dip to span ratio is *ca.* 1:6. This ratio is considered as a rule of thumb for efficient and aesthetically pleasing design [16]. Details of the different steps of the shape optimization are presented in the following subsections.

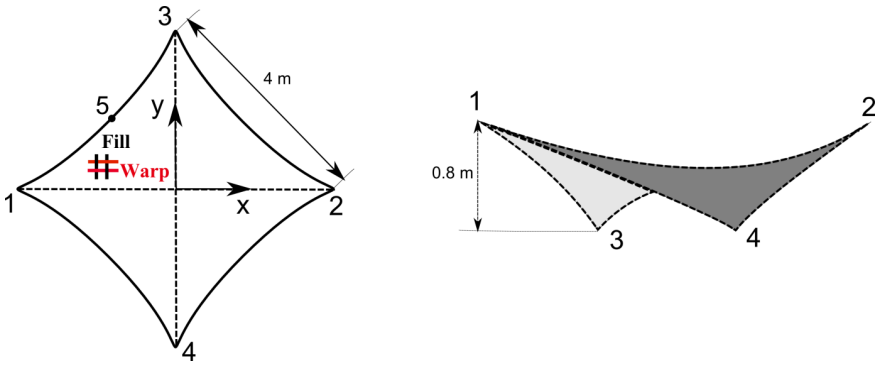

Figure 5.3: Schematic configuration of the hypar structure [9].

5.4.1 Parameterized geometry description

The ultimate target of this shape optimization problem is to find an optimum 3-D intermediate configuration of the membrane such that the stress fields in the resulting membrane, and the force in the cables are close to the desired levels as mentioned above. The geometry of the intermediate membrane can be described by a set of five control points *1, 2, 3, 4* and *5*, as shown in fig. 5.3. Herein, we assume that the shape of the membrane is symmetric with respect to the *x* and *y* directions (*cf.* fig. 5.3). Displacements of these points, denoted as p_1, p_2, p_3, p_4 and p_5 in fig. 5.4, govern the variation of the shape of the membrane. With prescribed coordinates of the control points, the outer edges of the membrane are created by using spline functions. Subsequently, from these edges, a 3-D non-uniform rational b-spline (NURBS) surface is created by using the "Filled Surface" feature in Solidworks [17].

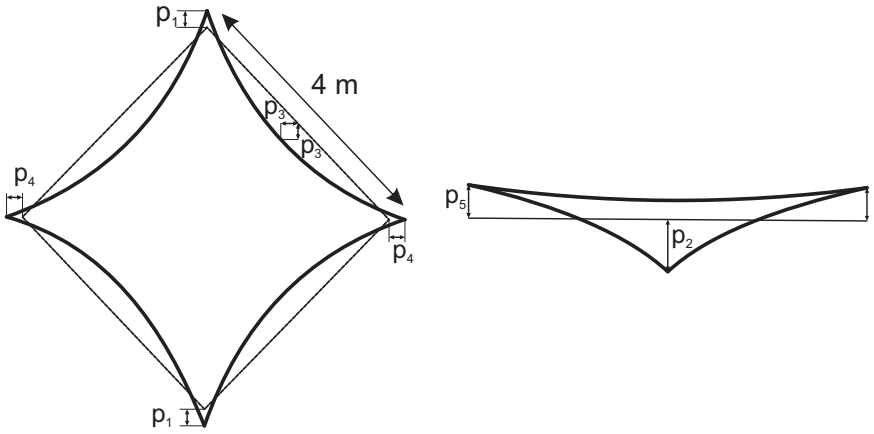

Figure 5.4: Parameterized geometry description of the hypar structure.

5.4.2 Objective function

Based on the parameterized geometry description above, the displacements of the control points with respect to the reference square (the dashed line in fig. 5.4) are the design variables of the considered shape optimization problem. The optimization can be formulated as those shown in eqs. (4.1) and (4.2). For the sake of convenience, these equations are repeated here:

Objective function:

$$W(\underline{P}) = w_1 \int_a (\underline{\sigma}^{\text{membrane}} - \underline{\sigma}_{ref}^{\text{membrane}}) : (\underline{\sigma}^{\text{membrane}} - \underline{\sigma}_{ref}^{\text{membrane}}) da + w_2 \int_l (\underline{\sigma}^{\text{cable}} - \underline{\sigma}_{ref}^{\text{cable}}) : (\underline{\sigma}^{\text{cable}} - \underline{\sigma}_{ref}^{\text{cable}}) dl \tag{5.1}$$

Constraints:

$$\underline{P}_l \leq \underline{P} \leq \underline{P}_u \tag{5.2}$$

where the vector $\underline{P}$ contains displacements of the control points, $\underline{P}_l$ and $\underline{P}_u$ are respectively their lower and upper values. $\underline{\sigma}^{\diamond}$ is the Cauchy stress tensor in the 3-D structure and $\underline{\sigma}_{ref}^{\diamond}$ is the reference stress tensor. a is the area of the resulting 3-D surface and l is the length of the deformed cable. w_1 and w_2 are the weights whose values reflect the importance of the associated components in the target function. ":" is the tensor contraction operator. In this work, to calculate this objective function, a structural analysis was done in ABAQUS/Standard. During the course of analysis, the control points $1, 2, 3$ and 4 were displaced in such a way that the height and the span of the structure are attained (*cf.* fig. 5.3).

5.4.3 Optimization algorithms

Similar to our previous study in chapter 4, the genetic algorithm (GA) is also used for controlling the process of approaching the optimum. GA is indeed a very powerful algorithm. However, it demanded many evaluations of the objective function. Thus, in this study, two other gradientless optimization algorithms, *viz.*, pattern search [18] and Bayesian optimization [19] are also used to find the optimum shape of the membrane.

The pattern search method is a subset of direct search methods, which neither compute nor explicitly approximate the derivative of the objective function. In the pattern search method, all the iterates lie on a scaled, translated integer lattice [18]. To create this lattice, a basis matrix and a generating matrix are required. At a certain iteration, the objective function is calculated at the current iterate as well as trial points, which lie on the lattice and are specified by a prescribed step length. The value of the objective function calculated at the current iterate is then compared to the counterparts at the trial points. If the value of the objective function calculated at a trial point is smaller than the counterpart at the current

iterate, then that trial point is chosen as an iterate for the next iteration and the step length is increased. If all the values calculated at trial points are bigger than the counterpart calculated at the current iterate, then the step length has to be reduced to generate new trial points. The iteration is terminated when either the change of the value of the objective function or the size of the step length is smaller than a prescribed tolerance. An example of using this method in shape optimization can be found in [20].

According to Kawaguchi et al. [21], Bayesian optimization is an efficient way to find global optima of a non-convex black-box deterministic function, which is the case for machine learning [19] and structural optimization [9, 22]. This method is especially suited for problems, in which the evaluation of the objective function is expensive because it demands a relatively low number of objective function evaluations. It has been shown in [23] that this method outperforms other state-of-the-art global optimization algorithms. The method can be split into two steps. At first, the objective function is surrogated by a probabilistic function. Typically, "Gaussian Process prior" is used in this step [19, 21]. In the second step, Bayesian optimization selects the next evaluation point by optimizing the acquisition function generated by the Gaussian Process.

The implementation for the shape optimization presented in this chapter is summarized in table 5.1 and fig. 5.5.

Table 5.1: Algorithm for implementation of the shape optimization for highly-curved tension fabric membrane structures.

(i)	**Pre-processing**. Given initial values for design variables $\boldsymbol{P}$, the weight factors w_i in the objective function W and the reference stresses in the cable and in the membrane → Create a 3-D surface using Solidworks VBA (Visual Basic for Applications) → Create an input file for ABAQUS/Standard
(ii)	**Finite Element Analysis** Running the analysis in ABAQUS/Standard and check if the simulation can go to the end of the load step
(iii)	**Post-processing**. If the simulation is prematurely terminated because of divergence → assign the penalty factor for the objective function Else → calculate the objective function using the formula eq. (5.1)
(iv)	**Optimization** If terminated conditions for optimization are reached, the optimization process stops and go to step (v). Otherwise, new values for the design variables are created and go to step (i)
(v)	**Fabric panel generation** Given the obtained optimum values for the design variables, the number of panels that designer would like to have and the tolerance that is used to judge if the residual strains in the intermediate membrane are negligible → Create the optimum 3D intermediate membrane using Solidworks VBA → Split the membrane based on geodesic lines (Command 'Shortpath' in Rhino) → Develop the 3D surface into different fabric panels using the 'Squish' feature → Check if the residual strains in the fabric panels are negligible: Yes: the program stops No: adjust the weight factors in the objective function and go to step (i)

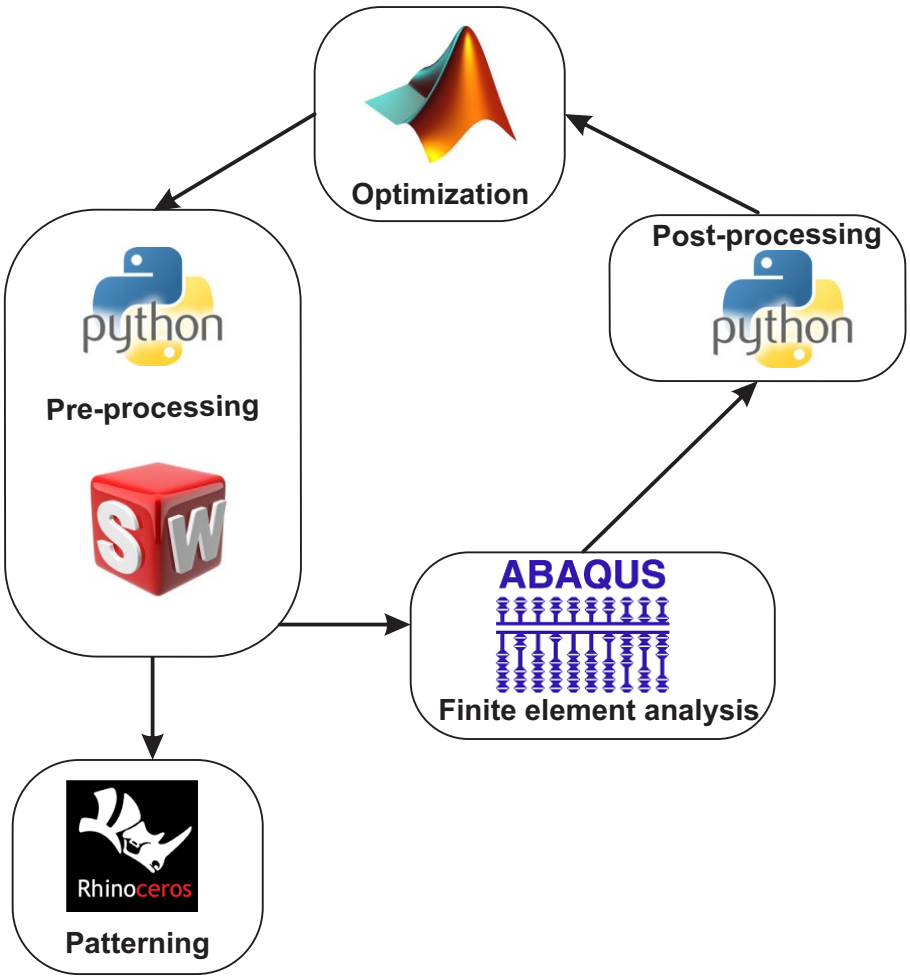

Figure 5.5: Software implementation of the shape optimization for the highly-curved membrane structures.

5.5 Numerical results

5.5.1 A comparison of different optimization algorithms

In order to identify which algorithm among GA, Pattern Search, and Bayesian optimization is the most efficient for the considered shape optimization, two combinations of the weight factors in the objective function (*cf.* table 5.2) are examined. In this work, the parameters for GA (*cf.* table 5.3) are taken from [24], in which the author also used GA for a five-variable structural shape optimization. Regarding the Pattern Search algorithm, the *"GPS Positive basis 2N"*, which is a commonly used pattern search algorithm, is used to create the pattern. Moreover, the Bayesian optimization used in this work is the one proposed in [21], in which the author used the *"Gaussian Process prior"* for the surrogate function and the *"upper confidence bound"* for the acquisition function. For the sake of simplicity, the orthotropic elasticity model is used for the fabric during simulations. The obtained results are summarized in table 5.4.

Table 5.2: Different combinations of the weight factors in the objective function eq. (5.1)

Combination	w_1	w_2
1	0.7	0.3
2	0.9	0.1

Table 5.3: Parameters for GA [24]

Population size	100
Number of generations	50
Selection scheme	Remainder stochastic sampling without replacement

From the obtained results, it is clear that the GA is the most expensive among the considered optimization algorithms. It demands respectively four times and *ca.* ten times greater in the number of function evaluations than the Bayesian optimization and the Pattern Search do. For the first weights combination, *i.e.,* $w_1 = 0.7$ and $w_2 = 0.3$ the result obtained by the GA is very close to the one found by the Pattern Search, but it is almost two times greater than the one found by the Bayesian optimization. Indeed, from fig. 5.6 the best result obtained from Bayesian optimization

Table 5.4: Comparison of different optimization algorithms for different combination of the weight factors.

	Number of the objective function evaluations	Minimum value of the objective function W
Combination 1		
Bayesian optimization	1000	0.550
GA	5000	0.988
Pattern Search	443	1.0854
Combination 2		
Bayesian optimization	1000	0.685
GA	5000	0.833
Pattern Search	375	1.172

can be achieved after *ca.* 700 iterations. Similar observation for the second weights combination, the results found by the Bayesian are better than the counterparts found by the GA and the Pattern Search. Therefore, in subsequent optimizations when the fabric plasticity model is used for the membrane we only employ the Bayesian optimization.

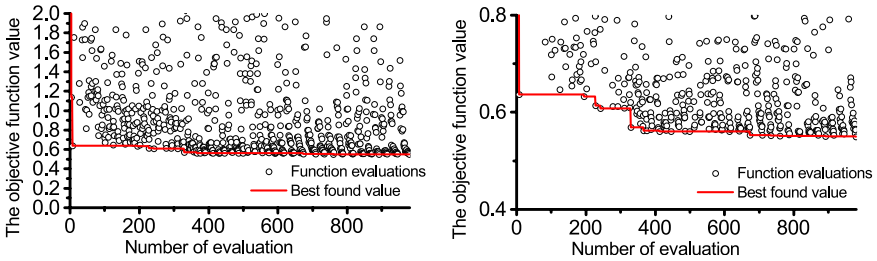

Figure 5.6: The distribution of the values of the objective function and the evolution of the best value over the iterations when the weight factors $w_1 = 0.7$ and $w_2 = 0.3$ are used: (a) the full range and (b) a smaller range is chosen to magnify the evolution of the best value over the iterations.

5.5.2 Optimum shapes when using elasticity

The stresses in the warp and fill directions in the membrane with the weight factors $w_1 = 0.7$ and $w_2 = 0.3$ are plotted in fig. 5.7 and the optimum values of the design variables are presented in table 5.6. Compared to the counterparts presented in chapter 4 (*cf.* fig. 5.8), the obtained results are better. This time, the stress fields in the membrane are closer to the prestress values (*i.e.*, 5 MPa) in the integral sense (*cf.* table 5.5), while the maximum stress at the corner is still bounded. Moreover, the force in the cable is also very close to the targeted one (20 kN). The obtained 3D intermediate membrane and the displacements of the material points in it to reach the final configuration is also plotted in fig. 5.9. This membrane is then split into six panels along geodesic lines and subsequently flattened by using the "Squish" feature in Rhino3D. In this feature, the 3-D intermediate membrane is discretized into a mesh. Subsequently, the mesh is flattened in such a way that the changes in facet area and the edge lengths are minimized. As mentioned earlier, when flattening a 3-D doubly curved surface, it is unavoidable to induce distortion into the fabric panels. This distortion in the fabric panels is presented in table 5.7. From this table, the biggest averaged strain occurs in the panel 1 (*cf.* fig. 5.10) and equals to 0.06%. Provided that the Young's moduli in the warp and fill directions are respectively 975.6 MPa and 716.1 MPa (*cf.* chapter 2), the corresponding stresses are 0.5854 MPa and 0.4296 MPa. These stresses are relatively small. Therefore, the stress-free assumption

in the 3-D intermediate membrane can be deemed to be valid. Another case for the weight factor combination with $w_1 = 0.9$ and $w_2 = 0.1$ is also considered. Again the stress fields in the membrane and the force in the boundary cable are very close to the targeted values (table 5.6). The maximum averaged strains in the flat fabric panel also occurs in the panel 1, but this time, it is only 0.05% (*cf.* table 5.7).

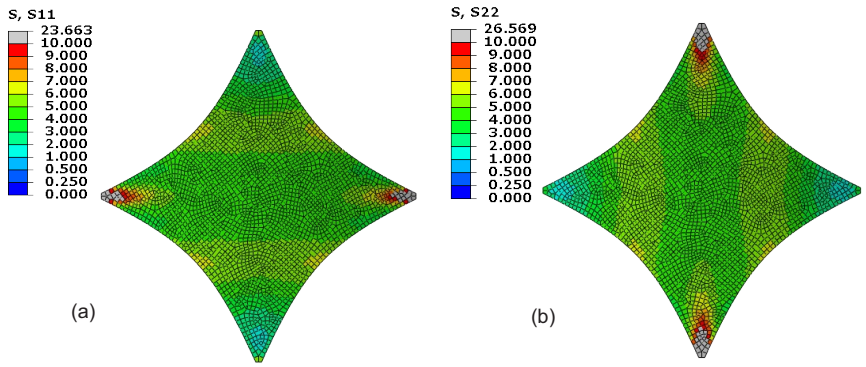

Figure 5.7: Stresses distribution in the optimum membrane in the warp (a) and the fill (b) directions when the orthotropic elasticity is used for the membrane for the case $w_1 = 0.7$ and $w_2 = 0.3$.

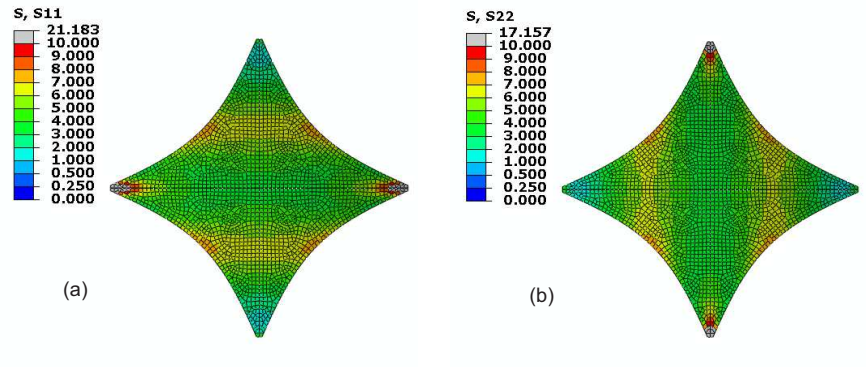

Figure 5.8: Stresses distribution in the optimum membrane in the warp (a) and the fill (b) directions found in the previous chapter when the orthotropic elasticity is used for the membrane for the case $w_1 = 0.7$ and $w_2 = 0.3$.

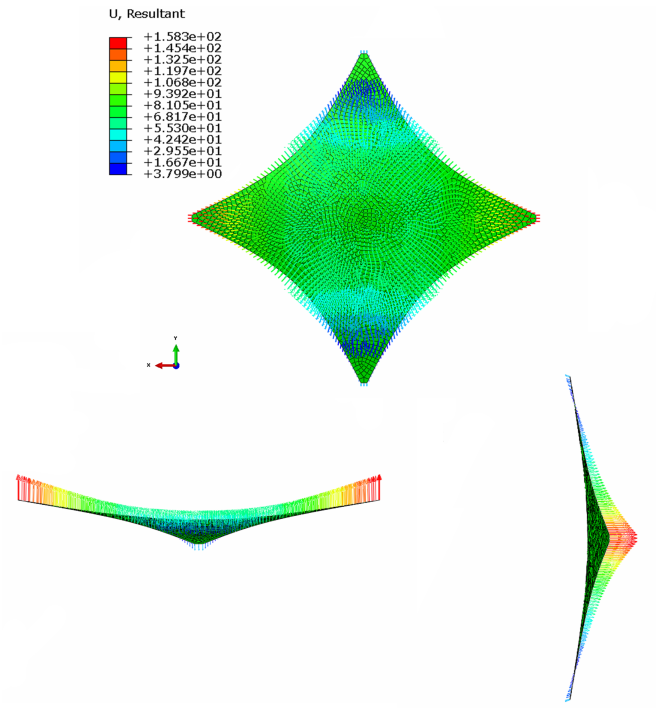

Figure 5.9: The optimum 3D intermediate membrane and the displacement of the material points in it to reach the final configuration when the orthotropic elasticity is used for the membrane and the weight factors are $w_1 = 0.7$ and $w_2 = 0.3$.

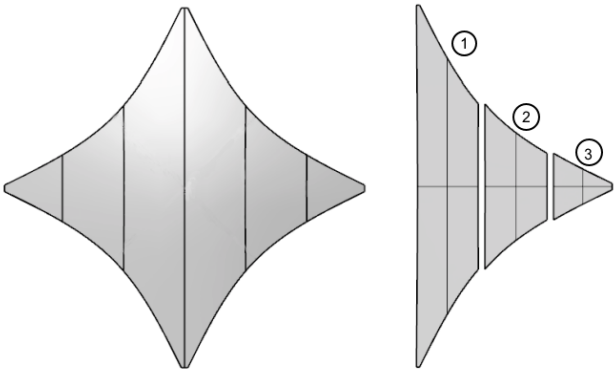

Figure 5.10: Flat fabric panels obtained from the optimum 3-D membrane when the orthotropic elasticity is used for the membrane and the weight factors are $w_1 = 0.7$ and $w_2 = 0.3$.

Table 5.5: Average (arithmetic mean) deviation of the stress and force components of the final structures found in this chapter (referred to as optimum 3D intermediate shape) and the counterparts found in chapter 4 (referred to as optimum planar shape) when linear orthotropic elasticity is used for the membrane.

	$\overline{\Delta\sigma_{11}}$(MPa)	$\overline{\Delta\sigma_{22}}$(MPa)	$\overline{\Delta F}$(kN)
Optimum 3D intermediate shape	0.829	0.786	0.001
Optimum planar shape	1.130	1.218	0.090

Table 5.6: Optimum values (in meter) of the design variable and the value of the objective function when the orthotropic elasticity is used for the membrane for different combinations of the weight factors.

Combination	p_1	p_2	p_3	p_4	p_5	W
1	-0.01125	0.3674	0.3097	0.0002	0.2417	0.55
2	-0.01152	0.3794	0.3116	-0.0037	0.2510	0.69

Table 5.7: Distortion after developing the optimum 3-D intermediate membrane into different flat fabric panels when the orthotropic elasticity is used for the membrane.

	Panel 1	Panel 2	Panel 3
Combination 1			
Averaged strain	0.06%	0.03%	0.01%
Combination 2			
Averaged strain	0.05%	0.03%	0.01%

5.5.3 Optimum shapes when using fabric-plasticity

The two above cases are also considered when the fabric plasticity model is used for the membrane during the shape optimization. The obtained results are presented in table 5.8. For the first case, when the weight factors $w_1 = 0.7$ and $w_2 = 0.3$ are used, the stress fields in the membrane are quite uniform and close to the targeted prestress (*cf.* fig. 5.11). The force in the cable is also close to 20 kN. Compared to the counterparts

presented in chapter 4, the obtained results are better (*cf.* table 5.9). It is expected because the assumption in the optimum shape is more flexible in this work than in the one presented in chapter 4. The optimum 3-D intermediate membrane is also split into six panels and flattened in Rhino3D. The averaged strain in the fabric panels is presented in table 5.10. This time, the averaged strains in the fabric panels are larger than the counterparts obtained in previous cases. The maximum averaged strain of 0.1% occurs in the panel 1. If this strain is in the warp direction, the resulting stress is 1.364 MPa. This stress value is rather large, and the stress-free assumption in the intermediate configuration is violated. In the second

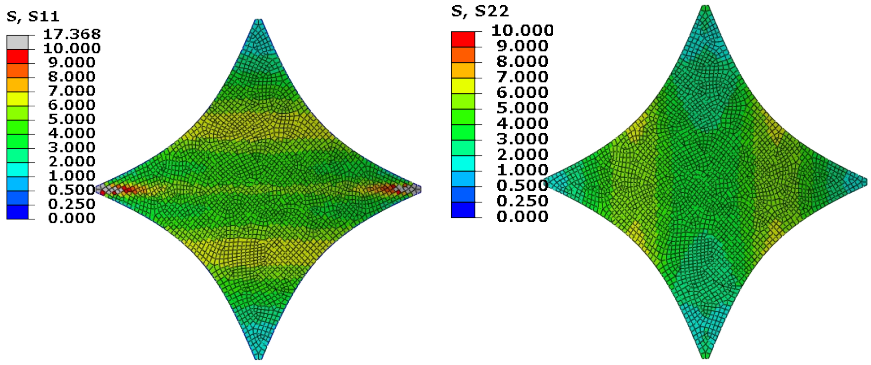

Figure 5.11: Stresses distribution in the membrane in the warp (a) and the fill (b) directions when the fabric-plasticity is used for the membrane for the case $w_1 = 0.7$ and $w_2 = 0.3$.

Table 5.8: Optimum values of the design variables (in meter) and the average deviations of the stress (in MPa) and force components (in kN) of the final structures for different combinations of the weight factors when fabric plasticity model is used for the membrane.

Combination	p_1	p_2	p_3	p_4	p_5	$\overline{\Delta\sigma_{11}}$(MPa)	$\overline{\Delta\sigma_{22}}$(MPa)	$\overline{\Delta F}$(kN)
1	-0.0333	0.3138	0.3500	-0.0000	0.3487	1.089	1.444	0.004
2	-0.0163	0.2527	0.3385	-0.0051	0.2894	1.110	1.584	0.063

case, when the weight factors $w_1 = 0.9$ and $w_2 = 0.1$ are used, the same stress patterns as the previous case are observed (*cf.* fig. 5.12). It can be concluded that the targeted prestresses are achieved in the membrane in the integral sense (*cf.* table 5.8). In addition, the peak stresses at the

Table 5.9: Average (arithmetic mean) deviations between the stress and force components of the final structures found in this chapter (referred to as optimum 3D intermediate shape) and the counterparts found in chapter 4 (referred to as optimum planar shape) when fabric plasticity model is used for the membrane.

	$\overline{\Delta\sigma_{11}}$(MPa)	$\overline{\Delta\sigma_{22}}$(MPa)	$\overline{\Delta F}$(kN)
Optimum 3D intermediate shape	1.089	1.4438	0.0036
Optimum planar shape	1.829	1.715	0.045

Table 5.10: Distortion after developing the optimum 3-D intermediate membrane into different flat fabric panels when the fabric plasticity is used for the membrane.

	Panel 1	Panel 2	Panel 3
Combination 1			
Averaged strain	0.10%	0.02%	0.01%
Combination 2			
Averaged strain	0.04%	0.03%	0.02%

corner of the membrane are also well-bounded. The force in the cable is just slightly higher than the targeted one (20.06 kN vs. 20 kN). The strains in the flattened fabric panels are presented in table 5.10. This time, the maximum strain is only 0.04%, thus the stress-free assumption in the intermediate membrane can be held. Hence the obtained results are deemed to be valid. The low strain in the flattened panels in this case is quite expected because compared to the previous case the optimum intermediate membrane in this case has lower curvature, manifested itself in the values of p_2 and p_5. It is quite interesting that the stress deviation in this case is greater than in the previous case, even though the weight factor associated with this deviation in the objective function has been increased. Indeed, this phenomenon can happen in a non-convex optimization [25].

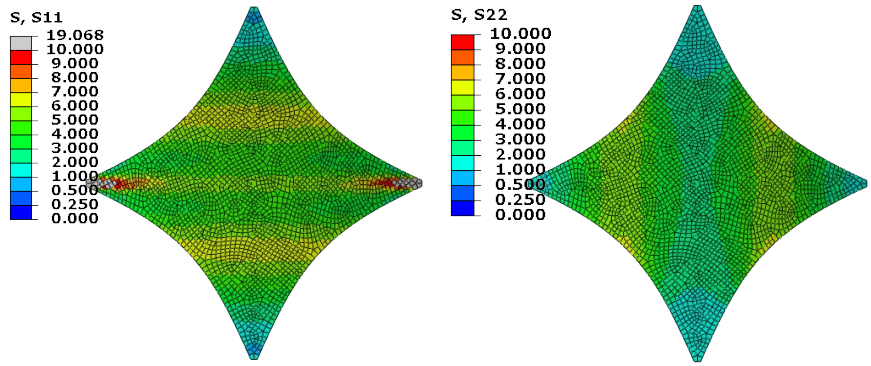

Figure 5.12: Stresses distribution in the membrane in the warp (a) and the fill (b) directions when the fabric-plasticity is used for the membrane for the case $w_1 = 0.9$ and $w_2 = 0.1$.

5.5.4 Further verification of the proposed method for a highly curved hyparstructure

Even though the results obtained from the proposed method are better than the ones presented in chapter 4, the considered hyparstructure has a rather modest height to side length ratio (0.8 m/ 4 m). Therefore, the proposed method is employed to design a more highly curved hyparstructure, whose height is equal to 1.4 m. The fabric plasticity and the orthotropic elasticity models are again employed respectively for the fabric membrane in the simulations. The optimum values of the design variables as well as the stress and force deviations of the above two cases are presented in table 5.11. The stress distribution in the deployed membrane is shown in figs. 5.13 and 5.14. As can be seen from these figures, in both cases the stresses are close to the targeted stress (5 MPa), even though the stress fields are more fluctuating compared to the case when the height of the structure is equal to 0.8 m. Moreover, the cable forces in both cases are also very close to the targeted one (20 kN), *i.e.,* 20.6 kN when the linear orthotropic elasticity is used for the membrane and 20.2 kN when the fabric plasticity is used for the membrane. The strains in the flattened fabric panels of these two cases are presented in table 5.12.

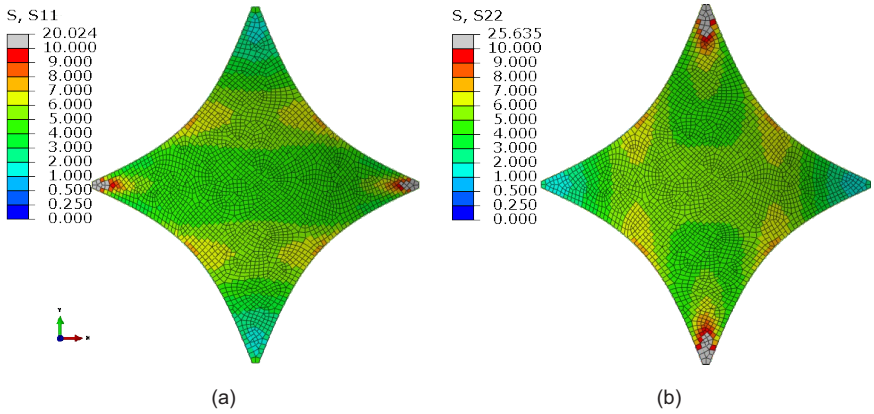

Figure 5.13: Stresses distribution in the membrane in the warp (a) and the fill (b) directions when the elasticity model is used for the membrane in case the height of the structure is equal to 1.4 m.

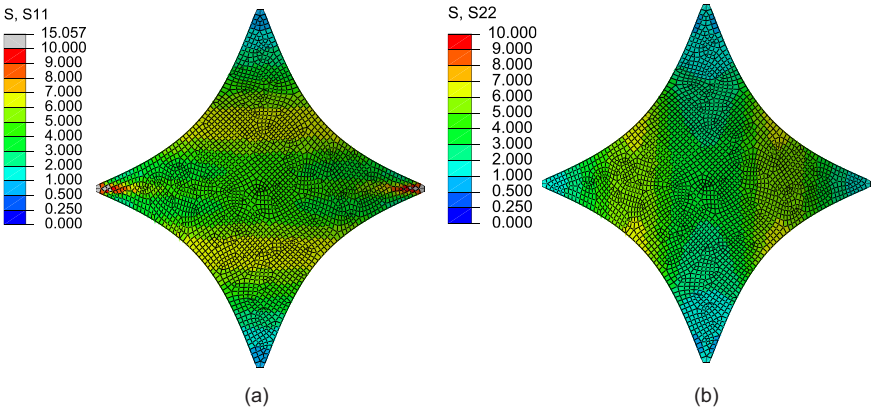

Figure 5.14: Stresses distribution in the membrane in the warp (a) and the fill (b) directions when the fabric plasticity model is used for the membrane in case the height of the structure is equal to 1.4 m.

Table 5.11: Optimum values of the design variables (in meter) and the average deviations of the stress (in MPa) and force components (in kN) of the final structures whose heigth is equal to 1.4 m when fabric plasticity (Fabric plas.) and linear orthotropic elasticity (Orth. elas.) models are respectively used for the membrane.

Material model	p_1	p_2	p_3	p_4	p_5	$\overline{\Delta\sigma_{11}}$(MPa)	$\overline{\Delta\sigma_{22}}$(MPa)	$\overline{\Delta F}$(kN)
Orth. elas.	0.0185	0.5398	0.3759	0.0370	0.5398	0.8530	0.8425	0.6013
Fabric plas.	0.0280	0.4907	0.4018	0.0444	0.4907	1.2199	1.5613	0.2033

Table 5.12: Distortion after developing the optimum 3-D intermediate membrane into different flat fabric panels in case the height of the structure is equal to 1.4 m (the order of the fabric panels is the same as the ones presented in fig. 5.10).

Material model	Panel 1	Panel 2	Panel 3
Orthotropic elasticity	0.09%	0.04%	0.01%
Fabric plasticity	0.08%	0.03%	0.01%

5.5.5 Compensation for fabric panels

In practice, when the orthotropic elasticity is used for the membrane, the designers have to apply compensation or reduction in the size of the flattened panels. The amount of fabric compensation is however not well-documented in the literature. Normally, the reduction of 1% is used as the rule of thumb [4] and the physical fabric cutting patterns are always smaller than the ones obtained from computer procedures [10]. It is however not always the case in our obtained results. In figs. 5.15 and 5.16, the fabric panels obtained from optimizations with the orthotropic elasticity and the fabric plasticity are compared. The differences among these fabric panels manifest the employed materials models for the membrane during the shape optimization and are referred to as computational compensation. The amount of computational compensation for each fabric panel is presented in table 5.13. Moreover, for the sake of comparison, the reduction of 1% is also applied to the panels, which are obtained from optimization with the orthotropic elasticity, to form so-called empirically compensated panels (*cf.* figs. 5.15 and 5.16). It can be seen from the results that the differences among panels obtained from optimizations with fabric plasticity and orthotropic elasticity are quite small, but larger

than 1%. The fabric panels obtained from optimization with fabric plasticity, *i.e.*, computationally compensated panels, are only smaller than the empirically compensated panels in the diagonal direction, but are larger in the warp and fill directions. Moreover, it can be seen from table 5.13 that the compensation for the panels is not uniform, but different from panel to panel and can be far different to 1%, as suggested by the designers in practice.

Table 5.13: Computational compensation for the fabric panels shown in figs. 5.15 and 5.16.

Hyparstructure's height (m)	Panel 1	Panel 2	Panel 3
0.8	2.2%	5%	4.3%
1.4	1.7%	5.4%	3.8%

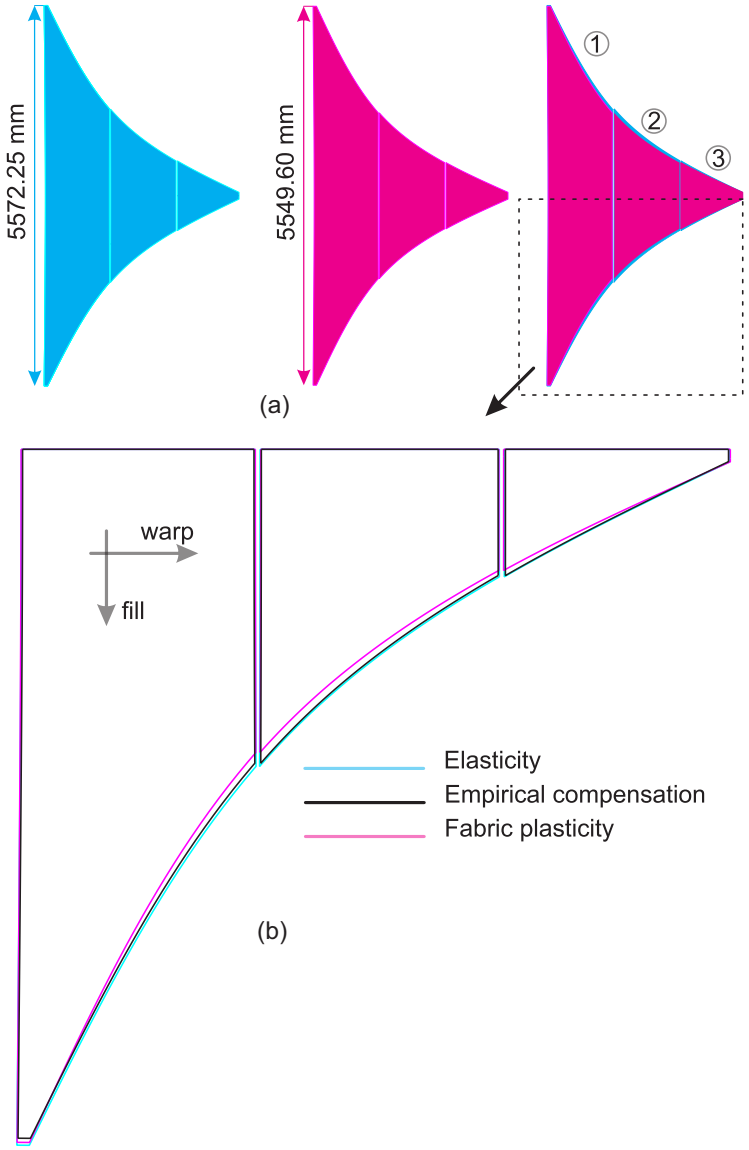

Figure 5.15: The fabric panels obtained from developing the optimum intermediate membrane in case the height of the hyparstructure is equal to 0.8 m: (a) Results from the shape optimization with the orthotropic elasticity (blue) and the fabric plasticity (magenta) are respectively used for the membrane, (b) Differences among the obtained fabric panels as well as the empirically compensated panels, which are derived from the optimum fabric panels with the orthotropic elasticity model.

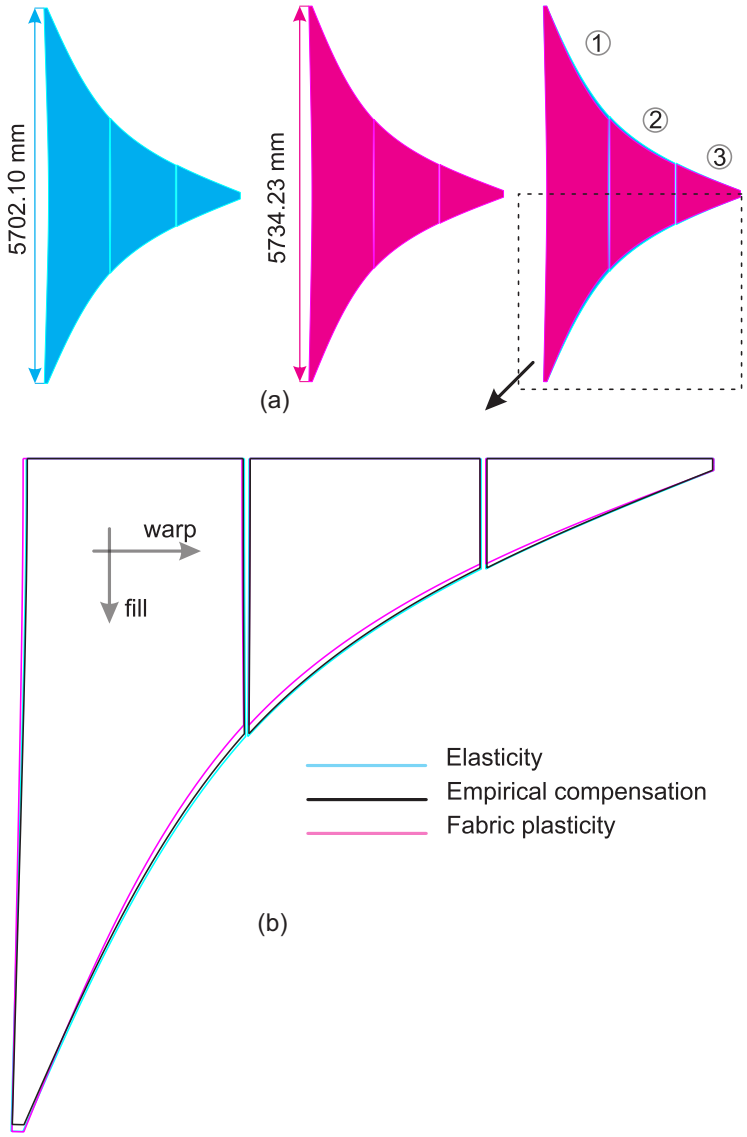

Figure 5.16: The fabric panels obtained from developing the optimum intermediate membrane in case the height of the hyparstructure is equal to 1.4 m: (a) Results from the shape optimization with the orthotropic elasticity (blue) and the fabric plasticity (magenta) are respectively used for the membrane, (b) Differences among the obtained fabric panels as well as the empirically compensated panels, which are derived from the optimum fabric panels with the orthotropic elasticity model.

5.6 Conclusions

In this chapter, a novel method in design and analysis of tensioned fabric membrane structures has been proposed. In this method, different stages in design and analysis are integrated in a single loop; it thus allows the information is well-transferred among them. Especially, different sources of nonlinearities, i.e., geometrical, material and boundary, can be included in the design and analysis stages. Hence, the computational model is closer to the physical one, and the obtained results are more reliable. In this work the method to apply compensation for fabric panels is also presented, this information can be valuable for the designers, but is rarely reported elsewhere. Moreover, this chapter is also one of the first works that employed Bayesian optimization in structural optimization applications. From the results, it can be seen that the Bayesian optimization outperforms the GA, which has been widely used in the research field. It thus provides a viable choice for structural optimization applications.

Bibliography

[1] W. Punurai, W. Tongpool, J. Héctor Morales, Implementation of genetic algorithm for optimum cutting pattern generation of wrinkle free finishing membrane structures, Finite Elements in Analysis and Design 58 (2012) 84–90. doi:10.1016/j.finel.2012.04.008.

[2] P. Gosling, B. Bridgens, A. Albrecht, H. Alpermann, A. Angeleri, M. Barnes, N. Bartle, R. Canobbio, F. Dieringer, S. Gellin, W. Lewis, N. Mageau, R. Mahadevan, J.-M. Marion, P. Marsden, E. Milligan, Y. Phang, K. Sahlin, B. Stimpfle, O. Suire, J. Uhlemann, Analysis and design of membrane structures: Results of a round robin exercise, Engineering Structures 48 (2013) 313–328. doi:10.1016/j.engstruct.2012.10.008.

[3] K.-U. Bletzinger, J. Linhard, R. Wüchner, EXTENDED AND INTEGRATED NUMERICAL FORM FINDING AND PATTERNING OF MEMBRANE STRUCTURES, Journal of the International Association for Shell and Spatial Structures 50 (1) (2009) 35–49.

[4] J.-Y. Kim, J.-B. Lee, A new technique for optimum cutting pattern generation of membrane structures, Engineering Structures 24 (6) (2002) 745–756. doi:10.1016/S0141-0296(02)00003-2.

[5] M. Ohsaki, J. Fujiwara, Developability conditions for prestress optimization of a curved surface, Computer Methods in Applied Mechanics and Engineering 192 (1–2) (2003) 77–94. doi:10.1016/S0045-7825(02)00523-6.

[6] M. Ohsaki, K. Uetani, Shape-stress trade-off design of membrane structures for specified sequence of boundary shapes, Computer Methods in Applied Mechanics and Engineering 182 (1–2) (2000) 73–88. doi:10.1016/S0045-7825(99)00086-9.

[7] R. B. Haber, J. F. Abel, D. P. Greenberg, An integrated design system for cable reinforced membranes using interactive computer graphics, Computers & Structures 14 (3–4) (1981) 261–280. doi:10.1016/0045-7949(81)90012-2.

[8] J. B. Pargana, D. Lloyd-Smith, B. A. Izzuddin, Fully integrated design and analysis of Tensioned Fabric Structures: Finite elements and

case studies, Engineering Structures 32 (4) (2010) 1054–1068. doi:10.1016/j.engstruct.2009.12.032.

[9] T. Dinh, A. Rezaei, W. Punurai, L. De Laet, M. Mollaert, D. Van Hemelrijck, W. Van Paepegem, A shape optimization approach to integrated design and nonlinear analysis of tensioned fabric membrane structures with boundary cables, International Journal of Solids and Structures 83 (2016) 114–125. doi:10.1016/j.ijsolstr.2016.01.004.

[10] S. Gale, W. J. Lewis, Patterning of tensile fabric structures with a discrete element model using dynamic relaxation, Computers & Structures 169 (2016) 112–121. doi:10.1016/j.compstruc.2016.03.005.

[11] R. M. PAULETTI, D. M. GUIRARDI, S. GOUVEIA, Modeling sliding cables and geodesic lines through dynamic relaxation, in: Symposium of the International Association for Shell and Spatial Structures (50th. 2009. Valencia). Evolution and Trends in Design, Analysis and Construction of Shell and Spatial Structures: Proceedings, Editorial de la Universitat Politécnica de Valencia., 2010.

[12] P. Wriggers, Nonlinear Finite Element Methods, Springer Berlin Heidelberg, Berlin, Heidelberg, 2008.

[13] J.-J. Li, S.-L. Chan, An integrated analysis of membrane structures with flexible supporting frames, Finite Elements in Analysis and Design 40 (5–6) (2004) 529–540. doi:10.1016/S0168-874X(03)00076-3.

[14] Hibbit, Karlsson, Sorensen, ABAQUS/Standard Analysis User's Manual, Hibbit, Karlsson, Sorensen Inc., 2014.

[15] W. A. Wall, M. A. Frenzel, C. Cyron, Isogeometric structural shape optimization, Computer Methods in Applied Mechanics and Engineering 197 (33–40) (2008) 2976–2988. doi:10.1016/j.cma.2008.01.025.

[16] B. Bridgens, M. Birchall, Form and function: The significance of material properties in the design of tensile fabric structures, Engineering Structures 44 (2012) 1–12. doi:10.1016/j.engstruct.2012.05.044.

[17] Matt Lombart, SolidWorks Surfacing and Complex Shape Modeling Bible (Apr. 2008).

[18] V. Torczon, On the Convergence of Pattern Search Algorithms, SIAM Journal on Optimization 7 (1) (1997) 1–25. doi:10.1137/S1052623493250780.

[19] J. Snoek, H. Larochelle, R. P. Adams, Practical bayesian optimization of machine learning algorithms, in: Advances in neural information processing systems, 2012, pp. 2951–2959.

[20] A. L. Marsden, M. Wang, J. E. Dennis Jr, Constrained aeroacoustic shape optimization using the surrogate management framework, Tech. rep., DTIC Document (2003).

[21] K. Kawaguchi, L. P. Kaelbling, T. Lozano-Pérez, Bayesian Optimization with Exponential Convergence, arXiv:1604.01348 [cs, stat]ArXiv: 1604.01348.

[22] R. Meske, J. Sauter, E. Schnack, Nonparametric gradient-less shape optimization for real-world applications, Structural and Multidisciplinary Optimization 30 (3) (2005) 201–218. doi:10.1007/s00158-005-0518-0.

[23] D. R. Jones, A taxonomy of global optimization methods based on response surfaces, Journal of global optimization 21 (4) (2001) 345–383.

[24] W. Annicchiarico, M. Cerrolaza, Structural shape optimization 3d finite-element models based on genetic algorithms and geometric modeling, Finite Elements in Analysis and Design 37 (5) (2001) 403–415. doi:10.1016/S0168-874X(00)00041-X.

[25] A. Messac, Optimization in Practice with MATLAB for Engineering Students and Professionals (Mar. 2015).

Chapter 6

Numerical Homogenization Procedure for Woven Fabrics

Thus far, the constitutive material model for the PVC coated fabric has been developed, carefully validated with the experimental data. Moreover, a dedicated design method that allows us to use this material model in design and analysis of tensioned membrane structures has been proposed. Nevertheless, the performance of the model is deteriorated when the load ratio in the warp and fill directions in the membrane is different from 1. This is quite expected because the material parameters of this model were calibrated in such a way that the discrepancies between simulation and experimental data with the load ratio of 1 are minimized (*cf.* chapter 2). To improve this material model, the experimental data with different load ratios in biaxial tests are required. However, experimental testing is time-consuming and expensive. Especially, at the moment it is not known in advance what load ratios are needed to further develop the constitutive material model. Thus, virtual testing is an intriguing alternative. Normally, the virtual testing for materials is conducted on a repeated unit cell (RUC) within the framework of multiscale modeling. On the other hand, the PVC coated fabric considered in this work is a kind of heterogeneous material. To predict the macroscopic mechanical behavior of this material well, it is necessary to understand the mechanical deformation mechanisms in the underlying structures, *e.g.*, micro- or meso-scale. The information obtained from mechanical analyses of these low scale structures can be transferred back to the macroscopic scale by using homogenization techniques. In this chapter, elements of

the homogenization-based multiscale method, *viz.*, the periodic boundary conditions, numerical homogenization scheme and the digital element method for woven fabrics, are presented in detail. These elements will provide analysis facilities for numerical modeling of the PVC coated woven fabric in the subsequent chapter. It is worth mentioning that the mechanical behavior of the studied PVC coated fabric is mainly governed by the underlying woven structure. Therefore, success in simulation of the dry woven fabric (without coating) will be a premise for the simulations of coated fabrics presented in the next chapter.

6.1 Introduction

Woven fabrics have recently received considerable attention because they are involved in different types of structures and materials, such as textile composites [1] and coated fabrics [2, 3]. In this chapter, these materials are referred to as woven fabric composites. It is evident that the mechanical properties of woven fabrics have a profound effect on the behavior of woven fabric composites, especially in case of coated fabrics [4]. A woven fabric is made by interlacing the so-called warp and fill yarns into a certain weave pattern. Classical weave patterns are plain, twill and satin shown in fig. 6.1. Each yarn contains a number of fibers with a diameter in the order of micrometers [5]. Indeed, the woven fabric materials have a hierarchically multi-scale nature. The fabric is composed of the yarns and the yarns are composed of a number of fibers. Therefore, mechanics of woven fabrics can be addressed at three different scales, *i.e.,* fabric level or macro-scale, yarn level or meso-scale and fiber level or micro-scale [6]. As a consequence, multiscale modeling is an eligible technique to provide a realistic description of the mechanical behavior of this kind of materials.

In this chapter, the elements of multiscale modeling for woven fabrics are presented. It commences with a literature study on woven fabrics modeling. Afterward, the digital element method, which is a dedicated simulation technique for woven fabrics, is introduced. It is followed by the theoretical background and the software implementation of the periodic boundary conditions and the numerical homogenization method. The chapter ends with the numerical simulation of a dry woven fabric under shear loading using the aforementioned numerical facilities.

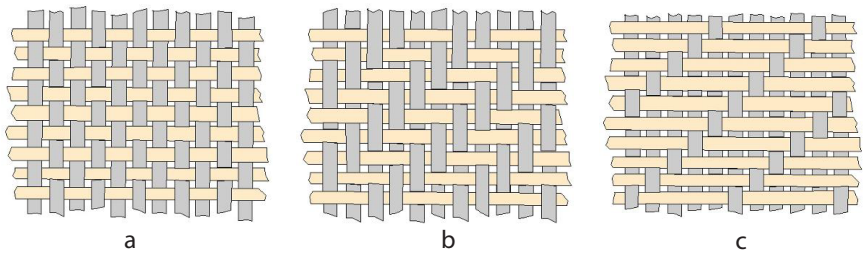

Figure 6.1: Classical weaving patterns: (a) plain weave, (b) twill weave and (c) satin weave (reprinted from *www.fibermaxcomposites.com*).

6.2 Woven fabrics modeling: a literature study

As mentioned earlier, mechanics of dry woven fabrics can be addressed at three different scales. Thus, models of woven fabrics can be divided into three categories depending on the scale they were proposed.

On macro-scale, woven fabrics can be considered as an anisotropic shell or membrane structure [7–9]. One of the material constitutive laws dedicated for woven fabrics was the hyperelasticity model for 3D woven fabrics proposed by Charmetant et al. [9]. In that work, the strain energy density formed through considering six deformation modes, *viz.*, transverse compression, in plane shear, longitudinal stretches and longitudinal shear in the warp and fill directions. That material model was used to simulate a deep drawing with a hemispherical punch. Compared with the experimental data, that model can provide reasonable results, but discrepancies between them are still visible. The reason is that the model cannot capture the local bending stiffness of the fibers, which has a significant effect on the woven fabric bending. Moreover, to calibrate that model, a sequence of tests, *viz.*, tension tests in the warp and fill direction, transverse compression test, in-plane and transverse shear tests, have to be done and inverse problems need solving to identify the material parameters. However, the mechanical behavior of the woven fabric shell (or membrane) can be derived by homogenizing the underlying meso-structure.

The meso-structure was either modeled by a pin-joined beam system [7] or a 3D finite element model [8]. In the former case, the structural configuration of the pin-joined beam system is linked with the macroscopic

deformation through an energy minimization method and subsequently macrosopic stresses are obtained from the internal forces of the pin-joined beam system by using the equilibrium conditions (*cf.* fig. 2.3). The problem with this approach is that the current beam theories are not sufficient to model the multi-fiber yarn, which has been shown in the work of Cornelissen and Akkerman [10]. Moreover, it is worth mentioning that this approach has been only widely applied for plain weave fabric, which has the simplest geometry among woven fabrics. Application of this approach for different kinds of weaving in 2D and 3D fabrics becomes cumbersome because of the complexity of the mathematical equations. In the latter case, a 3D finite element analysis on meso-structure of the woven fabric is performed, and the obtained result is then transferred to the macro scale using a homogenization scheme. Indeed, numerical models of woven fabrics at meso-scale are extensive. There are three different factors that are decisive for the performance of these models, *viz.*, the accuracy of the fabric yarn geometry, material constitutive law for the yarns and boundary conditions [9]. Contact between yarns plays a crucial role to predict the behavior of dry woven fabrics. Thus, the contact surfaces have to be described precisely. Ideally, there should be no interpenetration between yarns and no unreal voids. It is not a trivial task because the cross section of the yarns will change due to the reorganization of fibers in the micro-scale during the course of loading. In the work of Hivet and Boisse [11], the authors proposed a geometrical model for 2D fabrics. In their model, the cross sections of the yarn are varied along the yarn path. Different optical processes were used to determine the cross sections of the fabric yarn in different types of weaving. Based on these experimental observations, generic cross sections of the yarn at different locations in the yarn path were defined. Those authors claimed that this model ensured a realistic contact surface between yarns in the fabrics. Nevertheless, the model assumed that variations of the yarn thickness and width are small enough to ignore. This assumption can be invalid in case of tightly woven fabrics [12]. Regarding the constitutive law for the fabric yarn, one of the vital requirements is that it must account for the fibrous and discontinuous nature of the fabric yarns. Charmetant et al. [13] have proposed a material constitutive law for fabric yarns within the hyperelasticity framework. As a core of the model, they proposed a free energy function that accounts for four different deformation modes, *viz.*, elongation in fiber direction, compaction of the cross section, transverse shear and longitudinal shear. To calibrate this model, a sequence of

tests to characterize the aforementioned deformation modes are involved and the parameter identification is not straightforward. Regarding the boundary condition for meso-scale models, the periodic boundary conditions are de facto used. By using these conditions, it is ensured that the displacements among RUCs are continuous and the traction distributions on the opposite faces of any RUC are always the same.

The pioneering work in numerical modeling of woven fabrics at micro-scale, *i.e.*, fiber scale, was proposed by Wang and Sun [14]. They referred to their method as digital element method. In this method, the fiber was modeled as a sequence of cylinder bars, which are connected by frictionless pins and the cross section of the bars is a circle. While in the conventional finite element method, the element itself still maintains the physical properties of the discretized body, the individual cylinder bar in this case does not preserve the flexible nature of the fiber. However, this physical property can be mimicked by pinning different bars. The concept is similar to digital discretization that is why that method was referred to as digital element method [14]. Interaction among fibers is modeled so that the contact friction will be activated when the distance between two nodes of different fibers is smaller than the diameter of the fibers' cross section. This approach was further developed in subsequent works of Wang and her colleagues, such as [15–17], to mainly investigate the equilibrium geometry of woven fabrics. A similar approach was also proposed by Durville [18, 19]. However, in his works validation was missing. Döbrich et al. have also used this approach to model the mechanical properties of textile composites. Good results have been reported in Ref. [20]. Recently, Daelemans et al. have used the digital element method to simulate the woven geometry and mechanical behavior of a 3D dry fabric under different load cases [21]. Their results have been carefully tested with the corresponding experimental data and a very good agreement between numerical simulations and experimental data have been shown.

6.3 Digital element method: a dedicated simulation technique for woven fabrics

Although modeling woven fabrics at meso-scale is promising and the assumption of variable yarn cross section along the yarn path is a good approach to capture the realistic geometry of woven fabrics, its application for complex fabric structures is limited. Indeed, the yarn shape is affected

by the reorganization of the fiber at micro-scale during the course of loading. Thus, fabric geometry can be better captured at the micro scale, *i.e.*, fiber scale. The digital element method is a micromechanics-based approach, which was initially proposed to determine the geometry of 3-D braided fabrics [14]. There are three main concepts in this approach, *viz.*, digital fiber, digital yarn, and contact element [22] (*cf.* fig. 6.2). While the digital yarn is composed of a bundle of digital fibers, the digital fiber is composed of a sequence of cylinder bars, which are linked by frictionless pins. It is worth mentioning that the digital fiber can be modeled by a chain of pin-jointed truss elements in any finite element code. Additionally, the contact between truss elements has also been implemented in ABAQUS/Explicit [23].

In order to find the fabric micro geometry, the fabric topology and the targeted yarns prestresses are specified. The prescribed fabric configuration might not be in equilibrium. Such configuration can be found by using either an implicit or explicit integration scheme. Indeed, the fabric fibers can be rather soft and there are many contact elements involved in the equilibrium analysis. As a consequence, the dynamic explicit solver is a better choice [17]. Moreover, the fabric yarns are composed of hundreds or thousands of fibers in micro-scale. It is thus extremely computationally expensive if all of the fibers are included in the model. However, it is not the case when the digital element method is used. In the work of Miao et al. [16], a model that has 19 fibers per yarn was sufficient to predict a 3D braided fabric micro-geometries. In this context, a digital fiber does not represents for a single physical fiber, but for a cluster of physical fibers. It has been shown from the work of Wang and her colleagues that the digital element method is a promising method to determine realistically the geometry of fabrics (*cf.* fig. 6.3).

Indeed, different forms of the digital element method also exist. In [24], the authors employed the digital element method to model the geometry of a 3-D fabric in LS-Dyna. Different from the original work of Wang and Sun [14], in that work Mahadik and Hallet modeled the fiber with beam elements and a thermal drop was applied to the fibers to apply the tension force. Thus, the equilibrium configuration of the fabric can be found. In their model, 19 fibers were also used to model the fabric yarn and the diameter of each digital fiber is much larger than the diameter of the physical glass fiber. Those authors used beam elements instead of rod elements because the glass fiber in their considered fabric has a nonnegligible bending stiffness. However, in the classical beam theory,

the bending stiffness is coupled with the axial stiffness and the fact that the diameter of the digital fibers is much larger than the diameter of the physical ones. Therefore, using beam elements can lead to overestimate the bending stiffness of the digital fabric fibers in that case. Another

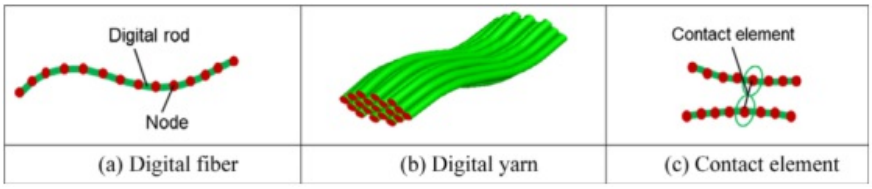

Figure 6.2: key concepts in the digital element method (reprinted from [17]).

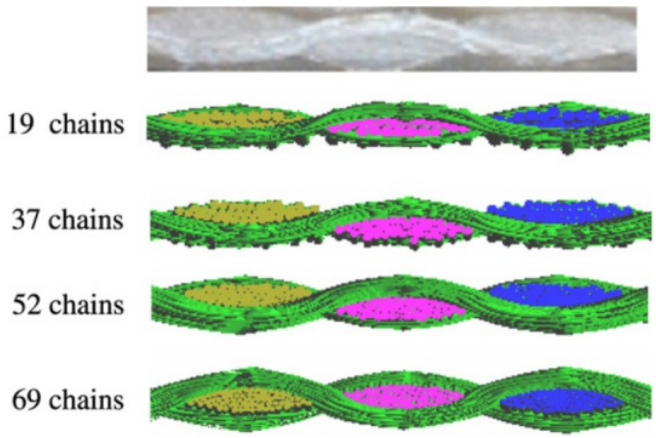

Figure 6.3: Comparison between the fabric geometry identified from a CT-scan measurement and the counterparts found from numerical simulations using the digital element method (reprinted from [16]).

form of the digital element method can be found in the works of Durville [19, 25]. In those works, the author proposed a kinematically enriched beam element for the fibers, so that the deformation of the beam's cross sections can be taken into account. Moreover, Durville also proposed a different approach in identifying the equilibrium configuration of the fabric. In his proposed method, the fabric fibers were laid in the same plane and interpenetrating each other. Subsequently, the superimposing order, which is used to prescribe the weaving pattern, is assigned at each

yarn crossing. Afterward, fibers belonging to different yarns were separated and move to the targeted positions set by the superimposing order until fibers from different yarns were really separated (*cf.* fig. 6.4). However, in his works, validation was missing. He proposed the kinematically enriched beam element for the fibers and believed that it could capture better the behavior the fabric fibers during deformation. Nevertheless, he did not compare the results obtained from the proposed beam and the classical one. In addition, it is evident that the extra degrees of freedom coming from the enrichment kinematics manifested themselves in the time of the simulations. In order to identify the geometry of a 2-D fabric, it took two to three days for the calculation time.

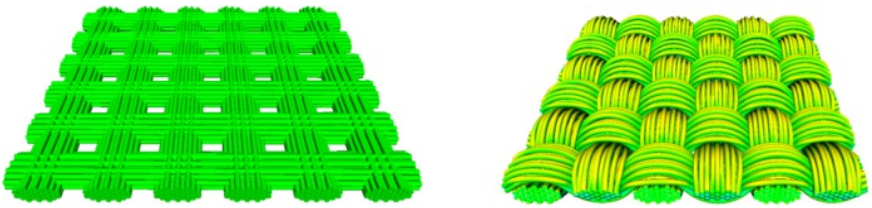

Figure 6.4: Initial configuration and computed equilibrium configuration of a 2-D fabric (reprinted from [26]).

6.4 Elements of the RUC-based homogenization technique and their implementation

The core of multiscale modeling is the RUC-based homogenization technique. Using this technique the strain from the coarse scale (*i.e.*, the macro-scale) can be transferred to the fine scale (*i.e.*, the micro/meso-scale) as boundary conditions. In return, the stress of the coarse scale can be obtained from the stress fields in the fine scale by using a certain homogenization scheme. In this work, we use periodic boundary conditions (PBC) and the numerical homogenization method to exchange the information between coarse and fine scales.

6.4.1 A practical implementation for periodic boundary conditions

RUC is the smallest cell that can be used to reconstruct the corresponding continuum medium. Therefore, boundary conditions, which are used to apply to an RUC, have to fulfill conditions such that the displacement between two integrated deformed RUCs has to be continuous, and there is no void or penetration between them. Periodic boundary conditions (PBC) can satisfy these requirements. In practice, the PBC are normally applied to the opposite surfaces of the RUC [27]. By using these boundary conditions, the spatial periodicity of the material points on surfaces ABB_1A_1 and BB_1C_1C are linked to the other surfaces DCC_1D_1 and AA_1D_1D and the control points 1, 2 and 3 (fig. 6.5) as follows:

$$\mathbf{x}^{ABB_1A_1} = \mathbf{x}^{DCC_1D_1} - \mathbf{x}^1 + \mathbf{x}^3, \tag{6.1}$$

$$\mathbf{x}^{BB_1C_1C} = \mathbf{x}^{AA_1D_1D} - \mathbf{x}^1 + \mathbf{x}^2, \tag{6.2}$$

where $\mathbf{x}^*$ is the position vector of a point $*$ with respect to a fixed coordinate system.

Since the conditions in equations 6.1 and 6.2 are also satisfied in the initial configuration, we can express them in terms of displacements as follows

$$\mathbf{u}^{\mathrm{ABB_1A_1}} = \mathbf{u}^{\mathrm{DCC_1D_1}} - \mathbf{u}^1 + \mathbf{u}^3, \tag{6.3}$$

$$\mathbf{u}^{\mathrm{BB_1C_1C}} = \mathbf{u}^{\mathrm{AA_1D_1D}} - \mathbf{u}^1 + \mathbf{u}^2. \tag{6.4}$$

The displacements of the corners 1, 2 and 3 are related to the macroscopic deformation gradient $\mathbf{F}^M$ as:

$$\mathbf{u}^{\mathrm{p}} = \mathbf{x}^{\mathrm{p}} - \mathbf{X}^{\mathrm{p}} = (\mathbf{F}^{\mathrm{M}} - \mathbf{I}) \cdot \mathbf{X}^{\mathrm{p}}, \qquad \mathrm{p} = 1, 2, 3, \tag{6.5}$$

where $\mathbf{X}^{\mathrm{p}}$ is the position vector of the corner p in the initial configuration and $\mathbf{I}$ is the second identity order tensor. The equations 6.3 and 6.4 can be implemented in ABAQUS by using the linear equation constraint, in which the value of the last two terms of the right hand side (RHS) will be imposed as displacements of the control points.

In this work, a Matlab program was implemented to impose the PBCs on an ABAQUS model. At first, it arranged the nodes on the faces of the

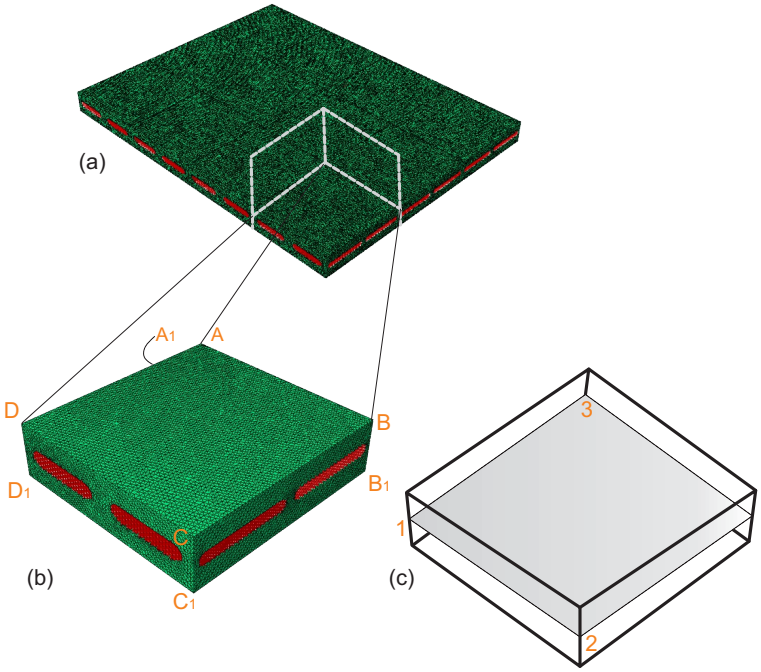

Figure 6.5: Implementation of PBC on opposite surfaces of the coated fabric unit cell: (a) a coated fabric sheet; (b) a repeated unit cell; (c) positions of the control points that govern deformation modes of the unit cell.

RUC into three groups. The first group contains only the nodes located at the corners of the RUC. The second group contains all nodes located on the edges of the RUC except for the ones at the corners. The last group contains the nodes on the faces of the RUC except for the ones at the corners and on the edges (*cf.* table 6.1). Afterward, this Matlab program found the matching nodes on two opposite surfaces as well as two opposite edges. It then retrieved the paired nodes and incorporated them into the linear equation constraint (*cf.* the Abaqus keyword "*Equation" [23]). However, the paired nodes can only be found in case of a conformal mesh. In practice, it is difficult to achieve such mesh, especially, when the geometry of the model is complicated. In [27], the author has proposed a method to tackle this problem. In that method, a copy of a selected surface is translated to the opposite one, then this copied surface is tied with the opposite surface (*cf.* the Abaqus keyword "*Tie" [23]). By doing

Table 6.1: Node sets used to impose the PBCs on the RUC.

Group 1	Group 2	Group 3
Corner_{A}	Edge_{AA_1}	$\mathrm{Face}_{AA_1D_1D}$
Corner_{A_1}	$\mathrm{Edge}_{A_1D_1}$	$\mathrm{Face}_{ABB_1A_1}$
Corner_{D_1}	Edge_{D_1D}	$\mathrm{Face}_{BCC_1B_1}$
Corner_{D}	Edge_{DA}	$\mathrm{Face}_{CDD_1C_1}$
Corner_{B}	Edge_{AB}	Face_{ABCD}
Corner_{B_1}	Edge_{BB_1}	$\mathrm{Face}_{A_1B_1C_1D_1}$
Corner_{C_1}	$\mathrm{Edge}_{B_1A_1}$	
Corner_{C}	Edge_{A_1A}	
	Edge_{CB}	
	$\mathrm{Edge}_{B_1C_1}$	
	Edge_{C_1C}	
	Edge_{DC}	
	$\mathrm{Edge}_{C_1D_1}$	

that the nodes on the opposite surface have the same displacements as the nodes on the copied surface. Subsequently, the linear equation constraint can be imposed on the nodes on the selected surface and their translated copy. Illustration of this process can be seen in fig. 6.6.

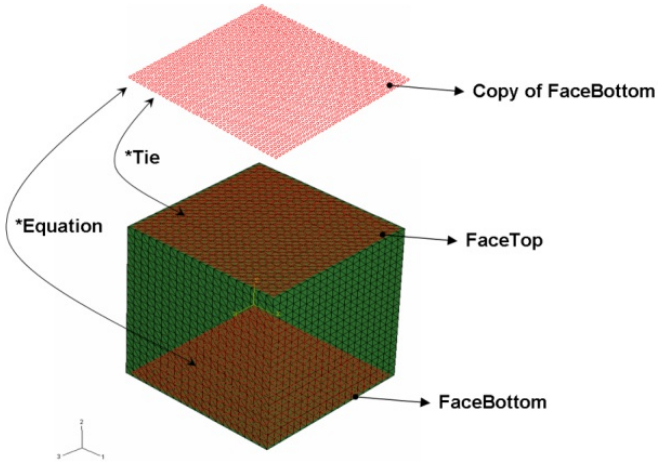

Figure 6.6: Implementation of PBC on opposite surfaces in case of non-conformal mesh (reprinted from [27]).

6.4.2 Numerical homogenization method for woven fabric materials within finite deformation framework

The averaged RUC stress tensor can be calculated from the stress field $\boldsymbol{\sigma}(\mathbf{x})$ in the RUC as follows [28]:

$$\bar{\boldsymbol{\sigma}} = \frac{1}{v_{\mathrm{RUC}}} \int_{\mathbf{x}\in v} \boldsymbol{\sigma}(\boldsymbol{x}) \mathrm{d}v, \tag{6.6}$$

where v_{RUC} is the deformed volume of the RUC. This integration can be done numerically with respect to the used element type and element geometry. However, this approach is not numerically efficient. Indeed, by using the divergence theorem and exploiting the equilibrium condition, the equation 6.6 can be expressed as:

$$\bar{\sigma}_{\mathrm{ij}} = \frac{1}{v_{\mathrm{RUC}}} \int_{\mathbf{x}\in\partial v} f_{\mathrm{j}} x_{\mathrm{i}} \mathrm{d}a, \tag{6.7}$$

where $\mathbf{f}$ and $\mathbf{x}$ are respectively the traction and position vectors of material points in the surface of the RUC. In [28], the authors have proved that by using the PBC equation 6.7 can be simplified as follows:

$$\bar{\sigma}_{\mathrm{ij}} = \frac{1}{v_{\mathrm{RUC}}} \int_{\mathbf{x}\in\partial v} f_{\mathrm{j}} x_{\mathrm{i}} \mathrm{d}a = \frac{1}{v_{\mathrm{RUC}}} \sum_{p=1}^{3} f_{\mathrm{j}}^{\mathrm{p}} x_{\mathrm{i}}^{\mathrm{p}}, \tag{6.8}$$

where $\mathbf{f}^{\mathrm{p}}$ and $\mathbf{x}^{\mathrm{p}}$ are respectively the traction and position vectors of the control points (*cf.* fig. 6.5).

6.5 Simulation of fabric shear using the digital element method

From the literature study mentioned above, the digital element method is indeed a very promising method for modeling woven fabrics. However, thus far there have been few works employing this method to characterize mechanical behavior of woven fabric materials. Actually, during the forming process the dry woven fabric can be subjected to a very complicated deformation, which is a combination of biaxial tension, in-plane shear, transverse compaction and out-of-plane bending. Among them, the in-plane shear deformation is significant [5, 29] and causes problems, such as the appearance of wrinkes [6, 30]. In this section, the digital element method is used to simulate the shear behavior of a dry woven fabric. The aims of this simulation are twofold: (i) to gain a better understanding of the fabric shear behavior to model the forming process with confidence, (ii) to investigate the digital element method for its potential to simulate mechanical loads on dry woven fabrics. The Chomarat 150 is chosen as a case study because the geometrical data of its unit cell and mechanical properties of the fabric fiber are available (*cf.* table 6.2). Moreover, the experimental data of the shear behavior of this fabric obtained from a picture frame test is also available and can be found in Ref. [31].

It has been revealed that regardless of the fiber type and weaving type the obtained shear-angle load is always a J-shaped curve. This curve can be divided into three stages. In the first stage, the initial shear stiffness is low and governed by friction among yarns. In the second stage, adjacent yarns come into contact, the shear stiffness is thus gradually increased. Eventually, in the last stage, the yarn lock-up happens. As a result, the shear stiffness increases significantly. It has been mentioned in [30–33] that there are four fundamental deformation mechanisms during shear, *viz.*, inter-yarn trellising, intra-yarn slipping, rotation at crossovers and lateral compression.

To characterize the dry fabric shear a picture frame test or a bias extension test can be used. There are extensive studies on these tests, among them are [5, 29, 31, 32, 34–37]. It has been concluded from these studies that

Table 6.2: Material and geometrical details for Chomarat 150TB (reproduced from [31]).

Total areal density	150 g/m^2
Warp areal density	82 g/m^2
Fill areal density	68 g/m^2
Fiber density	2.62 g/m^2
Fiber volume fraction of yarn	55%
Warp yarn spacing	1.686 mm
Fill yarn spacing	1.97 mm
Yarn width	0.819 mm
Fabric thickness	0.297 mm
Fiber modulus	73 GPa
Friction coefficient	0.3

the picture frame test is more appropriate to characterize the fabric shear at finite deformation regime. This frame is made by assembling four rods that are pinned together at the ends. In the test, a square fabric is placed in the frame in such a way that the warp and fill yarns are respectively parallel to the frame sides. A tensile force is applied at a corner of the frame, which is referred to as a crosshead in [32], while the opposite corner is fixed. As a consequence, the square configuration transforms into a rhombus (fig. 6.7). During the test, the force applied to the crosshead and the displacement of the crosshead are recorded. Based on these data, the shear force and shear angle are derived. It is assumed that during the course of deformation, only shearing of the fabric occurs and the yarns are not stretched provided that the edge effects are ignored [32, 34, 35]. At fiber scale, it has been shown by experimental studies that intra-yarn deformation occurs during the picture frame test [32] and the fibers in each yarn also slip relative to each other [38, 39]. It is worth mentioning that the boundary condition imposed on the fabric is really tricky. Harrison et al. [32] mentioned that if the edges of the fabric were loosely pinned in the frame, the required kinematics may not be induced. However, if these edges were tightly clamped in the frame, it would lead to spurious results.

Moreover, because the picture frame test has not been standardized and the frame size varies for different research groups, thus the normalization based on the energy method proposed in [32] is used. Following this method, the shear force will be normalized by the length of the frame.

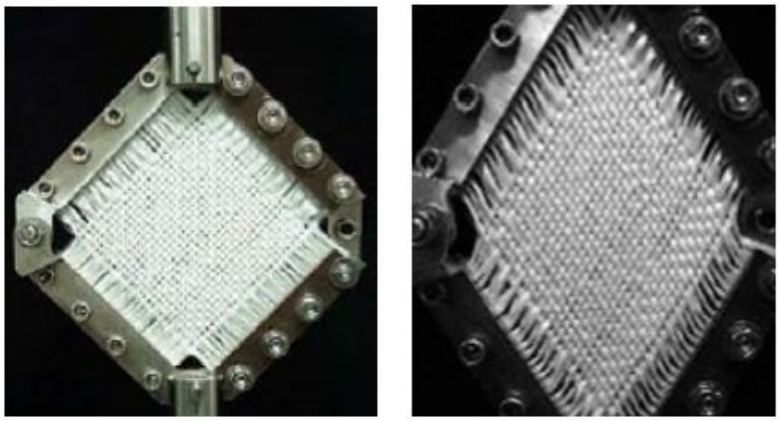

Figure 6.7: Initial and deformed configurations of the fabric specimen in the picture frame test set-up (reprinted from [31]).

This method was also used in [31], from where the experimental data used in this section are extracted (fig. 6.8). The geometry of the Chomarat

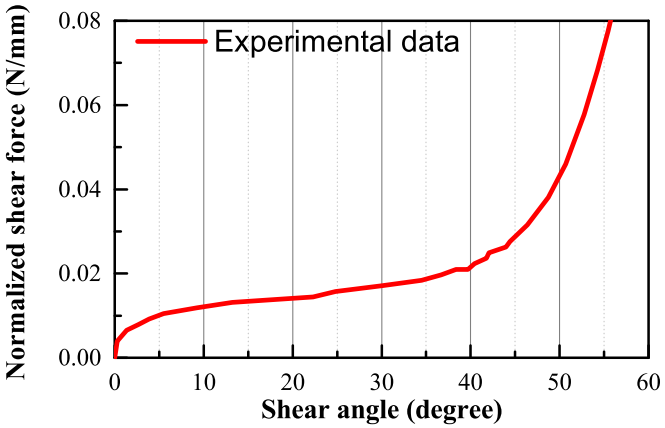

Figure 6.8: Normalized shear force and shear angle curved obtained from the picture frame test [31].

150 RUC is created based on micro-CT measurements provided in [38]. The yarn paths are splines, which are defined by specifying points at the crossovers. The positions of these points are derived from the space between the warp and fill yarns and the fabric thickness (*cf.* table 6.2).

The cross section of each yarn is assumed to be an ellipse and the fibers are distributed hexagonally in this ellipse (fig. 6.9)

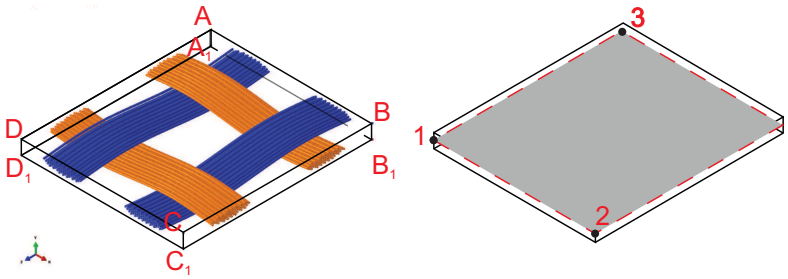

Figure 6.9: Unit cell of the Chomarat 150 and the position of the reference points, which are used to impose the boundary conditions.

6.5.1 Boundary conditions

The periodic boundary conditions presented in section 6.4.1 are employed to the RUC. To impose the shear deformation to the RUC, control point **2** is rotated counterclockwise around control point **1**, while control point **3** is rotated clockwise around control point **1**. It is assumed that the fabric yarns are not stretched and only fabric shear happens during the course of deformation in the picture frame test [40]. Therefore, the distances between the control points are kept constant during the course of rotation (*cf.* fig. 6.10).

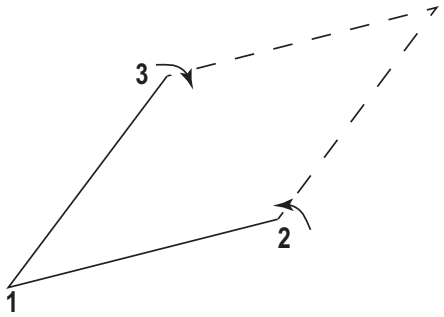

Figure 6.10: Illustration of the movement of the control nodes, which govern the deformation of the RUC.

6.5.2 Post-processing

I. Calculation of the normalized shear stress in the picture frame test

As mentioned in [40], to calculate the stress tensor we have to assume that the fabric is homogeneous and stress transfer within the material is the same as in continuum media. In [40], the authors mentioned that there is only a shear stress along the edges of the frames, denoted as τ_{s} (*cf.* fig. 6.11), and there is no normal stress on these edges. The shear stress is calculated as:

$$\tau_{\mathrm{s}} = F_{\mathrm{s}}/(L \cdot t), \tag{6.9}$$

where F_s is the projection of the tensile force that is applied to the crosshead. t is the thickness of the fabric and L is length of the frame edge. This formula is only applicable for the set-up in which the length of the frame is equal to the length of the fabric. However, in practice the fabric sample is cut-off at the corners to avoid wrinkles (*cf.* fig. 6.7). For this set-up, the shear stress is calculated as [41]:

$$\tau_{\mathrm{s}} = F_{\mathrm{s}} \frac{L_{\mathrm{frame}}}{L_{\mathrm{fabric}}^2 \cdot t}. \tag{6.10}$$

II. Calculation of the normalized shear stress of the RUC using computational homogenization method

The homogenized stresses of the RUC can be calculated by using eq. (6.8). The obtained stresses are indeed presented in the global coordinate. To compare with the normalized shear stress derived in subsection I., the obtained stresses have to be transformed from global coordinates x_1-x_3 to local coordinate η-ξ (*cf.* fig. 6.11) by using eq. (6.11).

$$\tau_{\eta\xi} = \tau_{\mathrm{s}} = -\frac{\sigma_{x_1} - \sigma_{x_3}}{2} \sin\gamma + \tau_{x_1 x_3} \cos\gamma. \tag{6.11}$$

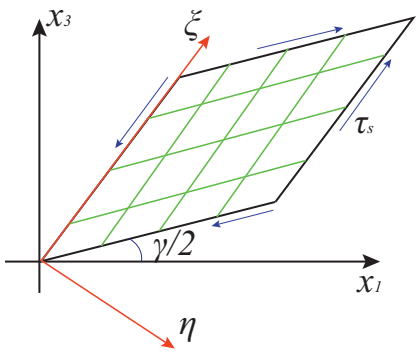

Figure 6.11: Stress transformation from the global x_1-x_3 coordinate system to the local η-ξ coordinate system.

6.6 Numerical results

As mentioned earlier, when using the digital element method, we do not have to use the same number of fibers of the considered fabric in the numerical model. In the work of Miao et al. [16] and Mahadik and Hallet [24], it has been reported that a model that has 19 fibers per yarn was sufficient to predict 3D braided fabric micro-geometries. In our case, the fibers are distributed hexagonally in the yarns, thus there is a coupling between the number of fibers in the thickness and the width directions of the yarn. As a consequence, the exact number of fibers per yarn cannot be assigned. Instead of using 19 fibers per yarn as the works mentioned above, the present author considers four cases in which the numbers of fibers per yarn are respectively equal to 11, 21, 44 and 61 (*cf.* fig. 6.12). While the number of fibers per yarn varies, the cross section of each fiber is also adjusted such that the yarn volume fraction can be preserved. Moreover, as mentioned in the work of Lomov et al. [39], when a fabric specimen is fixed onto the frame, it is possible that the fabric is tensioned. To apply this pretension, a linear temperature drop is applied to the fibers. Indeed, this temperature drop does not only impose the prestress in the fibers, but also causes reducing the crimp height of the fibers as well as changing the shape of the fabric yarn. It is worth mentioning that the abovementioned fabric pretension can affect the shear behavior of the fabric, especially in the low-strain regime [42]. However, this datum was missing in the Ref. [31], from where the experimental data are used in this work. Nevertheless, by testing with different values of the thermal drop,

the one that is equivalent to applying the strain of -0.15% in the fabric fibers is chosen.

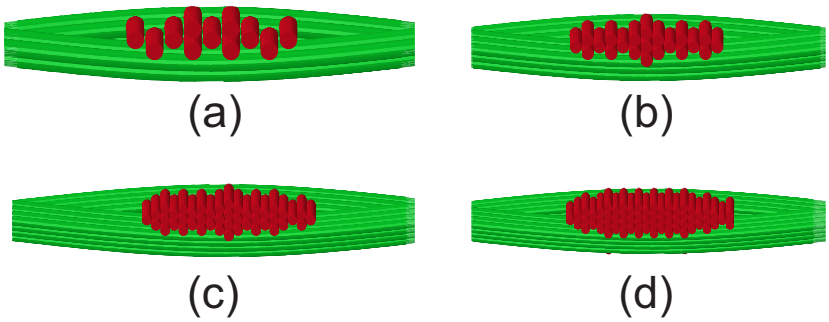

Figure 6.12: Different numbers of fibers per yarn are used to model the fabric yarn: (a) 11 fibers, (b) 21 fibers, (c) 44 fibers, and (d) 61 fibers.

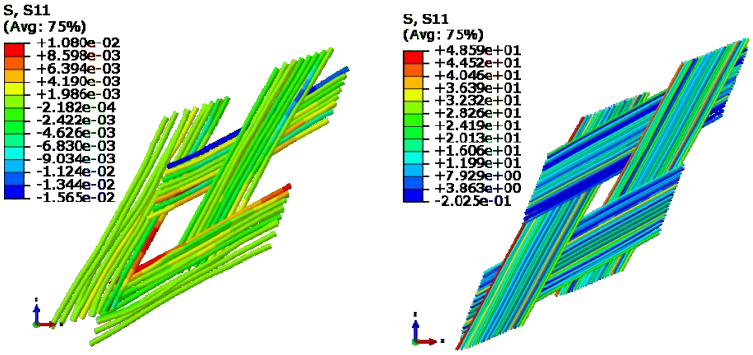

Figure 6.13: The deformed configuration of the 11-fiber-per-yarn and the 61-fiber-per-yarn fabric model.

The deformed configurations of the fabric when 11 fibers and 61 fibers are respectively used to model the fabric yarn are shown in fig. 6.13. The comparison of the homogenized shear behavior of the fabric when different numbers of fibers are used to model the fabric yarn is plotted in fig. 6.14. In addition, the homogenized shear behavior of the fabric when 61 fibers are used to model the fabric yarn and the corresponding experimental data are plotted in fig. 6.15. The numerical simulation by Lin et al. presented in [31], in which those authors used solid elements for fabric

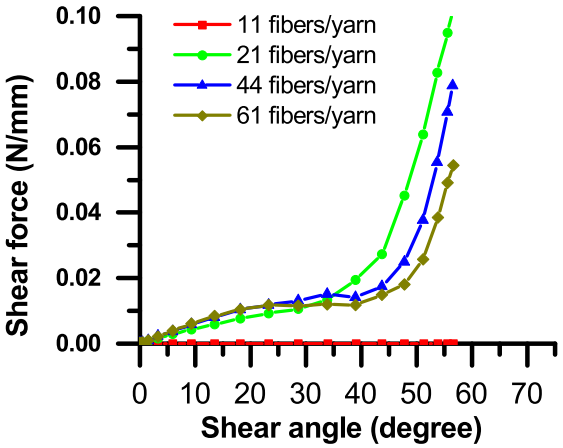

Figure 6.14: The influence of the number of fibers per yarn to the homogenized shear behavior of Chomarat 150.

yarns, is also plotted in fig. 6.15. It is clear from the obtained results that the number of fibers per yarn plays a crucial role and has a profound effect on the homogenized results. When the number of fibers per yarn is too low, the contact among the fibers cannot be properly described. As a consequence, the fibers are dispersed and the fabric is unwoven (*cf.* fig. 6.13). This phenomenon can also be observed in the homogenized shear behavior shown in fig. 6.15. The result obtained from the model with 11 fibers per yarn is almost zero during the course of deformation. When the contact among fibers is modeled properly, the typical J-shaped curve can be reproduced. The obtained result from the model with 21 fibers per yarn can bring a rough approximation for the shear behavior of the fabric. This observation is in line with the conclusion in [16, 24]. Those authors also recognized that the model with 19 fibers per yarn was sufficient to capture the microgeometry of 3D woven fabrics. It is worth mentioning that in those works, the conclusions were drawn by comparing the numerical results with the corresponding pictures obtained from CT-scan measurements in a qualitative sense. Moreover, it is evident that further refinement of the number of fiber per yarn can capture better not only the inter-yarn deformation, but also the intra-yarn deformation. These phenomena manifest themselves in the stiffer shear behavior that is obtained in the small shear angle regime, where the inter-yarn deformation is dominant, and at the larger locking angle, where the intra-

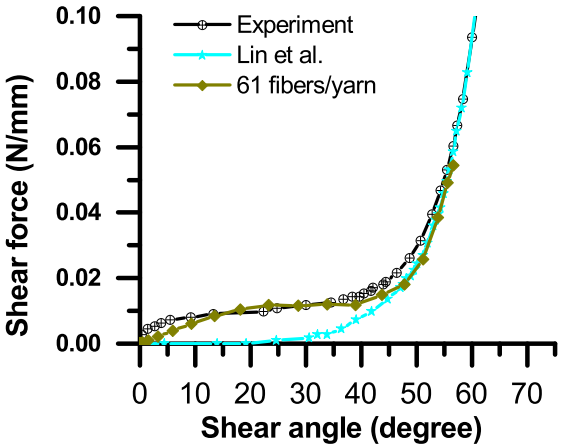

Figure 6.15: Comparison among the homogenized results obtained from the digital element method, the homogenized results obtained from Lin et al. (solid elements were used to model the fabric yarn) and the corresponding experimental data.

yarn deformation is dominant. Compared to the numerical simulation presented in [31], the result obtained from the model with 61-fiber-per-yarn is identical in the large shear angle regime, while in the small angle regime there is a clear improvement. This phenomenon can be explained by the fact that the intra-yarn shear was not considered in the numerical model presented in [31]. Moreover, in their model the fabric yarn was modeled with solid elements and the interaction among fibers in each yarn was not taken into account.

6.7 Conclusions

In this chapter, elements of multiscale modeling for woven fabrics, *viz.*, the periodic boundary conditions, the numerical homogenization method and the digital element method, are presented. Afterward, the fabric shear modeling of Chomarat 150, which is a dry woven fabric, is conducted using the aforementioned numerical facilities. The obtained results have significant improvement compared to the one available in the literature. It thus encourages the usage of the digital element method to model the mechanical behavior of the PVC coated fabric in the next chapter.

Bibliography

[1] A. P. Mouritz, M. K. Bannister, P. J. Falzon, K. H. Leong, Review of applications for advanced three-dimensional fibre textile composites, Composites Part A: Applied Science and Manufacturing 30 (12) (1999) 1445–1461. doi:10.1016/S1359-835X(99)00034-2.

[2] S. Kato, T. Yoshino, H. Minami, Formulation of constitutive equations for fabric membranes based on the concept of fabric lattice model, Engineering Structures 21 (8) (1999) 691–708. doi:10.1016/S0141-0296(98)00024-8.

[3] T. D. Dinh, A. Rezaei, L. De Laet, M. Mollaert, D. Van Hemelrijck, W. Van Paepegem, A new elasto-plastic material model for coated fabric, Engineering Structures 71 (2014) 222–233. doi:10.1016/j.engstruct.2014.04.027.

[4] J. B. Pargana, D. Lloyd-Smith, B. A. Izzuddin, Advanced material model for coated fabrics used in tensioned fabric structures, Engineering Structures 29 (7) (2007) 1323–1336. doi:10.1016/j.engstruct.2006.09.001.

[5] J. Cao, R. Akkerman, P. Boisse, J. Chen, H. Cheng, E. de Graaf, J. Gorczyca, P. Harrison, G. Hivet, J. Launay, W. Lee, L. Liu, S. Lomov, A. Long, E. de Luycker, F. Morestin, J. Padvoiskis, X. Peng, J. Sherwood, T. Stoilova, X. Tao, I. Verpoest, A. Willems, J. Wiggers, T. Yu, B. Zhu, Characterization of mechanical behavior of woven fabrics: Experimental methods and benchmark results, Composites Part A: Applied Science and Manufacturing 39 (6) (2008) 1037–1053. doi:10.1016/j.compositesa.2008.02.016.

[6] D. Durville, Simulation of the mechanical behaviour of woven fabrics at the scale of fibers, International Journal of Material Forming 3 (2) (2010) 1241–1251. doi:10.1007/s12289-009-0674-7.

[7] M. J. King, P. Jearanaisilawong, S. Socrate, A continuum constitutive model for the mechanical behavior of woven fabrics, International Journal of Solids and Structures 42 (13) (2005) 3867–3896. doi:10.1016/j.ijsolstr.2004.10.030.

[8] S. Fillep, J. Mergheim, P. Steinmann, Computational modelling and homogenization of technical textiles, Engineering Structures 50 (2013) 68–73. doi:10.1016/j.engstruct.2013.01.025.

[9] A. Charmetant, J. G. Orliac, E. Vidal-Sallé, P. Boisse, Hyperelastic model for large deformation analyses of 3d interlock composite preforms, Composites Science and Technology 72 (12) (2012) 1352–1360. doi:10.1016/j.compscitech.2012.05.006.

[10] B. Cornelissen, R. Akkerman, Analysis of yarn bending behaviour, in: Proceedings of ICCM-17: 17th international conference on composite materials, Edinburg, 2009.

[11] G. Hivet, P. Boisse, Consistent 3d geometrical model of fabric elementary cell. Application to a meshing preprocessor for 3d finite element analysis, Finite Elements in Analysis and Design 42 (1) (2005) 25–49.

[12] S. G. Ivanov, D. S. Ivanov, S. V. Lomov, I. Verpoest, F. Veyet, F. Boussu, Meso-FE models of tight 3d woven structures, in: European conference on composite materials (ECCM-15), Venice, Italy (24–28 June 2012), 2012.

[13] A. Charmetant, E. Vidal-Sallé, P. Boisse, Hyperelastic modelling for mesoscopic analyses of composite reinforcements, Composites Science and Technology 71 (14) (2011) 1623–1631. doi:10.1016/j.compscitech.2011.07.004.

[14] Y. Wang, X. Sun, Digital-element simulation of textile processes, Composites Science and Technology 61 (2) (2001) 311–319. doi:10.1016/S0266-3538(00)00223-2.

[15] B. A. Cheeseman, C. F. Yen, B. R. Scott, B. Powers, T. A. Bogetti, B. LaMattina, Y. Duan, M. Keefe, Y. Miao, Y. Wang, From Filaments to Fabric Packs-Simulating the Performance of Textile Protection Systems, Tech. rep., DTIC Document (2006).

[16] Y. Miao, E. Zhou, Y. Wang, B. A. Cheeseman, Mechanics of textile composites: Micro-geometry, Composites Science and Technology 68 (7–8) (2008) 1671–1678. doi:10.1016/j.compscitech.2008.02.018.

[17] L. Huang, Y. Wang, Y. Miao, D. Swenson, Y. Ma, C.-F. Yen, Dynamic relaxation approach with periodic boundary conditions in determining the 3-D woven textile micro-geometry, Composite Structures 106 (2013) 417–425. doi:10.1016/j.compstruct.2013.05.057.

[18] D. Durville, Numerical simulation of entangled materials mechanical properties, Journal of Materials Science 40 (22) (2005) 5941–5948. doi:10.1007/s10853-005-5061-2.

[19] D. Durville, Contact Modelling in Entangled Fibrous Materials, in: G. Zavarise, P. Wriggers (Eds.), Trends in Computational Contact Mechanics, no. 58 in Lecture Notes in Applied and Computational Mechanics, Springer Berlin Heidelberg, 2011, pp. 1–22.

[20] O. Döbrich, T. Gereke, C. Cherif, Modeling the mechanical properties of textile-reinforced composites with a near micro-scale approach, Composite Structures 135 (2016) 1–7. doi:10.1016/j.compstruct.2015.09.010.

[21] L. Daelemans, J. Faes, S. Allaoui, G. Hivet, M. Dierick, L. Van Hoorebeke, W. Van Paepegem, Finite element simulation of the woven geometry and mechanical behaviour of a 3d woven dry fabric under tensile and shear loading using the digital element method, Composites Science and Technology 137 (2016) 177–187. doi:10.1016/j.compscitech.2016.11.003.

[22] L. Huang, Determining micro- and macro- geometry of fabric and fabric reinforced compositesU.S. Army Research Laboratory, Albany Engineered Composites, Inc.

[23] Hibbit, Karlsson, Sorensen, ABAQUS/Explicit Analysis User's Manual, Hibbit, Karlsson, Sorensen Inc., 2014.

[24] Y. Mahadik, S. R. Hallett, Finite element modelling of tow geometry in 3d woven fabrics, Composites Part A: Applied Science and Manufacturing 41 (9) (2010) 1192–1200. doi:10.1016/j.compositesa.2010.05.001.

[25] D. Durville, Finite Element Simulation of the Mechanical Behaviour of Textile Composites at the Mesoscopic Scale of Individual Fibers, in: E. Oñate, B. Kröplin (Eds.), Textile Composites and Inflatable

Structures II, no. 8 in Computational Methods in Applied Sciences, Springer Netherlands, 2008, pp. 15–34.

[26] D. Durville, Finite element simulation of textile materials at mesoscopic scale, in: Finite element modelling of textiles and textile composites, Saint-Petersbourg, Russie, Fédération De, 2007.

[27] G. Al Kassem, Micromechanical material models for polymer composites through advanced numerical simulation techniques, Ph.D. thesis, RWTH Aachen (2009).

[28] M. G. D. Geers, V. G. Kouznetsova, W. a. M. Brekelmans, Computational homogenization, in: R. Pippan, P. Gumbsch (Eds.), Multiscale Modelling of Plasticity and Fracture by Means of Dislocation Mechanics, no. 522 in CISM International Centre for Mechanical Sciences, Springer Vienna, 2010, pp. 327–394, dOI: 10.1007/978-3-7091-0283-1_7.

[29] P. Badel, E. Vidal-Sallé, P. Boisse, Computational determination of in-plane shear mechanical behaviour of textile composite reinforcements, Computational Materials Science 40 (4) (2007) 439–448. doi:10.1016/j.commatsci.2007.01.022.

[30] B. Zhu, T. X. Yu, X. M. Tao, An experimental study of in-plane large shear deformation of woven fabric composite, Composites Science and Technology 67 (2) (2007) 252–261. doi:10.1016/j.compscitech.2006.08.011.

[31] H. Lin, M. J. Clifford, A. C. Long, M. Sherburn, Finite element modelling of fabric shear, Modelling and Simulation in Materials Science and Engineering 17 (1) (2009) 015008. doi:10.1088/0965-0393/17/1/015008.

[32] P. Harrison, M. J. Clifford, A. C. Long, Shear characterisation of viscous woven textile composites: a comparison between picture frame and bias extension experiments, Composites Science and Technology 64 (10–11) (2004) 1453–1465. doi:10.1016/j.compscitech.2003.10.015.

[33] S. V. Lomov, I. Verpoest, Model of shear of woven fabric and parametric description of shear resistance of glass woven reinforcements, Composites Science and Technology 66 (7–8) (2006) 919–933. doi:10.1016/j.compscitech.2005.08.010.

[34] P. Boisse, B. Zouari, J.-L. Daniel, Importance of in-plane shear rigidity in finite element analyses of woven fabric composite preforming, Composites Part A: Applied Science and Manufacturing 37 (12) (2006) 2201–2212. doi:10.1016/j.compositesa.2005.09.018.

[35] S. Gatouillat, E. Vidal-Sallé, P. Boisse, Advantages of the Meso/-Macro Approach for the Simulation of Fibre Composite Reinforcements, International Journal of Material Forming 3 (1) (2010) 643–646. doi:10.1007/s12289-010-0852-7.

[36] P. Harrison, F. Abdiwi, Z. Guo, P. Potluri, W. R. Yu, Characterising the shear–tension coupling and wrinkling behaviour of woven engineering fabrics, Composites Part A: Applied Science and Manufacturing 43 (6) (2012) 903–914. doi:10.1016/j.compositesa.2012.01.024.

[37] P. Harrison, Normalisation of biaxial bias extension test results considering shear tension coupling, Composites Part A: Applied Science and Manufacturing 43 (9) (2012) 1546–1554. doi:10.1016/j.compositesa.2012.04.014.

[38] M. Sherburn, Geometric and mechanical modelling of textiles, Ph.D. thesis, University of Nottingham (2007).

[39] S. V. Lomov, Picture Frame Test of Woven Composite Reinforcements with a Full-Field Strain Registration, Textile Research Journal 76 (3) (2006) 243–252. doi:10.1177/0040517506061032.

[40] L. Liu, J. Chen, X. Li, J. Sherwood, Two-dimensional macromechanics shear models of woven fabrics, Composites Part A: Applied Science and Manufacturing 36 (1) (2005) 105–114. doi:10.1016/j.compositesa.2004.07.004.

[41] X. Q. Peng, J. Cao, J. Chen, P. Xue, D. S. Lussier, L. Liu, Experimental and numerical analysis on normalization of picture frame tests for composite materials, Composites Science and Technology 64 (1) (2004) 11–21. doi:10.1016/S0266-3538(03)00202-1.

[42] J. Launay, G. Hivet, A. V. Duong, P. Boisse, Experimental analysis of the influence of tensions on in plane shear behaviour of woven composite reinforcements, Composites Science and Technology 68 (2) (2008) 506–515.

Chapter 7

A Hybrid Micro-meso-scale Unit Cell Model for Homogenization of the Nonlinear Orthotropic Material Behavior of Coated Fabrics Used in Tensioned Membrane Structures

Coated fabric material is a kind of textile composite. However, at micro scale the coating material is not fully impregnated inside the fabric yarn. Thus, the fabric fibers are free to slip relatively to each other during deformation. In this chapter a novel three-dimensional hybrid micro-meso unit cell model is proposed to predict the nonlinear mechanical behavior of coated fabrics using the digital element method. In the model, while the coating material is modeled with 3D solid elements, the fabric yarns are modeled as assemblies of truss elements. Thus, the material constitutive law used in this model is far simpler than the one in which the yarn is modeled with solid elements and the interaction among the fibers can be considered. Different load cases are examined, including uniaxial and biaxial stress states. In these analyses the periodic boundary

conditions are applied to the unit cell, and contact friction among the fibers is also considered. The results obtained from the analyses have a good correlation with the experimental data, which proves the validity of the model. Moreover, local mechanical deformation mechanisms of the coated fabric can be observed from these analyses, which provide a better understanding of the mechanical behavior of this kind of material.

7.1 Introduction

Compared to traditional textile composites, the PVC coated fabric is much less stiff. Its macroscopic mechanical behavior is severely nonlinear, anisotropic and irreversible deformation occurs very early in the loading stage (*cf.* chapter 2). One of the reasons for this peculiar behavior is that the coating material is not fully impregnated inside the fabric yarn. The fabric fibers are thus not held by the coating, but can slip relatively to each other during the course of deformation. Even though there have been some efforts in modeling coated fabrics, most of them are phenomenological models that cannot provide a direct relation between microstructure and the macroscopic mechanical behavior.

In this work, a computational model for coated fabrics is proposed, in which the fabric yarn is modeled as a bundle of truss elements instead of using solid elements, as others have done for textile composites. This model can provide a direct relation between the microstructure of the coated fabrics and their macroscopic mechanical behavior. Hence this work can fill the gap in the literature. The outline of this chapter is as follows. In the next section, a literature review of coated fabrics modeling at fine scales, *i.e.*, micro- and meso-scales, is conducted. Afterward, the ingredients of the proposed model, *viz.*, the geometry of the unit cell and material properties of the unit cell's constituents, are presented. This section is followed by numerical results. The chapter ends with some concluding remarks.

7.2 Coated fabrics modeling at fine scales

In fact, the coated fabric materials have a hierarchically multiscale nature. The fabric is composed of the yarns and the yarns are composed of a number of fibers. Therefore, mechanics of coated fabrics can be

addressed at three different scales, *i.e.,* fabric level or macro-scale, yarn level or meso-scale and fiber level or micro-scale. Models of coated fabrics can be divided into three categories depending on the scale they were proposed.

A literature review of coated fabrics models at macro-scale has been presented in chapter 2. Those models were aimed for structural analyses and cannot describe local deformation mechanisms during the course of deformation. These deformation mechanisms can be captured in the models proposed at meso- and micro-scales. In this chapter only models at these scales are reviewed.

Indeed, in the literature, there are numerous works related to dry fabrics and textile composites at meso- and micro-scales. However, the number of works dedicated to coated fabrics is very limited. Nevertheless, numerical modeling of coated fabrics at meso-scale has some things in common with modeling dry fabrics and textile composites. Normally, computational models for these materials are proposed within the framework of multiscale methods. One of the pioneering works using multiscale methods to model coated fabrics was done by Reese [1]. In her model, a 3D nonlinear truss element was used to model a polyester fabric yarn and low-order brick elements was employed to model a rubber coating (*cf.* fig. 7.1). A fabric sheet with ten yarns in each direction was subjected to different load cases to produce so-called computer experimental data. Those data was subsequently used to fit an elasto-plastic model at macro scale. Recently, within the framework of multiscale modeling a meso-scale layer-based yarn model was proposed for coated fabrics by Yang et al. [2]. The novelty of their model is in the way the fabric yarn was modeled. Instead of modeling the fabric yarn as a single solid, several vertical or horizontal solid layers have been used (*cf.* fig. 7.2). In this context, each solid layer represents for a cluster of fabric fibers. The material parameters of these solid layers were taken from the homogenized properties of the corresponding microstructure where the fibers were explicitly modeled. In general, the model can capture well the elastic behavior of the coated fabric in uniaxial stress state in both warp and fill directions. Even though the authors applied biaxial stress states to the model, the validation was not presented. Nevertheless, the obtained results from that work have been encouraging enough to merit further investigation.

In this chapter, a hybrid micro-meso-scale model for the coated fabric using the digital element method is proposed. Different from the model of

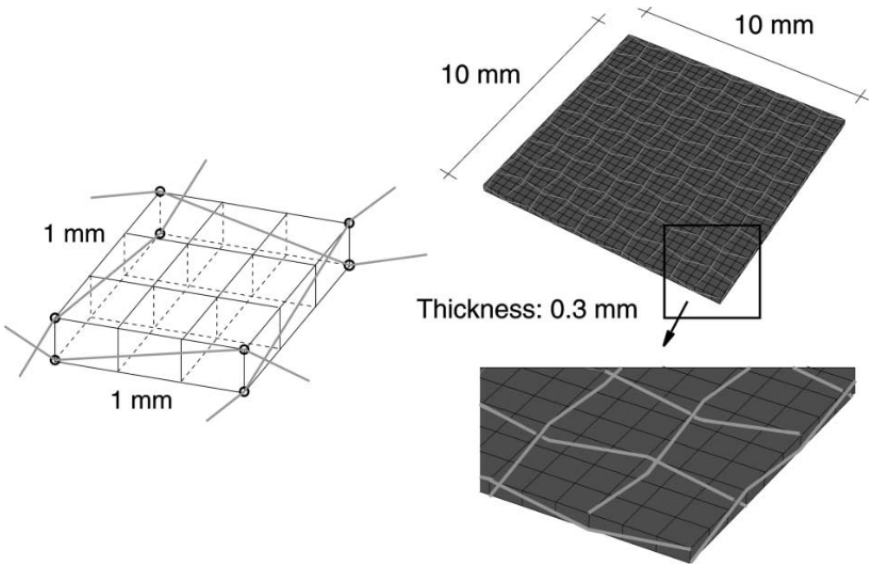

Figure 7.1: Computational model for rubber coating polyester fiber fabric (reprinted from [1]).

Yang et al. [2], the fabric yarn in this model is modeled by a bundle of truss elements and the contact friction among the fibers is incorporated directly into the model. Uniaxial stress state in the warp and fill direction as well as biaxial stress states are applied to the model, then the obtained results are compared to the experimental data to verify the model. Afterward, the model is employed to predict the mechanical behavior of the coated fabric when it is subjected to different stress ratios in the biaxial tests.

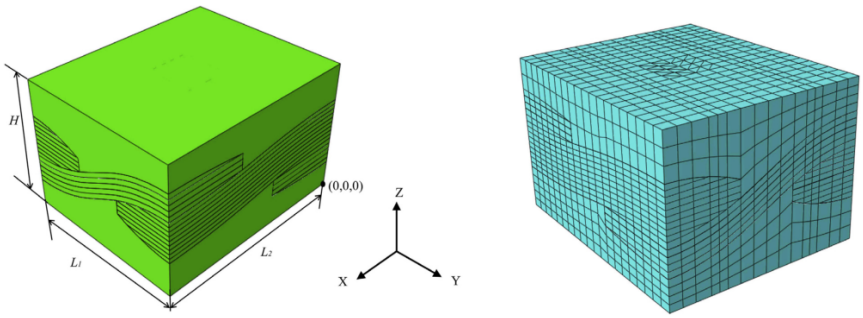

Figure 7.2: The meso-scale layer-based yarn model for a PVC coated polyester fiber fabric (reprinted from [2]).

7.3 Inputs of the unit cell

7.3.1 Microstructure of the PVC coated fabric

The material considered in this work is the PVC coated polyester fiber fabric, which was manufactured by Sioen Industry, Belgium. The microstructure of this material is captured by using the X-ray computed tomography (CT scan) technique. Its cross section in the warp and fill directions is exhibited in fig. 7.3. To create the micro-meso scale model of this material, we assumed that the cross section of the fabric yarn has a race-track shape, in which the fibers are distributed hexagonally. The geometrical data of this model is summarized in table 7.1 and its geometry as well as its mesh in ABAQUS/Explicit is plotted in fig. 7.4.

Table 7.1: Geometrical details for the PVC coated fabric.

Fiber volume fraction of the warp yarn	69.64%
Warp yarn spacing	1.595 mm
Warp yarn thickness	1.24 mm
Warp yarn width	0.25 mm
Fiber volume fraction of the fill yarn	70.84%
Fill yarn spacing	1.665 mm
Fill yarn thickness	0.18 mm
Fill yarn width	1.49 mm
Coated fabric thickness	0.83 mm

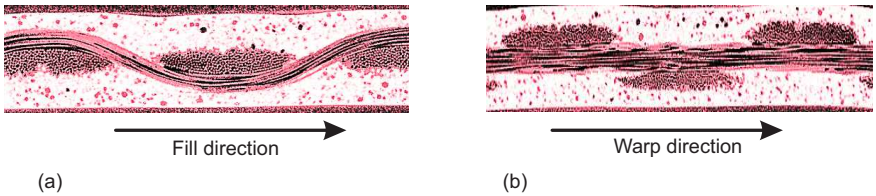

Figure 7.3: The microstructure of the PVC coated fabric: (a) The cross section in the warp direction; (b) the cross section in the fill yarn.

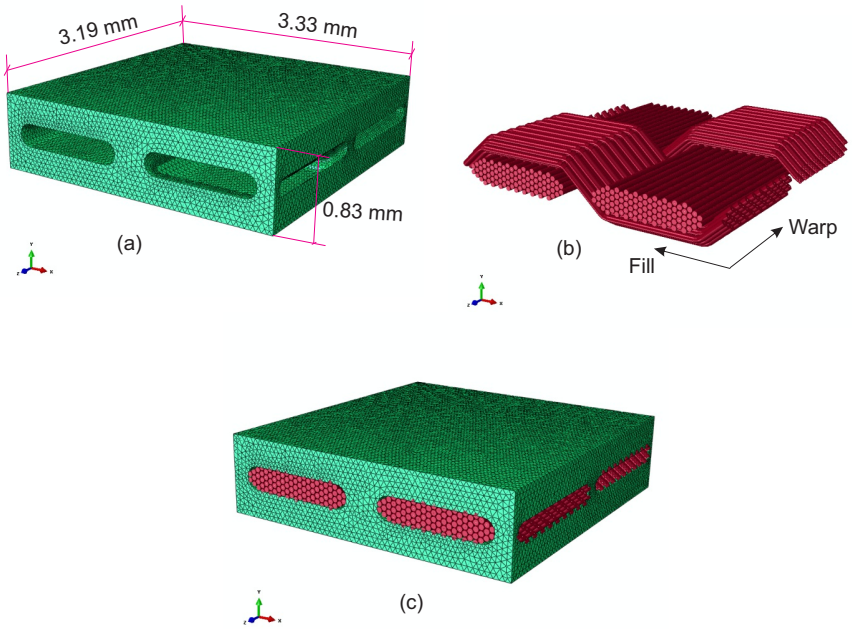

Figure 7.4: The idealized geometry of the PVC coated fabric: (a) the PVC coating, which is discretized by using the C3D10 elements (The midside nodes are not shown in ABAQUS/CAE); (b) the woven fabric structure, which is discretized by using the T3D2 elements, and (c) the assembled RUC.

7.3.2 Material properties of the unit cell's constituents

As can be seen from fig. 7.3, there are two material phases in the PVC coated fabric, *viz.*, PVC coating and polyester fiber. For the sake of mechanical characterization of these material phases, different uniaxial tension tests were carried out. The obtained stress-strain curves for the PVC coating and the individual polyester fiber are respectively shown in figs. 7.5 and 7.6. It is worth mentioning that it was rather difficult to perform cyclic loading for the fiber; therefore, we performed the test on different specimens in which the load levels were varied from 110 to 325 MPa. In the numerical simulations, the J_2 plasticity model is employed to model the elasto-plastic response of the PVC coating and the polyester fiber. By calibrating this model with the experimental data obtained from the uniaxial tests, the material parameters for the coating and fiber are derived (*cf.* table 7.2). Simulation for these uniaxial tests with the calibrated parameters is also performed to verify the model. As can be seen from figs. 7.5 and 7.6, the J_2 plasticity model can capture quite well the mechanical behavior of the coating and the fiber.

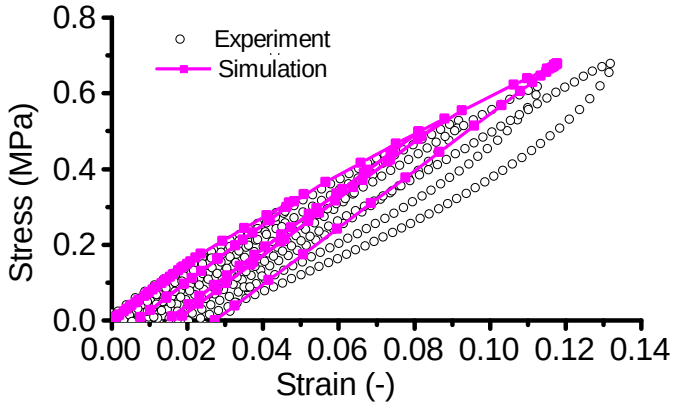

Figure 7.5: Experimental data and simulation for cyclic uniaxial tension tests for the PVC coating.

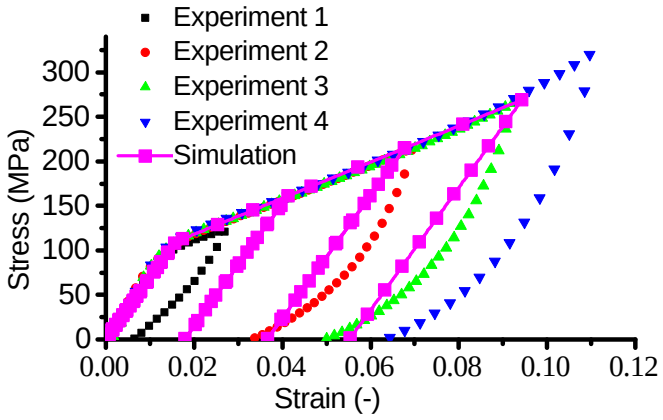

Figure 7.6: Experimental data and simulation for cyclic uniaxial tension tests for the polyester fiber.

Table 7.2: Material parameters of the PVC coating and the polyester fiber.

	PVC coating	Polyester fiber
E (MPa)	7.5	8270.7
H (MPa)	25.53	2992.2
σ_{yield} (MPa)	0.156	110

7.4 Numerical results

As can be seen from fig. 7.4 the fibers in the fill direction are rather idealized compared to the ones in reality (*cf.* fig. 7.3). Therefore, a linear temperature drop is applied to these fibers to bring them close to the physical ones. This strategy has initially proposed in the work of Mahadik and Hallet [3] and has been used in the previous chapter (*cf.* chapter 6). By testing with different values of the thermal drop, the one that is equivalent to applying the strain of -0.025 in the fill direction is chosen. The thermal effect on the fabric structure can be seen in fig. 7.7. Also, in micro-scale, the fabric yarns are composed of hundreds of fibers. It is thus extremely computationally expensive if all of the fibers are included in the model. However, it is not the case when the digital element method is used, as shown in the simulation of the fabric shear in the previous chapter (*cf.*

chapter 6). It has been shown in that simulation that the number of fibers has a profound effect on the homogenized results. Hence, it is necessary to conduct a study to know for which number of fibers per yarn, the computational model can capture the mechanical behavior of the PVC coated fabric. In this work, the number of fibers for each yarn is identified from the uniaxial tests; then the obtained model is validated with the data from a biaxial test when the stress ratio is equal to 1:1 (*cf.* chapter 2). In the numerical simulations of these tests, there are two load steps: at first, the aforementioned thermal load is applied, then displacements are applied to the control points to induce a certain stress state to the unit cell.

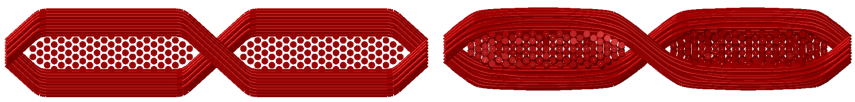

Figure 7.7: Thermal effect on the polyester fabric structure (left: initial configuration; right: deformed configuration).

Inside the fabric structure, there is indeed no coating material. However, we assume a perfect bonding at the interface of the fabric structure and the coating. As such, the fibers that are on the boundary of the yarn will be tied to the coating (*cf.* fig. 7.8). Moreover, there is contact among all fibers with the frictional coefficient of 0.25 [4].

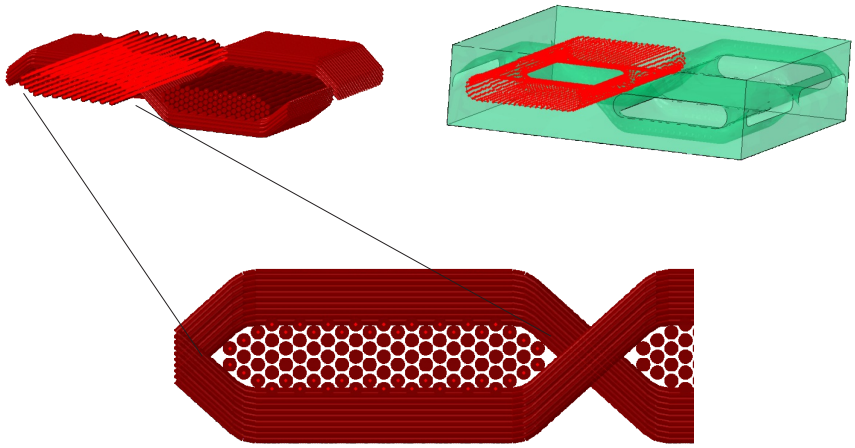

Figure 7.8: The fibers that are on the boundary of the fabric yarn are tied to the coating. Here the illustration is only for one yarn, but in the model, the tie connection is applied to all fabric yarns.

7.4.1 Uniaxial tests

The uniaxial tests in the warp and fill directions of the same PVC coated fabric were done and presented in chapter 2. The obtained stress-strain curves are plotted in fig. 7.9. From this figure, it can be seen that the mechanical behavior of this PVC coated fabric is severely nonlinear and highly orthotropic, *i.e.*, the behaviors in the warp and fill are remarkably different.

Because we assume that the fibers are distributed hexagonally inside the fabric yarn, there is a coupling between the number of fibers in the horizontal and vertical directions. In our software implementation, the maximum number of fibers layers is specified to distribute the fibers inside the yarn. To identify which number of fibers per yarn are sufficient for the model to capture the mechanical behavior of fabrics, four cases are considered (*cf.* fig. 7.10), *viz.*, (i) three layers of fibers in both the warp and fill directions (model 1); (ii) five layers of fibers in the warp direction and three layers of fibers in the fill direction (model 2); (iii) three layers of fibers in the warp direction and five layers of fibers in the fill direction (model 3); (iv) five layers of fibers in both the warp and fill directions (model 4). In these models, the diameter of each fiber is adjusted in such a way that

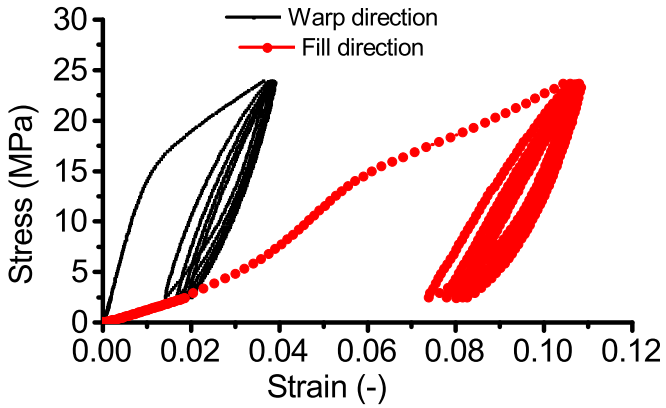

Figure 7.9: Experimental stress-strain curves of the uniaxial tests in the warp and fill direction of the considered PVC coated fabric (these tests were done at the ae-lab and MeMC, VUB).

the fiber volume fraction of the corresponding yarn is preserved.

The homogenized stress-strain curves of these models when they were subjected to uniaxial stress states in the warp and fill directions are respectively plotted in fig. 7.11 and fig. 7.12. In general, the homogenized curves obtained from these models can capture quite well the tendency of the counterparts in the experiments. In the warp direction, the result from the model 1 is rather soft compared to the experimental data. The results from model 3 and model 4 are almost identical and have a quite good correlation with the experimental data in both elastic and plastic regimes. It implies that the number of fibers used in the model 3 is sufficient. It is quite interesting to observe that the result obtained from the model 3 is better than the one from the model 2 in this load case although in the model 2 the number of fibers in the warp yarn, which is in line with the loading direction, is larger than the counterpart in the model 3. This phenomenon can be explained by the fact that the interaction of the fibers in the fill direction is more dominant than in the warp direction. This observation is indeed in line with the conclusion mentioned in [2]. Similar conclusions can be drawn from the results in the fill direction (*cf.* fig. 7.12). The discrepancy between the results from the model 3 and model 4 remains small. It is then again confirmed that the number of fibers used in the model 3 is sufficient. However, compared to the previous

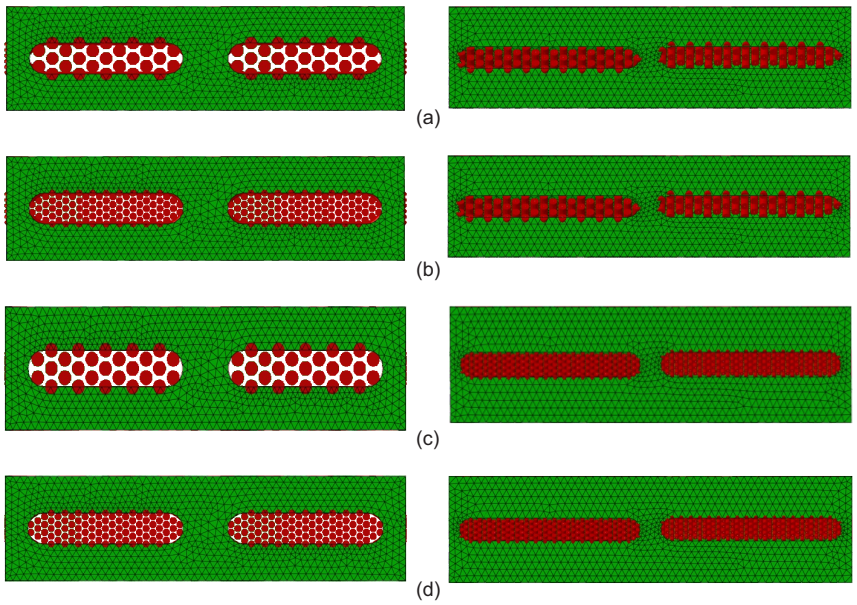

Figure 7.10: Four models that are employed to identify the sufficient number of fibers per yarn (left: the cross section of the warp yarn; right: the cross section of the fill yarn): (a) model 1, (b) model 2, (c) model 3, and (d) model 4.

case, this time the difference between the homogenized results and the experimental data is more visible, especially when the stress passes 15 MPa. The reason for these mismatches is because of the assumption of a perfect bonding between the coating material and the fibers in the yarn. The deformed configurations of the coated fabric unit cell when it was subjected to the uniaxial stress states in the warp and the fill directions are plotted in fig. 7.13. From the figure, it can be seen that the coating material has experienced a large deformation, not only in the loading direction but also in the lateral direction. This observation is chiefly clear in the case of the uniaxial test in the fill direction. For such a large deformation that the coating material has experienced in the uniaxial tests, especially in the fill direction, the perfect bonding between the coating material and the fibers is rather simplistic.

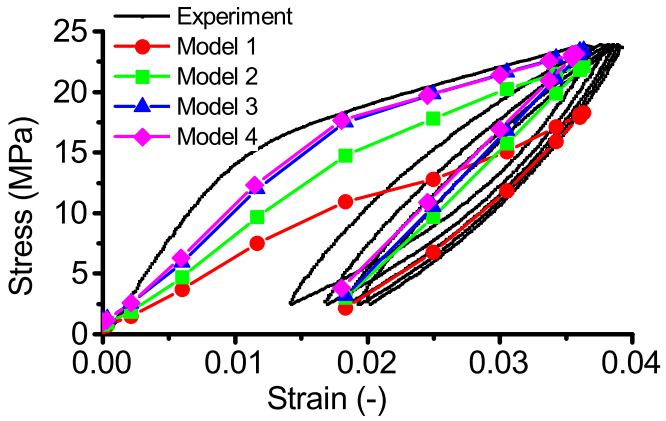

Figure 7.11: Stress-strain curves obtained from the uniaxial test in the warp direction of the PVC coated fabric: experiment *vs.* homogenization.

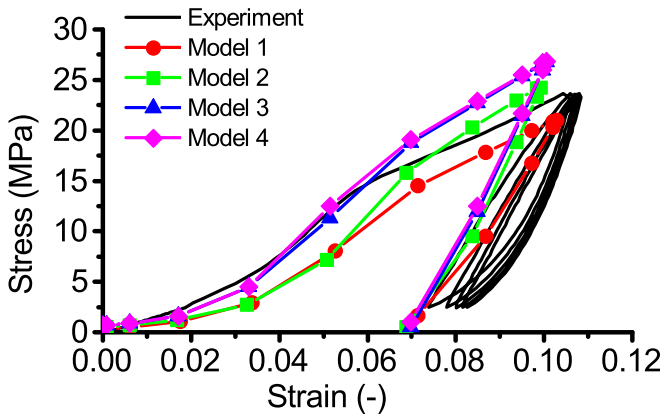

Figure 7.12: Stress-strain curves obtained from the uniaxial test in the fill direction of the PVC coated fabric: experiment *vs.* homogenization.

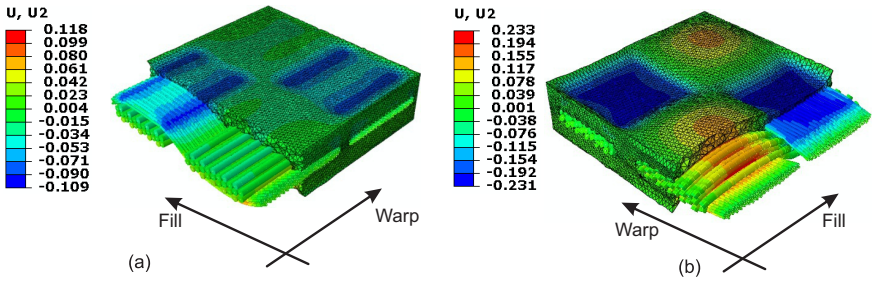

Figure 7.13: The displacement (mm) in the thickness direction of the coated fabric unit cell in the uniaxial tests: (a) in the warp direction and (b) in the fill direction (for the sake of clarity, a part of the coating material was removed in the figure).

7.4.2 Biaxial tests

From the results of the uniaxial tests, it can be seen that the model 3 can capture well the mechanical behavior of the PVC coated fabric. For validation, this model is subjected to biaxial stress states. In chapter 2, the biaxial test of the same coated fabric has been done in case the stress ratio in the warp and the fill directions, denoted as α, is equal to 1. The test was done on a cruciform specimen (*cf.* fig. 7.14). During the experiment, the strains in the center of the cruciform were recorded by using the digital image correlation technique and the equivalent stresses were calculated as the load applied to the arms of the cruciform divided by the cross section of the arms. Certainly, these equivalent stresses are different from the stresses in the center of the cruciform. Therefore, the stress-strain curves plotted in fig. 7.15 do not reflect the constitutive behavior of the coated fabric in the biaxial stress state. However, in chapter 2, we have proposed a phenomenological material model for the coated fabric, *i.e.*, fabric plasticity, and that model can capture well the mechanical behavior of the coated fabric in the biaxial test. Therefore, when the model 3 is subjected to the biaxial stress state of stress ratio $\alpha = 1$, the homogenized stress-strain curve is compared to the stress-strain curve extracted at the center of the cruciform in the numerical continuum model when the fabric plasticity is used for the membrane. These curves are plotted in fig. 7.16. As can be seen from this figure, the homogenized results of the model 3

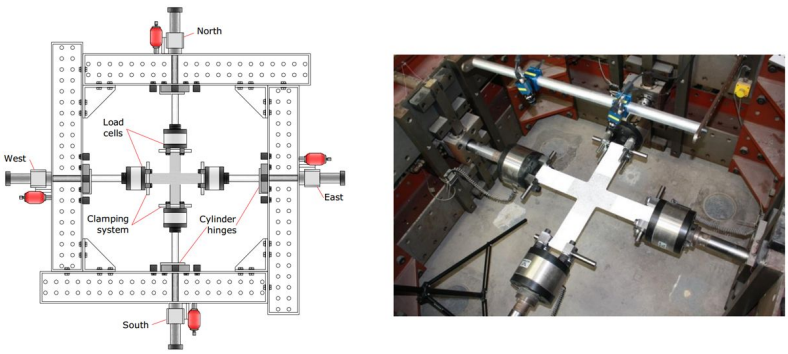

Figure 7.14: The biaxial tension tests was done on the coated fabric cruciform specimen (*cf.* chapter 2).

have a good correlation to the counterparts of the fabric plasticity model in both elastic and plastic regimes. In the warp direction, the results from the model 3 and the fabric plasticity are almost identical in the elastic

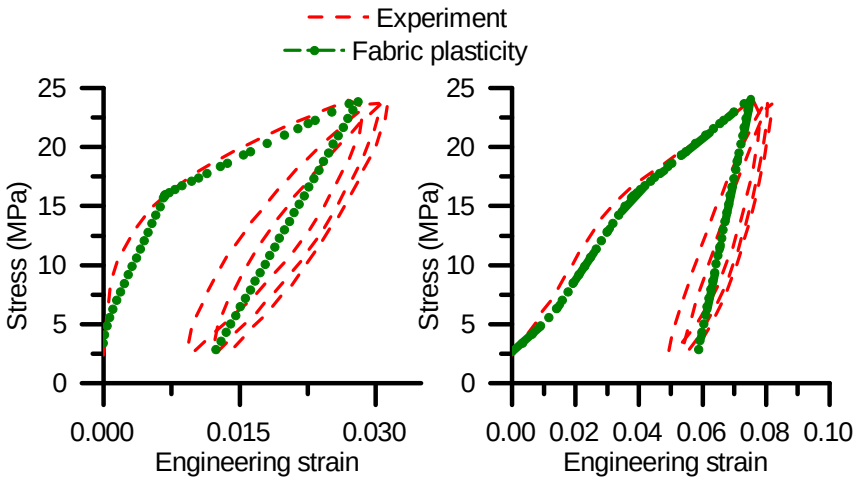

Figure 7.15: The correlation between the experimental data and the fabric plasticity model with the stress ratio $\alpha = 1$ (*cf.* chapter 2).

regime; the discrepancy is only visible when the stress state is in the plastic regime. It is worth mentioning that in the fabric plasticity model, we assumed that the linear hardening law governs the relation between stress and strain when the material is in the plastic regime. However, in the experiment, the relation between stress and strain in this regime remains nonlinear (*cf.* fig. 7.15). Therefore, it is believed that the results from homogenization, in this case, are more realistic.

Thus far, it has been shown that the model 3 can capture the mechanical behavior of the coated fabric not only in uniaxial stress states but also in the biaxial stress state. We then use this model to create virtual experimental data for the coated fabric when it is subjected to biaxial stresses with different stress ratios α. Indeed, these data are necessary to further develop the fabric plasticity model that was proposed in chapter 2. Different stress ratios α have been examined, and the homogenized stress-strain curves are plotted in fig. 7.17. It can be seen in this figure that when the stress ratio $\alpha = 0.25$, the stress in the warp direction is positive, while the strain in this direction is negative. It indeed manifests the peculiar mechanical behavior of the coated fabric, so-called negative strain phenomenon [5].

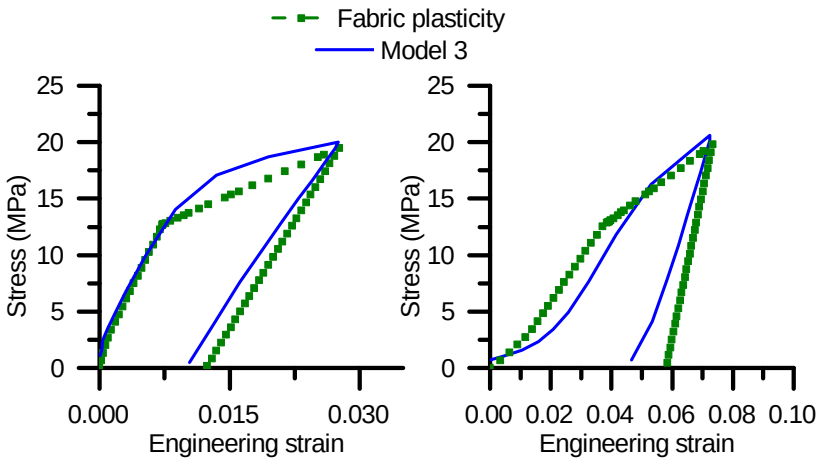

Figure 7.16: The constitutive stress-strain curves obtained from numerical homogenization of the model 3 and the fabric plasticity model with the stress ratio $\alpha = 1$.

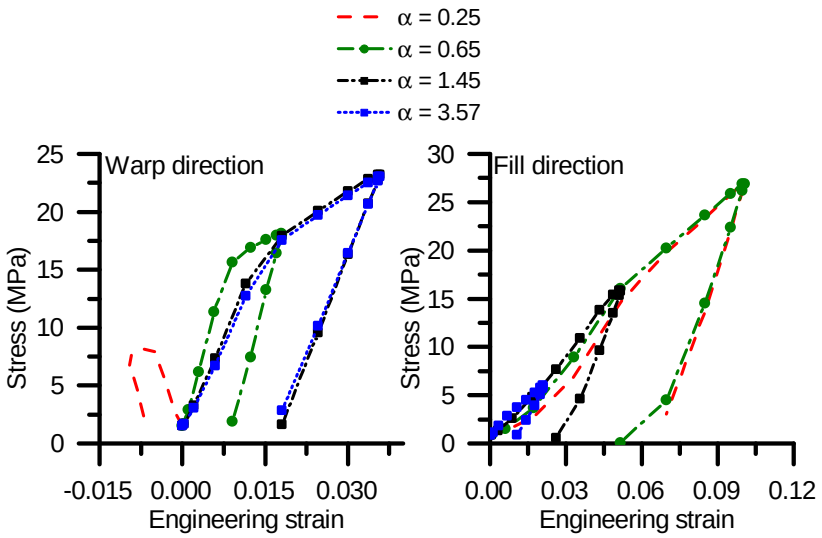

Figure 7.17: The stress-strain curves obtained from numerical homogenization of the model 3 under different the stress ratios α: (a) in the warp direction and (b) in the fill direction.

7.5 Conclusions

In this chapter, a numerical model for the PVC coated fabrics used in tensioned fabric membrane structures is proposed using the digital element method. The ultimate target of this work is to provide a direct link between the micro-meso structure of the coated fabric and its macroscopic mechanical behavior. In the proposed model, the fabric fibers are explicitly modeled with truss elements and interactions among them are thus incorporated directly into the homogenized macroscopic mechanical behavior of the studied coated fabric. The numerical model demonstrates good performance in capturing the peculiar mechanical behavior of the coated fabrics in both uniaxial tests and biaxial tests, including anisotropy, severe nonlinearity, irreversible deformation and stress ratio dependence. Further developments of this model can be carried out by incorporating the hysteresis effect in the material models of the coated fabric constituents, *i.e.*, the coating and the fiber materials. Moreover, a more sophisticated interaction between the coating and fibers can improve the performance of the proposed model.

Bibliography

[1] S. Reese, Meso-macro modelling of fibre-reinforced rubber-like composites exhibiting large elastoplastic deformation, International Journal of Solids and Structures 40 (4) (2003) 951–980. doi:10.1016/S0020-7683(02)00602-9.

[2] Y. Yang, P. Zeng, M.-J. Pindera, Capturing the Multiscale Effects in the Response of Coated Woven Fabrics, Composite Structuresdoi:10.1016/j.compstruct.2015.10.027.

[3] Y. Mahadik, S. R. Hallett, Finite element modelling of tow geometry in 3d woven fabrics, Composites Part A: Applied Science and Manufacturing 41 (9) (2010) 1192–1200. doi:10.1016/j.compositesa.2010.05.001.

[4] M. M. Robins, R. W. Rennell, R. D. Arnell, The friction of polyester textile fibres, Journal of Physics D: Applied Physics 17 (1984) 1349–1360.

[5] B. N. Bridgens, P. D. Gosling, Direct stress–strain representation for coated woven fabrics, Computers & Structures 82 (23–26) (2004) 1913–1927. doi:10.1016/j.compstruc.2003.07.005.

Appendix A

List of Experiments

As mentioned in chapter 1, this dissertation is a part of the project *"Integrated analysis and experimental verification of kinematic form active analysis (KFAS) for architectural applications"*. This project was executed in strong collaboration of three following partners: (i) the research group Mechanics of Materials and Structures (MMS) of the Department of Materials Science and Engineering at Ghent University; (ii) the architectural engineering research laboratory (ae-lab) of the department of Architectural Engineering at Vrije Universiteit Brussel; (iii) the research group Mechanics of Materials and Constructions (MeMC) at Vrije Universiteit Brussel. In this project, the numerical simulations were performed under the supervision of the MMS research group and these simulations were presented in this dissertation. The experiments were performed under the supervision of the ae-lab and the MeMC research groups. Most of the experimental data presented in the dissertation were provided by P. Tapali, M. Van Craenenbroeck and S. Puystiens from Vrije Universiteit Brussel.

Table A.1: List of experiments done at Vrije Universiteit Brussel.

Date	Tests	Testing device/instrument
Before June 2012	Uniaxial, biaxial and bias extension tests (Sioen T2107)	Instron DIC
February 2013	Loading of a 2D membrane Series of loading and unloading	Overhead crane 100 kN load cell, 2x10 kN load cell DIC
April 2013	Loading of a 2D membrane Series of loading and unloading	Overhead crane 100 kN load cell, 2x10 kN load cell DIC
June 2013	Tension tests belts (Loadlok 25MM BS2800daN) 1 x continuous; 2 x cyclic loading (up to failure)	Instron
August 2013	Tension tests belts (Loadlok 25MM BS2800daN) 6 x cyclic loading (up to failure)	Instron
August 2013	Uniaxial tension tests membrane (Sioen T2107) 8 x continuous; 6 x cyclic loading (warp, fill and $45°$)	Instron DIC
October 2013	Biaxial tests (Sioen T2107) 3 x MSAJ protocol (preliminary tests)	Biaxial bench DIC
February 2014	Validation/calibration of the new RVDT's (on uniaxial membrane specimens)	Instron DIC
March 2014	Biaxial tests (Sioen T2107 and T2103) 4 x MSAJ; 4 x adapted protocol	Biaxial bench DIC, RVDT's
April 2014 May 2014	Compensation tests membrane material (Sioen T2107) 2 x biaxial 3D foldable membrane	Biaxial bench DIC Overhead crane 100 kN load cell, 4 x 10 kN load cell DIC
July 2014	Tension tests belts (Loadlok 50MM BS6000daN) 1 x continuous; 4 x cyclic loading	Instron
July 2014	3D foldable membrane Pretensioning, opening and closing	Overhead crane 100 kN load cell, 4 x 10 kN load cell DIC
August 2014	Biaxial tests for 3D membrane test 2 x biaxial	Biaxial bench DIC
September 2014	3D foldable membrane pretensioning, opening and closing	Overhead crane 100 kN load cell 4 x 10 kN load cell and DIC